AWARD NUMBER: W81XWH-19-1-0590

TITLE: SOS2 is a tractable therapeutic target to limit therapeutic resistance in non-small cell lung cancer

PRINCIPAL INVESTIGATOR: Robert L. Kortum, MD

RECIPIENT: The Henry M. Jackson Foundation for the Advancement of Military Medicine, Inc.

REPORT DATE: AUGUST 2020

TYPE OF REPORT: Annual

PREPARED FOR: U.S. Army Medical Research and Materiel Command
Fort Detrick, Maryland 21702-5012

DISTRIBUTION STATEMENT: Approved for Public Release;
Distribution Unlimited

The views, opinions and/or findings contained in this report are those of the author(s) and should not be construed as an official Department of the Army position, policy or decision unless so designated by other documentation.

REPORT DOCUMENTATION PAGE

Form Approved
OMB No. 0704-0188

1. REPORT DATE	**2. REPORT TYPE**	**3. DATES COVERED**
AUGUST 2020	**ANNUAL**	**1AUG2019 - 31JUL2020**

4. TITLE AND SUBTITLE
SOS2 is a tractable therapeutic target to limit therapeutic resistance in non-small cell lung cancer

5a. CONTRACT NUMBER

5b. GRANT NUMBER
W81XWH-19-1-0590

5c. PROGRAM ELEMENT NUMBER

6. AUTHOR(S)
Dr. Robert Kortum

E-Mail: robert.kortum@usuhs.edu

5d. PROJECT NUMBER

5e. TASK NUMBER

5f. WORK UNIT NUMBER

7. PERFORMING ORGANIZATION NAME(S) AND ADDRESS(ES)
The Henry M. Jackson Foundation for the
Advancement of Military Medicine, Inc.
6720A Rockledge Drive, Suite 100
Bethesda, Maryland 20817

8. PERFORMING ORGANIZATION REPORT NUMBER

9. SPONSORING / MONITORING AGENCY NAME(S) AND ADDRESS(ES)

U.S. Army Medical Research and Development Command
Fort Detrick, Maryland 21702-5012

10. SPONSOR/MONITOR'S ACRONYM(S)

11. SPONSOR/MONITOR'S REPORT NUMBER(S)

12. DISTRIBUTION / AVAILABILITY STATEMENT

Approved for Public Release; Distribution Unlimited

13. SUPPLEMENTARY NOTES

14. ABSTRACT

Our objective is to characterize SOS2 as a bona fide therapeutic target whose inhibition will limit therapeutic resistance in EGFR- and KRAS-mutated NSCLC. We hypothesize that SOS2 deletion reduces RTK-stimulated PI3K/AKT signaling to limit therapeutic resistance in EGFR- and KRAS-mutated NSCLCs. In year 1 of the proposal, we found that SOS2 deletion significantly reduces the development of osimertinib resistance in EGFR-mutated NSCLC cells, whereas SOS1 inhibition shows strong synergy with osimertinib in initial cell killing after initial treatment. Further, we found that SOS2 deletion reduces transforming (3D) growth of EGFR-mutated NSCLC cells at limiting serum concentrations. In KRAS-mutated NSCLC cells, we found that SOS2 deletion reduces transforming (3D) growth and synergizes with MEK inhibitors to limit cell survival. We have also published two primary research articles and one review based on these data.

15. SUBJECT TERMS
Lung cancer, KRAS, EGFR, MEK, osimertinib, trametinib, Son of Sevenless, SOS2, SOS1

16. SECURITY CLASSIFICATION OF:			**17. LIMITATION OF ABSTRACT**	**18. NUMBER OF PAGES**	**19a. NAME OF RESPONSIBLE PERSON**
					USAMRMC
a. REPORT	**b. ABSTRACT**	**c. THIS PAGE**			**19b. TELEPHONE NUMBER** *(include area code)*
Unclassified	Unclassified	Unclassified	Unclassified	27	

Standard Form 298 (Rev. 8-98)
Prescribed by ANSI Std. Z39.18

TABLE OF CONTENTS

1. **INTRODUCTION:** Narrative that briefly (one paragraph) describes the subject, purpose and scope of the research.

   This is the year-one annual report for the research project "SOS2 is a tractable therapeutic target to limit therapeutic resistance in non-small cell lung cancer"; the subject of this is to examine SOS2 as novel therapeutic targets in NSCLC harboring EGFR or KRAS mutations. The purpose of this research is to test the hypothesis that that *SOS2* deletion reduces RTK-stimulated PI3K/AKT signaling to limit therapeutic resistance in EGFR- and KRAS-mutated NSCLCs. The scope of the project is to obtain preliminary data to allow the investigator to write a full lung cancer proposal (CDMRP or R01) at the end of the cycle investigating novel therapeutic targets in lung cancer.

2. **KEYWORDS:** Provide a brief list of keywords (limit to 20 words).

Lung cancer, KRAS, EGFR, MEK, osimertinib, trametinib, Son of Sevenless, SOS2, SOS1

3. **ACCOMPLISHMENTS:** The PI is reminded that the recipient organization is required to obtain prior written approval from the awarding agency grants official whenever there are significant changes in the project or its direction.

What were the major goals of the project?
List the major goals of the project as stated in the approved SOW. If the application listed milestones/target dates for important activities or phases of the project, identify these dates and show actual completion dates or the percentage of completion.

Aim 1, **Major Task 1: Determine whether *SOS2* deletion synergizes with Osimertinib treatment to limit RAS effector signaling and inhibit cell growth.**

1. Confirm SOS2 deletion using CRISPR/Cas9 in NSCLC cell lines (month 3). Completed 09/2019
2. Determine dose-response curves for each EGFR mutant NSCLC cell line to osimertinib treatment +/- *SOS2* deletion (month 9). 75% complete as of 08/2020.
3. Determine the effect of *SOS2* deletion on ERK and AKT activation in NSCLC cell lines treated with Osimertinib (month 9). 75% complete as of 08/2020.

Aim 1, **Major Task 2: Characterize the extent to which *SOS2* deletion delays the development of Osimertinib resistance in EGFR (T790M) lung cancer cell lines.**

1. Examine which concentration of osimertinib inhibits growth but allows the outgrowth of resistant clones in each parental NSCLC cell line (month 8). 75% complete as of 08/2020.
2. Examine the effect of *SOS2* deletion on the development of osimertinib resistance by time-to-progression (month 13). 10% complete as of 08/2020.
3. Examine the effect of *SOS2* deletion on the development of osimertinib resistance in 96-well format (month 18). 66% complete as of 08/2020.
4. Transfer resistant clones from 96-well plates to 24-well plates for further expansion in major task 3 (month 18). 50% complete as of 08/2020.

Aim 1, Major Task 3: Determine whether SOS2 deletion alters the mechanism by with lung cancer cell lines become resistant to osimertinib.

1. Expand multiple WT and *SOS2* KO osimertinib resistant sub clones from a 24 well plate to multiple 10 cm dishes (month 18). 50% complete as of 08/2020.
2. Generate genomic DNA, protein lysate, and a frozen vial of cells for each osimertib resistant clone (month 18). 50% complete as of 08/2020.
3. Examine protein lysates by dot-blot for ERK and AKT phosphorylation versus parental cell lines +/- osimertinib treatment (month 20). Not started.
4. Perform whole-exome sequencing of resistant samples (month 23).
5. Compare and analyze the mutation spectrum in NSCLC cell lines resistant to osimertinib +/- *SOS2* deletion (month 24). Not started

Aim 2, Major Task 1: Determine the extent to which SOS2 contributes to RTK-dependent PI3K pathway activation in *KRAS* mutated NSCLC cell lines cultured in 3D.

1. Verification of PI3K and PTEN status in KRAS mutated cell lines (month 4). Completed 12/2019
2. Establishment of 3D culture conditions for assessing RTK-stimulated signaling (month 8). Completed 02/2020.
1. Successful deletion of *SOS2* in *KRAS* mutated lung cancer cell lines (month 10). 33% complete as of 08/2020.
2. Assessment of pERK and pAKT in above cells (month 13). Not started

Aim 2, Major Task 2: Characterize the extent to which *PI3KCA*/*PTEN* mutations or *PTEN* expression level alterations influence the vulnerability of *KRAS* mutant NSCLC cell lines to *SOS2* deletion.

1. Assess each *KRAS* mutated cell line to be studied for its ability to (i) form spheroids and (ii) grow/proliferate in spheroid culture (month 14). 33% complete as of 08/2020.
2. Perform assessment of 2D proliferation in cells above cells (month 18). 33% complete as of 08/2020.
3. Perform assessment of 3D transformation in cells above cells (month 18). 33% complete as of 08/2020.

Aim 2, Major Task 3: Examine whether *PIK3CA* or *PTEN* mutation status predicts the responsiveness of *KRAS* mutated tumors to combining pharmacologic MEK inhibition with *SOS2* deletion.

1. Assess dose-response to trametinib treatment in *KRAS* mutated cells +/- *SOS2* deletion (month 20). 25% complete as of 08/2020
2. Assess time-to-progression in trametinib -treated *KRAS* mutated cells +/- *SOS2* deletion (month 22). Not started.
3. Assess RAS effector activation in trametinib -treated *KRAS* mutated cells +/- *SOS2* deletion (month 24). Not started

What was accomplished under these goals?

For this reporting period describe: 1) major activities; 2) specific objectives; 3) significant results or key outcomes, including major findings, developments, or conclusions (both positive and negative); and/or 4) other achievements. Include a discussion of stated goals not met.

Description shall include pertinent data and graphs in sufficient detail to explain any significant results achieved. A succinct description of the methodology used shall be provided. As the project progresses to completion, the emphasis in reporting in this section should shift from reporting activities to reporting accomplishments.

Aim 1, **Major Task 1: Determine whether *SOS2* deletion synergizes with Osimertinib treatment to limit RAS effector signaling and inhibit cell growth.**

1. *Confirm SOS2 deletion using CRISPR/Cas9 in NSCLC cell lines.*

   While this proposal is focused on SOS2, the experiments were done in parallel with experiments where we had deleted SOS1. As such, the figure showd both *SOS1* and *SOS2* deletion. We have designed and tested several sgRNAs that target either SOS1 or SOS2, and have found at least 3 sgRNAs that delete SOS1 or SOS2 in >80% of cells. We have successfully deleted both SOS1 and SOS2 in seven different NSCLC cell lines (HCC827, H1650, H1975, H3255, H3255-TM, PC9, PC9-TM). This includes all *EGFR*-mutated cell lines in the current proposal. We have also tested the effects of *SOS1* or *SOS2* deletion in all seven cell lines, and found that SOS1 more consistently alters oncogenic transformation compared to SOS2. These data are found in Fig. 1 (below), and are also part of our recently accepted manuscript at eLife.

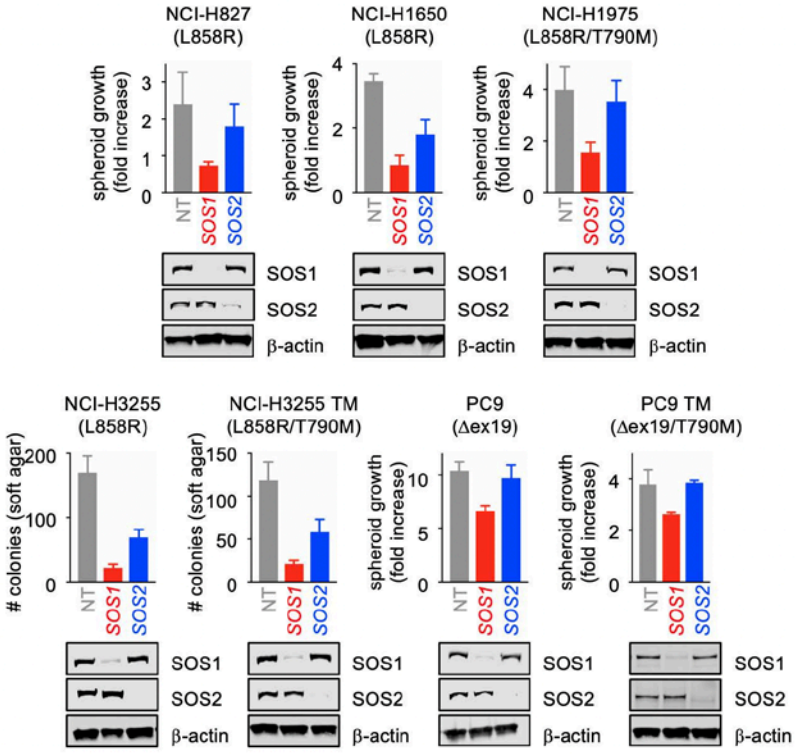

Fig. 1 (LC180213). SOS1 is required for transformation in *EGFR*-mutated NSCLC cells. *SOS1* or *SOS2* were deleted in seven different EGFR-mutated NSCLC cell lines using CRISPR/Cas9. Western blots confirming deletion are shown. We found that *SOS1* deletion consistently reduced anchorage-independent (3D, transforming) growth in all EGFR-mutated NSCLC cell lines we examined. In contrast, *SOS2* deletion had a more variable effect on 3D transforming growth of NSCLC cell lines.

2. *Determine dose-response curves for each EGFR mutant NSCLC cell line to osimertinib treatment +/- SOS2 deletion.*

We have assessed the dose-response curve for Osimertinib in NT versus SOS2 KO cells in all of the cell lines over a four day period. We found that in 10% serum, *SOS2* deletion does not alter osimertinib-induced killing in either 2D or 3D culture after 4 days of treatment (see Fig. 2 as an example in H1975 cells and Fig. 3 as an example in PC9 cells). Further, *SOS2* deletion does not enhance the marked synergy we observe between Osimertinib and the SOS1 inhibitor BAY-293 in three different NSCLC cell lines (Fig. 4 and our recently published eLife paper.

However, we have found that *SOS2* deletion has a significant effect on the ability of osimertinib to inhibit transformation in 3D culture. These experiments require that cells be cultured long enough for transformation to be observed. First, when modeling HGF-stimulated osimertinib resistance in H1975 cells, we found that either *SOS1* or *SOS2* deletion reduced the dose of osimertinib required to inhibit transformation (Fig. 2). Further, under reduced serum conditions (2%), *SOS2* deletion reduces overall transforming growth and enhances osimertinib-induced killing in PC9 cells (Fig. 3). These experiments were ongoing when we had to shut the lab down due to the coronavirus pandemic. We are starting them back up now that we can resume our lab work at 50% capacity.

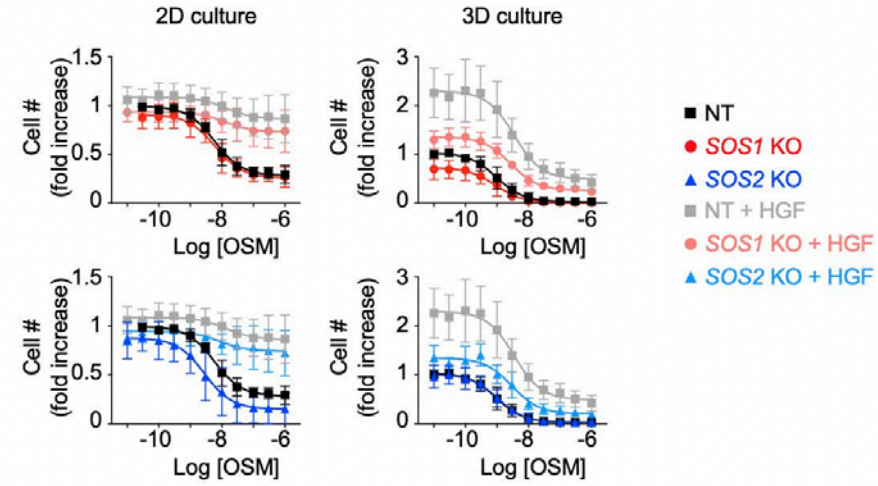

Fig. 2 (LC180213). *SOS1* or *SOS2* deletion inhibit HGF-dependent osimertinib resistance in 3D cultured H1975 cells. NT controls, *SOS1* KO or *SOS2* KO cells were cultured under either 2D or 3D conditions and treated with increasing doses osimertinib alone or in the presence of 30 ng/mL HGF to induce osimertinib resistance. Western blots confirming deletion are in Fig. 1. We found that while *SOS1* KO or *SOS2* KO alone did not alter the osimertinib dose-response curve in 10% serum, either *SOS1* KO or *SOS2* KO blocked HGF-induced osimertinib resistance under 3D culture conditions.

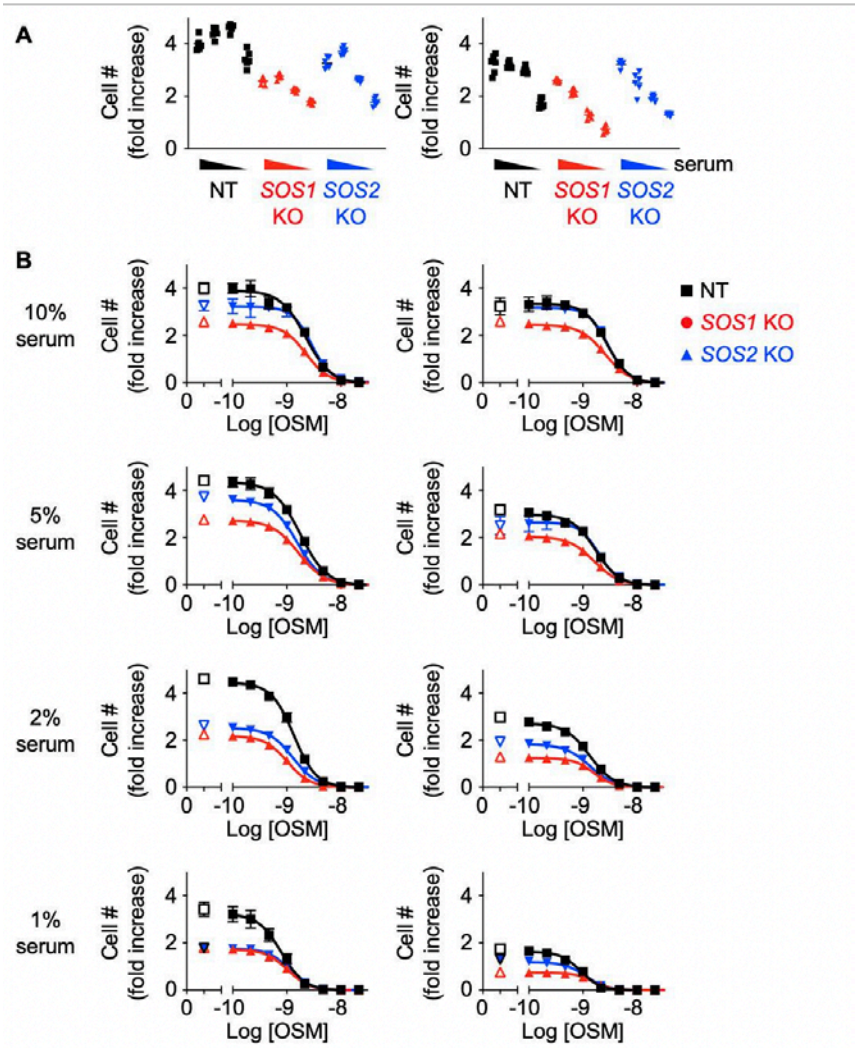

Fig. 3 (LC180213). *SOS2* deletion enhances osimertinib-induced inhibition of transformation in PC9 cells. NT controls, *SOS1* KO or *SOS2* KO PC9 cells were cultured under 3D conditions in decreasing doses of serum (10%, 5%, 2%, or 1%). Cells were either left untreated (A) or were treated with increasing doses of osimertinib, and cell number was assessed at day 0, day 4, and day 7. We had previously found that *SOS1* KO inhibits transformation. Strikingly, we also found that *SOS2* KO inhibits transformation at limiting serum conditions (A) and may enhance the ability of osimertinib to inhibit transforming growth (B). Western blots confirming deletion are in Fig. 1.

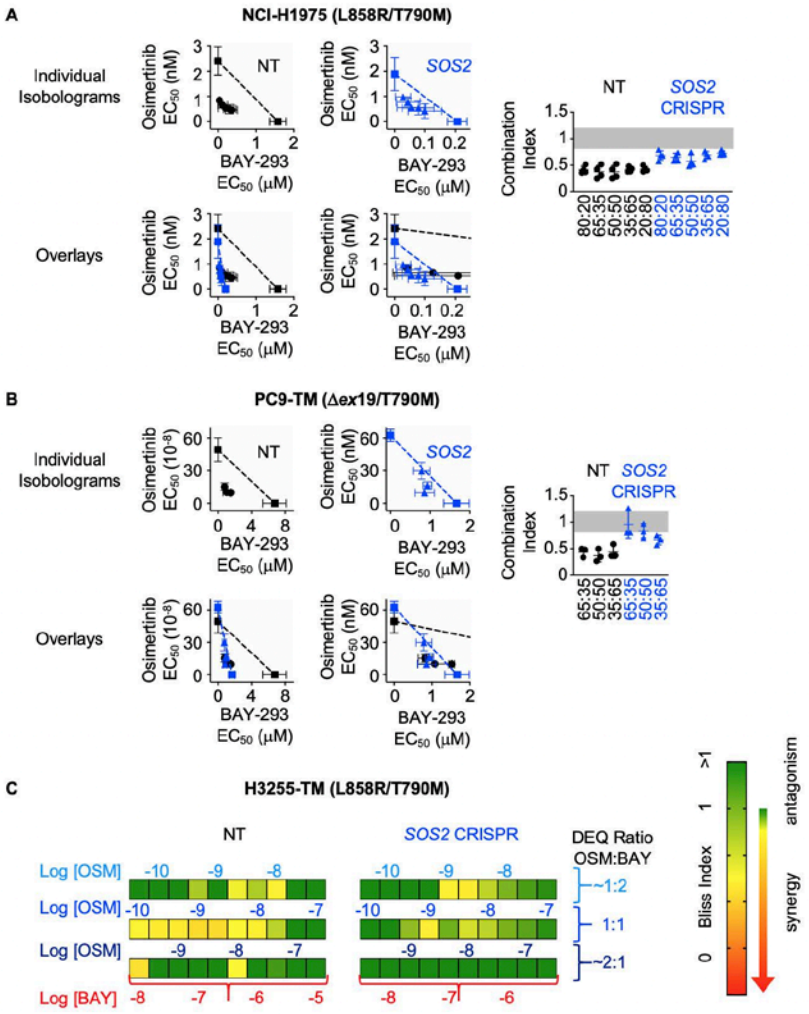

Figure 4 (LC180213). *SOS2* deletion does not enhance the synergistic interaction between SOS1 inhibition and EGFR-TKI treatment.
(A-B) Isobologram analysis (left) and Combination Index (right) from dose-equivalent treatments of osimertinib and BAY-293 in H1975 (**A**) or PC9-TM (**B**) cells where *SOS2* has been deleted (blue) versus NT controls (black). Overlay plots on two different BAY-293 dosing scales are shown below the individual isobologram plots. Additive effects occur on the dashed lines of the isobologram plot and have a CI 0.8-1.2 (gray box), whereas synergistic interactions fall below the dashed lines and have a CI < 0.8.
(C) Bliss Index heatmaps for H3255-TM cells where *SOS2* has been deleted versus NT controls treated at at 1:2, 1:1, and 2:1 ratios of osimertinib and BAY-293 based on dose equivalencies.
Data are presented as mean +/- s.d. from three independent experiments.
For each experiment, three technical replicates were assessed.

3. *Determine the effect of SOS2 deletion on ERK and AKT activation in NSCLC cell lines treated with Osimertinib.*

In our recently accepted eLife manuscript, we assessed the individual and combined effects of *SOS2* deletion and SOS1 inhibition (using BAY-293) on osimertinib-induced inhibition of RAS effector signaling in 3D culture (Fig. 5). Intriguingly, we found that either *SOS2* deletion or SOS1 inhibition significantly inhibited pERK in both H1975 and PC9-TM cells, and that the combination of SOS2 deletion and SOS1 inhibition further enhanced this inhibition. In contrast, SOS2 deletion did not alter pAKT, whereas SOS1 inhibition showed a significant inhibition of pAKT. We are currently following these

studies up in other cell lines to assess whether the effect of *SOS2* deletion on osimertinib-induced inhibition of pERK or pAKT changes under reduced serum conditions (see Fig. 3). These samples are made for H1975 and PC9 cells.

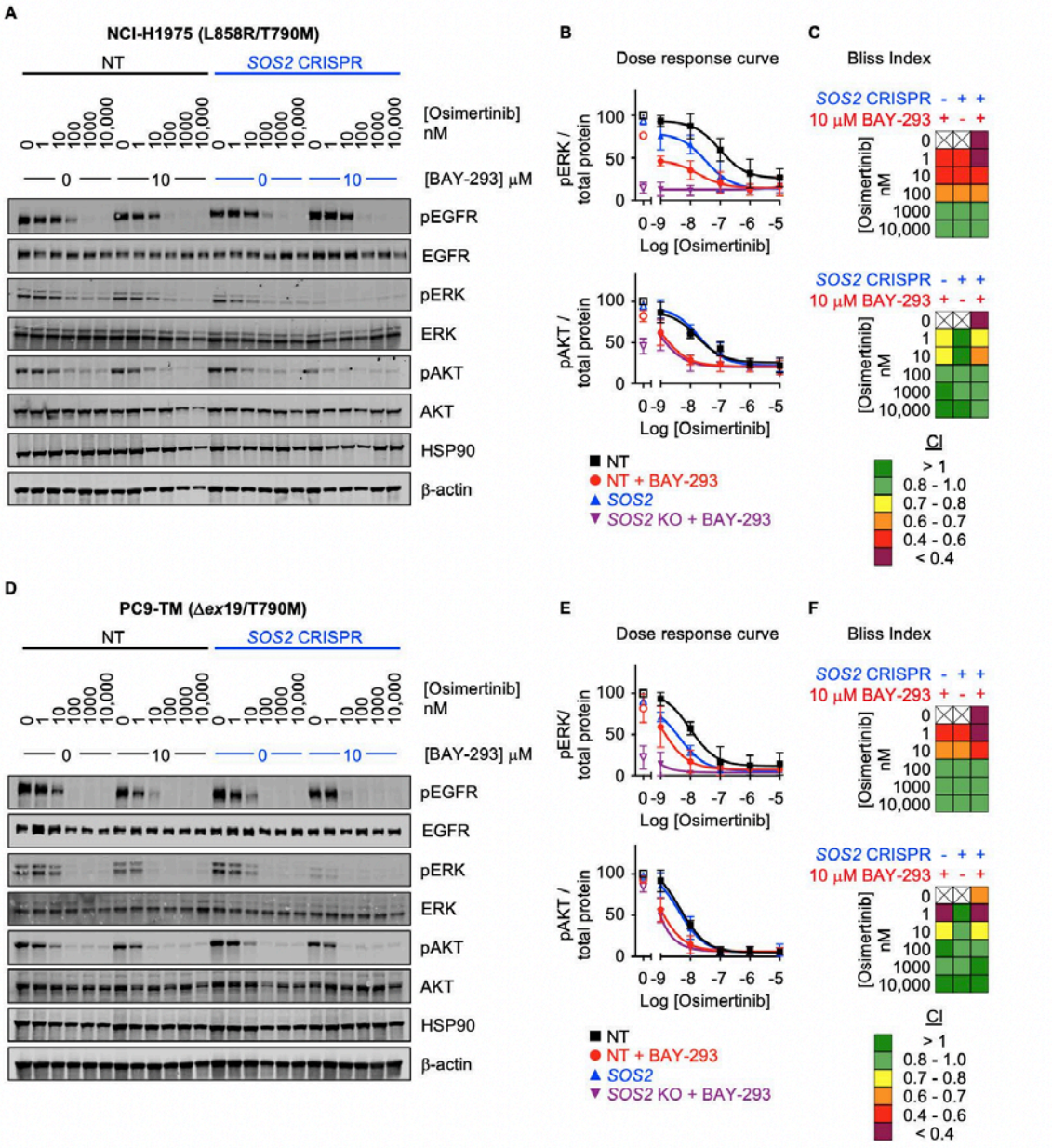

Figure 5 (LC180213). *SOS2 deletion* and SOS1 inhibition synergizes with mutant EGFR inhibition to inhibit downstream effector signaling.
Western blots **(A, D)**, pERK and pAKT quantitation **(B, E)**, and Bliss Indices **(C, F)** of WCLs of NCI-H1975 cells (A-C, top) or PC9-TM cells (D-F, bottom) cultured under 3D spheroid conditions for 48 hours and then treated with the indicated concentrations of the EGFR-TKI osimertinib and/or the SOS1 inhibitor BAY-293 for 6 hours. Western blots are for pEGFR, EGFR, pAKT, AKT, pERK1/2, ERK1/2, HSP90, and b-actin. pERK and pAKT quantifications were calculated using a weighted average of total protein western blots. Combination Indices are based on pERK / Total protein and pAKT / Total protein quantitations. Increasingly synergistic combinations are indicated in yellow, orange, red, or purple. Phosphoprotein quantitations are presented as mean +/- s.d. from three independent experiments. Bliss indices are presented as mean from three independent experiments.
For each experiment, three technical replicates were assessed.

Aim 1, **Major Task 2: Characterize the extent to which *SOS2* deletion delays the development of Osimertinib resistance in EGFR (T790M) lung cancer cell lines.**

1. *Examine which concentration of osimertinib inhibits growth but allows the outgrowth of resistant clones in each parental NSCLC cell line.*

   When performing the initial experiments in H1975 cells, we found that very different concentrations of osimertinib would be required for time-to-progression versus 96-well resistance experiments, with TTP experiments needing to be performed at much lower concentrations of osimertinib than 96-well resistance assays. We hypothesize that this difference is due to the trypinization/replating that occurs in TTP assays versus allowing quiescent cells to remain attached for the 96-well resistance assays. We have worked out the concentrations required for the 96-well plate assays and are well on our way to completing these (see Fig. 6). We had a number of TTP experiments ongoing in March 2020, which we were required to stop due to the university shutting down for the coronavirus pandemic. We will re-start these experiments this fall.

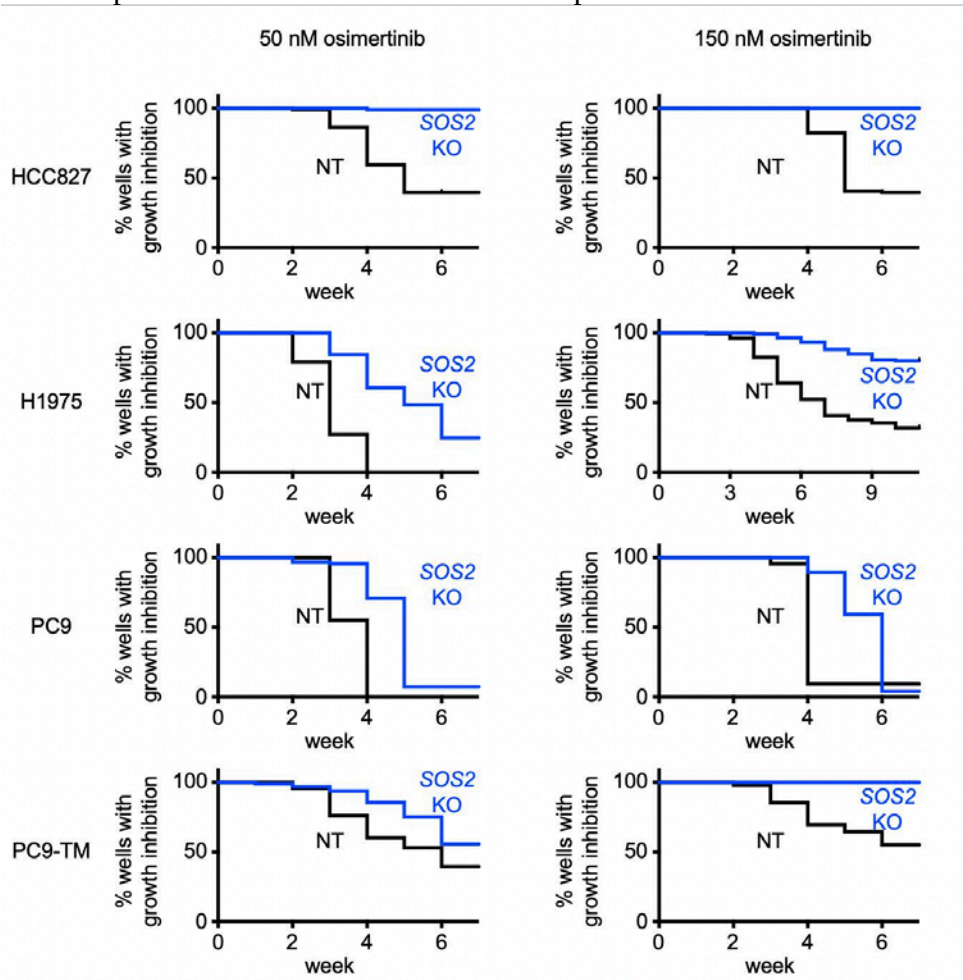

Figure 6 (LC180213). *SOS2 deletion* limits osimertinib resistance in cell culture models
Multi-well resistance experiments showing that *SOS2* deletion delays the development of osimertinib resistance and reduces the overall number of osimertinib resistant colonies in EGFR-mutated NSCLC cell lines treated with 50 nM (left) or 150 nM (right) osimertinib when compared to NT control.

2. *Examine the effect of SOS2 deletion on the development of osimertinib resistance by time-to-progression.*

   We had a number of TTP experiments ongoing in March 2020, which we were required to stop due to the university shutting down for the coronavirus pandemic. We will re-start these experiments this fall.

3. *Examine the effect of SOS2 deletion on the development of osimertinib resistance in 96-well format.*

   We have assessed the effects of *SOS2* deletion on the development of osimertinib using the 96-well (trial) format in four different *EGFR*-mutated NSCLC cell lines. We found that in all four cases, SOS2 deletion delayed the development of osimertinib resistance (Fig. 6). Further, in three of the four cell lines SOS2 deletion reduced the overall number of osimertinib resistant populations. For the one cell line that this did not occur (PC9), we are repeating the experiment at a higher concentration of osimertinib (300 nM). We have not yet started these experiments in H3255 or H3255-TM cells, as they have different and more complex media requirements compared to HCC827, H1975, PC9, and PC9-TM cells. Experiments in H3255 and H3255-tm cells will be performed in the upcoming year.

4. *Transfer resistant clones from 96-well plates to 24-well plates for further expansion in major task 3.*

   We have transfrered 26 NT and 31 *SOS2* KO clones for H1975 cells resistant to either 150 nM or 300 nM osimertinib into 24 well plates, and further expanded these (see below). New resistance experiments to confirm the data shown in Fig. 6 were started August 2020, and further resistant clones will be expanded from these experiments.

Aim 1, Major Task 3: Determine whether SOS2 deletion alters the mechanism by with lung cancer cell lines become resistant to osimertinib.

1. *Expand multiple WT and SOS2 KO osimertinib resistant sub clones from a 24 well plate to multiple 10 cm dishes.*

   We have expanded 26 NT and 31 *SOS2* KO clones for H1975 cells resistant to either 150 nM or 300 nM osimertinib into 4 x 10 cm Dishes. These were then banked for genomic DNA, protein lysate, and a frozen vial of cells.

2. *Generate genomic DNA, protein lysate, and a frozen vial of cells for each osimertib resistant clone.*

We have expanded 26 NT and 31 *SOS2* KO clones for H1975 cells resistant to either 150 nM or 300 nM osimertinib into 4 x 10 cm Dishes. These were then banked for genomic DNA, protein lysate, and a frozen vial of cells.

3. *Examine protein lysates by dot-blot for ERK and AKT phosphorylation versus parental cell lines +/- osimertinib treatment.*

   We are currently optimizing our pERK and pAKT dot blots to ensure that we can perform appropriate background correction for these experiments. Once we have the protocol optimized, we will perform dot-blots on the bio-banked H1975 resistant samples as a pilot experiment, and then expand our studies to other resistant clones as they become available.

4. *Perform whole-exome sequencing of resistant samples.*

   These experiments have not been initiated.

5. *Compare and analyze the mutation spectrum in NSCLC cell lines resistant to osimertinib +/- SOS2 deletion (month 24).*

   These experiments have not been initiated.

Aim 2, Major Task 1: Determine the extent to which SOS2 contributes to RTK-dependent PI3K pathway activation in *KRAS* mutated NSCLC cell lines cultured in 3D.

1. *Verification of PI3K and PTEN status in KRAS mutated cell lines.*

   We have obtained all of the KRAS mutated cell lines outlined in the proposal and have verified the PI3K and PTEN mutational status in each cell line.

2. *Establishment of 3D culture conditions for assessing RTK-stimulated signaling.*

   We have gone through an iterative process to optimize RTK-stimulated signaling experiments in a 3D environment. These experiments have been significantly enhanced by the use of 24-well Aggrewell plates from StemCell, which have 1200 individual micropatterned 'wells' in a single large well. We now routinely plate 500-750 cells / spheroid and change the media from 2% - 0.25% over a 48 hour period prior to growth factor stimulation.

3. *Successful deletion of SOS2 in KRAS mutated lung cancer cell lines.*

   We have successfully deleted SOS2 in three of the cell lines, H23, H358, and H460 (see Fig. 7 below). We have also examined both 2D proliferation and 3D transformation in these cells (see Aim 2, major task 2).

4. *Assessment of pERK and pAKT in above cells (month 13).*

   These experiments have not been initiated.

Aim 2, Major Task 2: Characterize the extent to which *PI3KCA*/*PTEN* mutations or *PTEN* expression level alterations influence the vulnerability of *KRAS* mutant NSCLC cell lines to *SOS2* deletion.

1. *Assess each KRAS mutated cell line to be studied for its ability to (i) form spheroids and (ii) grow/proliferate in spheroid culture.*

   We have confirmed spheroid growth in H23, H358, and H460 cells (see Fig. 7). We will confirm spheroid growth in other *KRAS*-mutated NSCLC cell lines as we pull them out of culture.

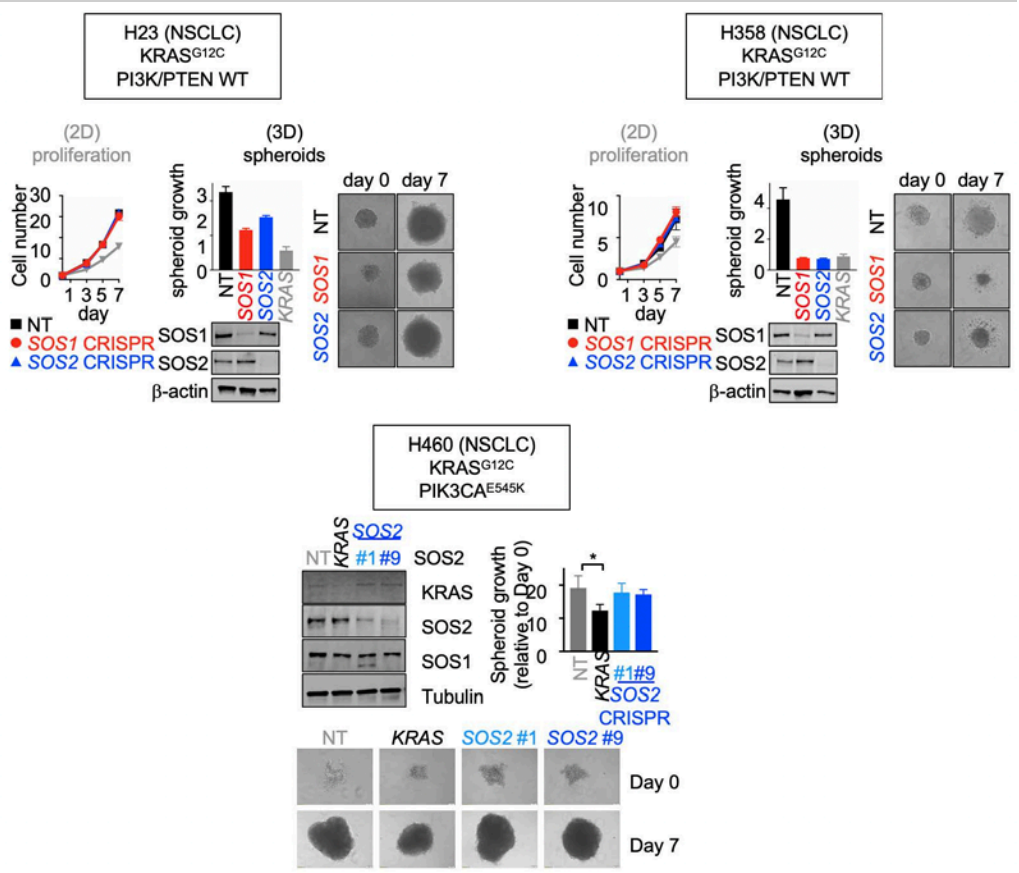

Figure 7 (LC180213). *SOS2* deletion reduces 3D transformation in KRAS-mutated NSCLC cell lines with WT PI3K/PTEN.
A. SOS1 or *SOS2* were deleted in *KRAS-mutated*/*PIK3CA* WT (H23 and H358) NSCLC cell lines using CRISPR/Cas9. Western blots confirming deletion are shown. We found that either *SOS1* deletion or *SOS2* deletion consistently reduced anchorage-independent (3D, transforming) growth but not 2D anchorage-dependent proliferation in both cell lines. Cells where *KRAS* was deleted were used as a positive control. B. *SOS2* was deleted in *KRAS-mutated*/*PIK3CA*-mutated H460 NSCLC cells using CRISPR/Cas9. Western blots confirming deletion are shown. In contrast to H23 and H358 cells in **A**, *SOS2* deletion did not reduce oncogenic transformation in H460 cells as assessed by spheroid growth. Cells where *KRAS* was deleted were used as a positive control.

2. *Perform assessment of 2D proliferation in cells above cells.*

   We have assessed 2D proliferation in H23, H358, and H460 cells where we have deleted *SOS2* versus NT controls. For both H23 and H358 cells, *SOS1* KO experiments were performed in parallel. As expected, *SOS2* deletion did not alter 2D proliferation in any of the *KRAS*-mutated cell lines we've tested thus far (Fig. 7). Experiments assessing *SOS2* deletion will be performed in other cell lines in the next year.

3. *Perform assessment of 3D transformation in cells above cells.*

   We have assessed 3D transformation (spheroid growth) in H23, H358, and H460 cells where we have deleted *SOS2* versus NT controls. For both H23 and H358 cells, *SOS1* KO experiments were performed in parallel. As expected, *SOS2* deletion reduced spheroid growth in cells where the PI3K/PTEN axis is WT (H23 and H358 cells), but not in H460 cells that have mutated PIK3CA (Fig. 7). Experiments assessing *SOS2* deletion will be performed in other cell lines in the next year.

Aim 2, Major Task 3: Examine whether *PIK3CA* or *PTEN* mutation status predicts the responsiveness of *KRAS* mutated tumors to combining pharmacologic MEK inhibition with *SOS2* deletion.

1. *Assess dose-response to trametinib treatment in KRAS mutated cells +/- SOS2 deletion.*

   We have thus far assessed the dose response to trametinib in H358 and H460 cells where SOS2 has been deleted versus NT controls. We found that SOS2 deletion synergized with MEK inhibition to inhibit growth of *KRAS*-mutated/*PIK3CA* WT cells as well as the combination of MEK + PI3K inhibition. In contrast, this synergy was lost in cells with mutated *PIK3CA* (Fig. 8).

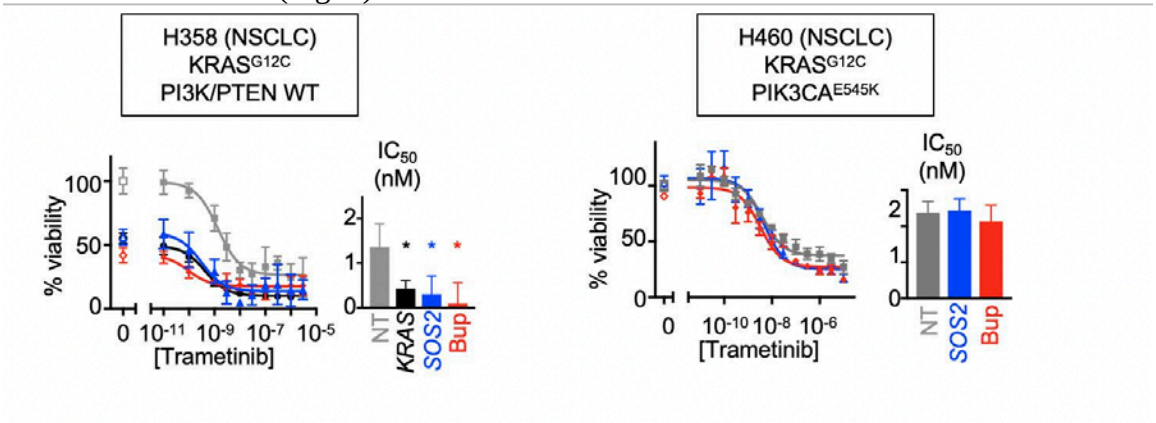

Figure 8 (LC180213). *SOS2* deletion synergizes with the MEK inhibitor trametinib in KRAS-mutated NSCLC cell lines with WT PI3K/PTEN.
SOS2 was deleted in H358 (*KRAS*-mutated/*PIK3CA* WT) and H460 (*KRAS*-mutated/*PIK3CA*-mutated) NSCLC cells using CRISPR/Cas9. *SOS2 KO* cells and NT control cells were treated with increasing doses of trametinib. NT cells were also treated with trametinib + an IC_{50} dose of buparlisib as a control for inhibiting PI3K. We found that SOS2 deletion synergized with MEK inhibition to inhibit growth of *KRAS*-mutated/*PIK3CA* WT cells as well as the combination of MEK + PI3K inhibition. In contrast, this synergy was lost in cells with mutated *PIK3CA*.

2. *Assess time-to-progression in trametinib -treated KRAS mutated cells +/- SOS2 deletion.*

   These experiments have not been initiated.

3. *Assess RAS effector activation in trametinib -treated KRAS mutated cells +/- SOS2 deletion.*

   These experiments have not been initiated.

What opportunities for training and professional development has the project provided?
If the project was not intended to provide training and professional development opportunities or there is nothing significant to report during this reporting period, state "Nothing to Report."

Describe opportunities for training and professional development provided to anyone who worked on the project or anyone who was involved in the activities supported by the project. "Training" activities are those in which individuals with advanced professional skills and experience assist others in attaining greater proficiency. Training activities may include, for example, courses or one-on-one work with a mentor. "Professional development" activities result in increased knowledge or skill in one's area of expertise and may include workshops, conferences, seminars, study groups, and individual study. Include participation in conferences, workshops, and seminars not listed under major activities.

I have presented this work at research seminars for three different departments at the NCI (Pediatric Oncology Branch, Laboratory of Cell and Developmental Signaling, Laboratory of Cancer Biology and Genetics.

Describe how the results were disseminated to communities of interest. Include any outreach activities that were undertaken to reach members of communities who are not usually aware of these project activities, for the purpose of enhancing public understanding and increasing interest in learning and careers in science, technology, and the humanities.

The EGFR findings were published in the recently accepted manuscript:
Theard PT, Sheffels E, Sealover NE, Linke AJ, Pratico DJ, and **Kortum RL** (2020). Marked Synergy by Vertical Inhibition of EGFR signaling in NSCLC Spheroids: SOS1 as a therapeutic target in EGFR-mutated cancer. *eLife, accepted*.
We have also presented the research findings at the above conferences.

We also wrote an invited review outlining our work on targeting SOS in KRAS-mutated cells for the NCI RAS dialogue:

> Sheffels E and **Kortum RL** (2020). SOS Signaling in *RAS*-mutated cancers. *NCI RAS Initiative: RAS Dialogue,* June 2020. https://www.cancer.gov/research/key-initiatives/ras/ras-central/blog/2020/kortum-sos-proteins-in-kras-cancers

Describe briefly what you plan to do during the next reporting period to accomplish the goals and objectives.

We will continue to perform the experiments outlined in the SOW. We are currently writing a methods paper using this technique for Bio-Protocols and will submit this in September 2020. We plan to submit a second manuscript on the EGFR/SOS2 data (Aim 1) by the end of the calendar year. We plan to submit a KRAS manuscript in either late 2020 or early 2021.

4. IMPACT: Describe distinctive contributions, major accomplishments, innovations, successes, or any change in practice or behavior that has come about as a result of the project relative to:

What was the impact on the development of the principal discipline(s) of the project?
If there is nothing significant to report during this reporting period, state "Nothing to Report."

Describe how findings, results, techniques that were developed or extended, or other products from the project made an impact or are likely to make an impact on the base of knowledge, theory, and research in the principal disciplinary field(s) of the project. Summarize using language that an intelligent lay audience can understand (Scientific American style).

Most current studies of genes whose deletion may change oncogenic proliferation are done under anchorage-dependent (attached, 2D) conditions. We previously reported that *SOS2* deletion affects KRAS-mutant tumorigenesis, but only under in anchorage-independent (3D) conditions, and not in 2D cultures, has significant implications to how the field assesses modifiers of KRAS-driven tumorigenesis.

We have now found a similar requirement for performing 3D culture experiments in *EGFR*-mutated NSCLC cells. In our eLife manuscript, we show that there is significant synergy between EGFR and SOS1 inhibition, but only under 3D culture conditions. This finding suggests that we must take care in choosing the appropriate culture system to identify and test

novel therapeutic targets to treat *EGFR* and *KRAS* mutant tumors, and that anchorage-independent 3D growth screens should be used to supplement current 2D screening efforts. Further, these data suggest that 3D culture systems might be needed in all NSCLC cell lines.

What was the impact on other disciplines?
If there is nothing significant to report during this reporting period, state "Nothing to Report."

Describe how the findings, results, or techniques that were developed or improved, or other products from the project made an impact or are likely to make an impact on other disciplines.

Nothing to report

What was the impact on technology transfer?
If there is nothing significant to report during this reporting period, state "Nothing to Report."

Describe ways in which the project made an impact, or is likely to make an impact, on commercial technology or public use, including:

- *transfer of results to entities in government or industry;*
- *instances where the research has led to the initiation of a start-up company; or*
- *adoption of new practices.*

Our work has led directly to a CRADA (Cooperative Research And Development Agreement) between our lab and Boehringer Ingelheim assessing their clinical SOS1 inhibitors in *EGFR*-mutated NSCLC. These are already in phase 1 trials for *KRAS* mutated cancers.

What was the impact on society beyond science and technology?
If there is nothing significant to report during this reporting period, state "Nothing to Report."

Describe how results from the project made an impact, or are likely to make an impact, beyond the bounds of science, engineering, and the academic world on areas such as:

- *improving public knowledge, attitudes, skills, and abilities;*
- *changing behavior, practices, decision making, policies (including regulatory policies), or social actions; or*
- *improving social, economic, civic, or environmental conditions.*

Nothing to report

5. **CHANGES/PROBLEMS:** The PD/PI is reminded that the recipient organization is required to obtain prior written approval from the awarding agency grants official whenever there are significant changes in the project or its direction. If not previously reported in writing, provide the following additional information or state, "Nothing to Report," if applicable:
Remember that significant changes in objectives and scope require prior approval of the agency.

Nothing to report

Actual or anticipated problems or delays and actions or plans to resolve them
Describe problems or delays encountered during the reporting period and actions or plans to resolve them.

We were forced to shut down our laboratory in March 2020 due to the coronavirus pandemic. This caused us to stop/throw away many ongoing resistance experiments, as these require long-term (several months) of culture. Fortunately, we were able to start back up at 50% capacity in July 2020, and are currently operating at 50% capacity in the laboratory. The shut-down and loss of ongoing experiments significantly set us behind on the work. That being said, we anticipate completing all of the Aims on budget. However, we will need an extension on the time to spend the funds into a third year.

Changes that had a significant impact on expenditures
Describe changes during the reporting period that may have had a significant impact on expenditures, for example, delays in hiring staff or favorable developments that enable meeting objectives at less cost than anticipated.

See above – coronavirus pandemic.

Significant changes in use or care of human subjects, vertebrate animals, biohazards, and/or select agents
Describe significant deviations, unexpected outcomes, or changes in approved protocols for the use or care of human subjects, vertebrate animals, biohazards, and/or select agents during the reporting period. If required, were these changes approved by the applicable institution

committee (or equivalent) and reported to the agency? Also specify the applicable Institutional Review Board/Institutional Animal Care and Use Committee approval dates.

Significant changes in use or care of human subjects

n/a

Significant changes in use or care of vertebrate animals

n/a

Significant changes in use of biohazards and/or select agents

n/a

6. PRODUCTS: List any products resulting from the project during the reporting period. If there is nothing to report under a particular item, state "Nothing to Report."

- **Publications, conference papers, and presentations**
  Report only the major publication(s) resulting from the work under this award.

  Journal publications. *List peer-reviewed articles or papers appearing in scientific, technical, or professional journals. Identify for each publication: Author(s); title; journal; volume: year; page numbers; status of publication (published; accepted, awaiting publication; submitted, under review; other); acknowledgement of federal support (yes/no).*

  Two peer-reviewed articles have been published thus far with this grant support. In both articles, we acknowledgement the federal grant support from the CDMPR/LCRP grant LC18213.

  1. Theard PT, Sheffels E, Sealover NE, Linke AJ, Pratico DJ, and **Kortum RL** (2020). Marked Synergy by Vertical Inhibition of EGFR signaling in NSCLC Spheroids: SOS1 as a therapeutic target in EGFR-mutated cancer. *eLife, accepted*.

2. Terrell EM, Durrant DE, Ritt DA, Sheffels E, Sealover NE, Esposito D, Zhou Z, Hancock J, **Kortum RL**, and Morrison DK (2019). Distinct Binding Preferences Between Individual Ras and Raf Family Members and the Impact on Oncogenic Ras Signaling. *Mol Cell,* **76:**872-84.

Books or other non-periodical, one-time publications. *Report any book, monograph, dissertation, abstract, or the like published as or in a separate publication, rather than a periodical or series. Include any significant publication in the proceedings of a one-time conference or in the report of a one-time study, commission, or the like. Identify for each one-time publication: author(s); title; editor; title of collection, if applicable; bibliographic information; year; type of publication (e.g., book, thesis or dissertation); status of publication (published; accepted, awaiting publication; submitted, under review; other); acknowledgement of federal support (yes/no).*

We were invited to write the June 2020 NCI RAS dialogue. There was no opportunity to cite support in this format:
Sheffels E and **Kortum RL** (2020). SOS Signaling in *RAS*-mutated cancers. *NCI RAS Initiative: RAS Dialogue,* June 2020.
https://www.cancer.gov/research/key-initiatives/ras/ras-central/blog/2020/kortum-sos-proteins-in-kras-cancers

My first student, Erin Sheffels, completed her PhD dissertation. CDMRP support was acknowledged:

Sheffels E (2020). The RasGEFs SOS1 and SOS2 are Potential Therapeutic Targets in RAS-Driven Cancers. USU MCB Program Doctoral Dissertation.

Other publications, conference papers and presentations. *Identify any other publications, conference papers and/or presentations not reported above. Specify the status of the publication as noted above. List presentations made during the last year (international, national, local societies, military meetings, etc.). Use an asterisk (*) if presentation produced a manuscript.*

This represents a list of all conference presentations between 07/2018 -06/2019. The publications have been listed above.

1. Sheffels E, Sealover NE, Theard PL, and **Kortum RL**, *"3D culture conditions reveal therapeutic signaling vulnerabilities in RAS-mutant cancer cells"* USUHS Research Days Graduate Student Colloquium, May 2020. Poster presentation.

2. Theard PL and **Kortum RL**, *"Marked Synergy be Bertical Inibition of EGFR signaling in NSCLC Spheroids: SOS1 as a therapeutic target in EGFR-mutated cancer"* USUHS Research Days Graduate Student Colloquium, May 2020. Poster

presentation.

3. Sealover NE, Linke A, Theard PL, Sheffels E, Yohe M, and **Kortum RL**, *"Assessing potential therapeutic approaches in Rhabdomyosarcoma"* USUHS Research Days Graduate Student Colloquium, May 2020. Poster presentation.

4. Pratico D, Theard PL, and **Kortum RL**, *"Investigation of Therapeutic Resistance of EGFR-driven NSCLC Cells Through Imaging and Dose Response Curves"* USUHS Research Days Graduate Student Colloquium, May 2020. Poster presentation.

5. Sheffels E, Sealover NE, Theard PL, and **Kortum RL**, *"3D culture conditions reveal therapeutic signaling vulnerabilities in RAS-mutant cancer cells"* ASCB/EMBO Annual Meeting, Washington D.C., December 2019. Poster presentation.

6. Theard PL and **Kortum RL**, *"SOS1 and SOS2 are therapeutic targets that play unique roles in mutant EGFR-driven NSCLC cells"* ASCB/EMBO Annual Meeting, Washington D.C., December 2019. Poster presentation.

7. Sheffels E, Sealover NE, Theard PL, and **Kortum RL**, *"Anchorage-independent growth conditions reveal a differential SOS2 dependence for transformation and survival in RAS-mutant cancer cells"* 12th Annual Combined Signaling Retreat, NCI, NIH. November 2019. Poster presentation.

8. Theard PL and **Kortum RL**, *"SOS1 and SOS2 are therapeutic targets that play unique roles in mutant EGFR-driven NSCLC cells"* 12th Annual Combined Signaling Retreat, NCI, NIH. November 2019. Poster presentation.

9. Sealover NE, Sheffels E, and **Kortum RL**, *"Toward a comprehensive understanding of how RasGEF-WT RAS signaling influences mutant RAS-driven transformation"* 12th Annual Combined Signaling Retreat, NCI, NIH. November 2019. Poster presentation.

- **Website(s) or other Internet site(s)**
  List the URL for any Internet site(s) that disseminates the results of the research activities. A short description of each site should be provided. It is not necessary to include the publications already specified above in this section.

Not applicable

- **Technologies or techniques**
  Identify technologies or techniques that resulted from the research activities. Describe the technologies or techniques were shared.

The use of 3D spheroid cultures to assess the combined genetic and pharmacologic inhibition of transformation in *EGFR* mutated cells. This technique is in the published *eLife* manuscript. We are currently writing a methods paper using this technique for Bio-Protocols.

- **Inventions, patent applications, and/or licenses**
  Identify inventions, patent applications with date, and/or licenses that have resulted from the research. Submission of this information as part of an interim research performance progress report is not a substitute for any other invention reporting required under the terms and conditions of an award.

  Not applicable.

- **Other Products**
  Identify any other reportable outcomes that were developed under this project. Reportable outcomes are defined as a research result that is or relates to a product, scientific advance, or research tool that makes a meaningful contribution toward the understanding, prevention, diagnosis, prognosis, treatment and /or rehabilitation of a disease, injury or condition, or to improve the quality of life. Examples include:
  - *data or databases;*
  - *physical collections;*
  - *audio or video products;*
  - *software;*
  - *models;*
  - *educational aids or curricula;*
  - *instruments or equipment;*
  - *research material (e.g., Germplasm; cell lines, DNA probes, animal models);*
  - *clinical interventions;*
  - *new business creation; and*
  - *other.*

  Not applicable.

7. PARTICIPANTS & OTHER COLLABORATING ORGANIZATIONS

What individuals have worked on the project?

Provide the following information for: (1) PDs/PIs; and (2) each person who has worked at least one person month per year on the project during the reporting period, regardless of the source of compensation (a person month equals approximately 160 hours of effort). If information is unchanged from a previous submission, provide the name only and indicate "no change".

Name:	Robert Kortum, MD/PhD
Project Role:	PI
Researcher Identifier (e.g. ORCID ID):	
Nearest person month worked:	1.8
Contribution to Project:	Dr. Kortum has performed many of the experiments with graduate students and technicians, and has analyzed all of the data.
Funding Support:	DoD/USU
Name:	Amanda Linke
Project Role:	Technician
Researcher Identifier (e.g. ORCID ID):	
Nearest person month worked:	9
Contribution to Project:	Amanda Linke is supporting both Patricia Theard on Aim 1/EGFR experiments and Nancy Sealover and Erin Sheffels on Aim 2/KRAS experiments. Amanda is an author on the eLife manuscript.
Funding Support:	CDMRP/LC180213
Name:	Nancy Sealover
Project Role:	Graduate Student (former technician)
Researcher Identifier (e.g. ORCID ID):	
Nearest person month worked:	10
Contribution to Project:	Erin Sheffels and Nancy Sealover performed KRAS experiments and assisted with EGFR experiments. Erin is a co-author on both the eLife and Molecular Cell manuscripts.
Funding Support:	CDMRP/LC180213
Name:	Erin Sheffels
Project Role:	Graduate Student
Researcher Identifier (e.g. ORCID ID):	
Nearest person month worked:	11

Contribution to Project:	Erin Sheffels and Nancy Sealover performed KRAS experiments and assisted with EGFR experiments. Nancy is a co-author on both the eLife and Molecular Cell manuscripts.
Funding Support:	HJF Fellowship
Name:	Patricia Theard
Project Role:	MD/PhD Student
Researcher Identifier (e.g. ORCID ID):	
Nearest person month worked:	10
Contribution to Project:	Patricia Theard is performing all of the EGFR experiments with the help of Amanda Linke and Dr. Kortum outlined in Aim 1. Patricia is the first author on the eLife manuscript.
Funding Support:	DoD/USU MD/PhD program

Has there been a change in the active other support of the PD/PI(s) or senior/key personnel since the last reporting period?
If there is nothing significant to report during this reporting period, state "Nothing to Report."

If the active support has changed for the PD/PI(s) or senior/key personnel, then describe what the change has been. Changes may occur, for example, if a previously active grant has closed and/or if a previously pending grant is now active. Annotate this information so it is clear what has changed from the previous submission. Submission of other support information is not necessary for pending changes or for changes in the level of effort for active support reported previously. The awarding agency may require prior written approval if a change in active other support significantly impacts the effort on the project that is the subject of the project report.

Nothing to report

What other organizations were involved as partners?
If there is nothing significant to report during this reporting period, state "Nothing to Report."

Describe partner organizations – academic institutions, other nonprofits, industrial or commercial firms, state or local governments, schools or school systems, or other organizations (foreign or domestic) – that were involved with the project. Partner organizations may have provided financial or in-kind support, supplied facilities or equipment, collaborated in the research, exchanged personnel, or otherwise contributed.

Provide the following information for each partnership:
Organization Name:
Location of Organization: (if foreign location list country)
Partner's contribution to the project (identify one or more)

- *Financial support;*
- *In-kind support (e.g., partner makes software, computers, equipment, etc., available to project staff);*
- *Facilities (e.g., project staff use the partner's facilities for project activities);*
- *Collaboration (e.g., partner's staff work with project staff on the project);*
- *Personnel exchanges (e.g., project staff and/or partner's staff use each other's facilities, work at each other's site); and*
- *Other.*

Nothing to report

8. **SPECIAL REPORTING REQUIREMENTS**

   COLLABORATIVE AWARDS: N/A

   QUAD CHARTS: N/A

9. **APPENDICES:** Please see attached.

Marked Synergy by Vertical Inhibition of EGFR signaling in NSCLC Spheroids: SOS1 as a therapeutic target in EGFR-mutated cancer

Patricia L. Theard[1], Erin Sheffels[1], Nancy E. Sealover[1], Amanda J. Linke[1], David J. Pratico[1], and Robert L. Kortum[1]*

[1]Department of Pharmacology and Molecular Therapeutics, Uniformed Services University of the Health Sciences, Bethesda, MD 20814, USA.

*Corresponding author. Email: robert.kortum@usuhs.edu

Abstract

Drug treatment of 3D cancer spheroids more accurately reflects in vivo therapeutic responses compared to adherent culture studies. In EGFR-mutated lung adenocarcinoma, EGFR-TKIs show enhanced efficacy in spheroid cultures. Simultaneous inhibition of multiple parallel RTKs further enhances EGFR-TKI effectiveness. We show that the common RTK signaling intermediate SOS1 was required for 3D spheroid growth of EGFR-mutated NSCLC cells. Using two distinct measures of pharmacologic synergy, we demonstrated that SOS1 inhibition strongly synergized with EGFR-TKI treatment only in 3D spheroid cultures. Combined EGFR- and SOS1-inhibition markedly inhibited Raf/MEK/ERK and PI3K/AKT signaling. Finally, broad assessment of the pharmacologic landscape of drug-drug interactions downstream of mutated EGFR revealed synergy when combining an EGFR-TKI with inhibitors of proximal signaling intermediates SOS1 and SHP2, but not inhibitors of downstream RAS effector pathways. These data indicate that vertical inhibition of proximal EGFR signaling should be pursued as a potential therapy to treat EGFR-mutated tumors.

Introduction

Lung cancer is the leading cause of cancer-related death worldwide; adenocarcinomas are the most common subtype of lung cancer. Oncogenic driver mutations in the RTK/RAS pathway are found in over 75% of lung adenocarcinomas (*1*). Activating EGFR mutations occur in 10-30% of lung adenocarcinomas, and are the major cause of lung cancer in never-smokers. In patients whose tumors harbor either an L858R mutation or an exon 19 deletion (85% of EGFR mutated tumors), first-generation EGFR-tyrosine kinase inhibitors (TKIs) erlotinib and gefitinib enhance progression free survival (*2-4*). However, resistance to first generation TKI invariably occurs. In most cases, acquired resistance to first generation EGFR-TKIs occurs via either a secondary EGFR 'gatekeeper mutation' (T790M, 50-60% of cases) that renders the receptor insensitive to first generation EGFR-TKIs or oncogenic shift to alternative RTKs (15-30%). To treat patients with T790M-mutated resistant tumors, the third generation EGFR-TKI osimertinib, which selectively targets activating EGFR mutant proteins including T790M but spares wild-type EGFR, was developed (*5, 6*). However, despite further enhancing survival of patients with EGFR-mutant tumors, resistance again emerges.

Unlike first-generation EGFR-TKIs, mechanisms driving osimertinib resistance are more variable, including both EGFR-dependent (10-30%) and EGFR-independent mechanisms (*7-10*). The most common EGFR-independent resistance mechanisms involve reactivation of the RTK/RAS/effector pathway (*10*), often via enhanced signaling through parallel RTKs (*7-9, 11-16*). Here, combining osimertinib with individual RTK inhibitors can both inhibit the development of resistance through the inhibited RTK and kill cancer cells with resistance driven by the specific RTK being inhibited. However, simultaneous inhibition of multiple RTKs with osimertinib may be required to eliminate oncogenic shift to alternative RTKs (*8*). Downstream

of RAS, co-targeting intermediates of the RAF/MEK/ERK and PI3K/AKT pathways enhances of osimertinib effectiveness, however, signaling through the uninhibited effector pathway may drive resistance (*17-20*). Thus, it may be important for therapeutic combinations including osimertinib to stifle all downstream RTK/RAS signaling to be effective.

Recent studies suggest that pharmacologic assessments of targeted therapeutics should be performed under 3D culture conditions rather than in 2D adherent cultures (*21, 22*). 3D spheroids show altered growth characteristics, changes in cell surface proteins, altered metabolism, changes in activation of signaling pathways or altered responses to targeted pathway inhibitors, and are more resistant to drug-induced apoptosis compared to 2D adherent cultures signaling (*23-26*). These differences may be particularly relevant in *EGFR*-mutated NSCLC. *EGFR*-mutated cells show differential RTK expression and phosphorylation in 3D versus 2D conditions (*27*). Further, EGFR-mutated cells respond more robustly to first-generation EGFR-TKIs in 3D cultures, and these responses more closely resemble responses seen *in vivo* (*28*). These data highlight the need for pharmacologic assessment of therapeutics designed to treat *EGFR*-mutated NSCLC under 3D culture conditions.

The ubiquitously expressed RasGEFs (guanine nucleotide exchange factors) SOS1 and SOS2 (son of sevenless 1 and 2) are common signaling intermediates of RTK-mediated RAS activation. Although not initially considered as drug targets because of the low oncogenic potential of SOS (*29*), there has been renewed interest in SOS proteins as therapeutic targets for cancer treatment. We and others have shown that SOS1 and SOS2 may be important therapeutic targets in KRAS-mutated cancer cells (*30-32*), and a specific SOS1 inhibitor (BAY-293) has recently been identified (*33*). Here, we investigate SOS1 and SOS2 as potential therapeutic targets in EGFR-mutated lung adenocarcinoma cells. Using two distinct measures of

pharmacologic synergy, we demonstrate that SOS1 inhibition using BAY-293 synergizes with osimertinib only under 3D spheroid culture conditions, and in doing so add to the growing evidence that pharmacologic assessment of novel therapeutics designed to treat cancer must be performed under 3D culture conditions (*27, 31, 34-36*). By assessing the pharmacologic landscape of EGFR/RAS pathway inhibitors, we demonstrate that inhibition of proximal signaling is required to synergize with osimertinib, and that combined EGFR and SOS1 inhibition synergizes to inhibit RAS effector signaling in 3D culture. These findings have significant therapeutic implications for the development of combination therapies to treat EGFR-mutated lung adenocarcinoma.

Results

SOS1 deletion inhibits transformation in EGFR-mutated NSCLC cells

Previous studies showed that EGFR-mutated NSCLC cell lines show much more robust responsiveness to first generation EGFR-TKIs in 3D culture (monoculture cancer cell line spheroids or monoculture or mixed culture organoids in ECM/Matrigel) compared to 2D adherent culture, and further that 3D conditions more readily mirror EGFR-TKI responses seen *in vivo* (*28*). To confirm these findings and extend them to third generation EGFR-TKIs, we assessed dose-dependent survival of both first-generation EGFR-TKI sensitive (HCC827, exon 19 deletion [Δ*ex*19]) or resistant (NCI-H1975, L858R/T790M) NSCLC cell lines to either gefitinib or osimertinib treatment under both adherent (2D) or spheroid (3D) culture conditions (Fig. 1A). HCC827 and H1975 cells were plated in either adherent or spheroid cultures, allowed to rest for 48 hours, and then treated with increasing doses of either the first-generation EGFR-TKI gefitinib or the third-generation EGFR-TKI osimertinib for four days. HCC827 cells showed responsiveness to both EGFR-TKIs under 2D and 3D culture conditions, however in both cases 3D spheroid cultures showed a > 1-log enhancement in EGFR-TKI efficacy and enhanced overall growth inhibition. While NCI-H1975 cells were not sensitive to gefitinib, osimertinib treatment of H1975 cells showed enhanced efficacy and increased overall growth inhibition in 3D spheroids over 2D adherent cultures.

SOS1 and SOS2 are ubiquitously expressed RasGEFs responsible for transmitting EGFR signaling to downstream effector pathways. To determine whether SOS1 or SOS2 were required for 2D anchorage-dependent proliferation or 3D spheroid growth in EGFR-mutated NSCLC cells, *SOS1* (Figure 1-figure supplement 1 and (*37*)) or *SOS2* (*31*) were deleted in pooled populations of HCC827 and H1975 cells to avoid clonal effects, and both proliferation and

spheroid growth were assessed versus NT controls (Fig. 1B and C). In adherent culture, neither *SOS1* nor *SOS2* deletion altered proliferation (Fig. 1B). In contrast, *SOS1* deletion completely inhibited spheroid growth in both HCC827 and H1975 cells, indicating that SOS1 was required to maintain the transformed phenotype in both cell lines. To determine whether SOS1 was generally required for mutant EGFR-driven transformation, we further deleted *SOS1* or *SOS2* in both first-generation sensitive NCI-H3255 (L858R) and PC9 (Δ*ex*19) cells and in subcultures of these cell lines that had acquired T790M mutations after continuous EGFR-TKI treatment (H3255-TM (*38*) and PC9-TM (*39*)). In all cases, *SOS1* deletion significantly diminished oncogenic transformation, whereas *SOS2* deletion had variable effects on transformation depending on the EGFR mutated cell line examined (Fig. 1D). These data indicate that SOS1 is the major RasGEF responsible for oncogenesis downstream of mutated EGFR.

BAY-293 was recently described as a specific inhibitor for SOS1 (*33*). To determine whether SOS1 inhibition was similarly more effective in 3D spheroids over 2D adherent culture, we assessed dose-dependent survival of H1975 cells after BAY-293 treatment under both 2D and 3D culture conditions (Fig. 1E). Similar to what we observed after either EGFR-TKI treatment (Fig. 1A) or *SOS1* deletion (Fig. 1C and D), BAY-293 showed enhanced efficacy and increased overall growth inhibition in 3D spheroids over 2D adherent cultures. To confirm the specificity of BAY-293 for SOS1, we further treated 3D spheroid cultured H1975, PC9-TM, and H3255-TM cells where either *SOS1* or *SOS2* had been deleted versus NT controls with increasing doses of BAY-293 for four days, and assessed cell viability within the spheroids using Cell Titre Glo (Fig. 1F and Figure 1-figure supplement 2). BAY-293 treatment did not inhibit survival of spheroids where *SOS1* had been deleted, indicating the specificity of BAY-293 for SOS1. Further, cells where *SOS2* had been deleted showed an approximately 1-log enhancement in

BAY-293 efficacy and enhanced overall growth inhibition compared to NT controls, indicating that SOS1 and SOS2 have some overlapping functions in supporting survival of spheroid cultured EGFR-mutated NSCLC cells. For these experiments, the untreated sample cell number at day four of treatment for each cell line (NT, *SOS1* KO, *SOS2* KO) was set to 100%, so differences in transformation (see Fig. 1B-D) will not be appreciated. Further, for NCI-H1915 and NCI-H3255 cells, *SOS1* deletion does not show transformation differences after four days. Overall, these data suggest that EGFR-mutated NSCLC cells are more sensitive to either mutant EGFR or SOS1 inhibition in 3D spheroid culture compared to traditional 2D adherent conditions.

SOS1 inhibition synergizes with EGFR-TKIs to inhibit cell survival under anchorage independent (3D) culture conditions.

Previous studies reported that combining osimertinib with an alternative RTK inhibitor may inhibit or treat the development of resistance driven by that specific RTK (*7*-*9*), whereas simultaneous inhibition of multiple parallel RTKs with osimertinib may be required to effectively potentiate osimertinib action (*8*). Further, while many studies show enhanced drug activity in combination therapies versus osimertinib treatment alone, they do not assess whether the effects of the 2-drug combinations are truly synergistic; synergistic interactions between therapeutics allow for maximization of the therapeutic effect while minimizing adverse events and may be required for effective therapeutic combinations with targeted agents (*40*).

SOS1 is a common downstream mediator of RTK signaling. We hypothesized that SOS1 could be an effective drug target to synergize with EGFR-TKI inhibition to treat EGFR-mutated lung adenocarcinoma. To directly assess synergy between osimertinib and SOS1 inhibition, we use two distinct methods based on the most widely established reference models of drug

additivity. The first method, isobologram analysis, assesses changes in the dose-response curves for mixtures of two drugs compared to sham mixtures of each individual drug with itself. The second method, Bliss independence analysis, assesses whether a mixture of two individual drug doses has a greater effect than would be expected if the two drugs acted independently. We will first describe and then use each method in turn to determine the whether SOS1 inhibition using BAY-293 could synergize with the EGFR-TKI osimertinib in *EGFR*-mutated lung adenocarcinoma cells.

Isobologram analysis is a dose-effect analysis based on the principle of Loewe additivity, which states that a drug mixed with itself, and by extension a mixture of two or more similar drugs, will show additive effects. For two drugs (Drug A and Drug B) that have parallel dose-response curves so that a constant potency ratio is maintained at all doses of A and B (Fig. 2A), treatment using any dose-equivalent (DEQ) mixture of Drugs A and B will show a similar effect to treatment with either Drug A or Drug B alone if the effects of the two drugs are additive. In contrast, if the two drugs show synergism, then the effect seen by treatment with DEQ mixtures of A and B will be greater than the effect for either drug alone. By generating dose-response curves for different DEQ mixtures of Drugs A and B (Fig. 2B), one can compare the EC_{50} of each DEQ mixture to the EC_{50} of Drug A or Drug B alone on an isobologram plot (Fig. 2C). The EC_{50} of each individual drug is plotted as the x- or y-intercept, and the calculated contribution of each drug to the overall EC_{50} for each DEQ mix is plotted as a single point ($EC_{50,A}$, $EC_{50,B}$) on the graph. If the EC_{50} values for each DEQ mix fall along the straight line (isobole) that connects the individual drug EC_{50} values, then the drug-drug interaction is additive. In contrast, points that fall above or below the isobole indicate antagonism or synergy. The extent to which two drugs interact can be further quantified from the EC_{50} data as a combination index (CI) (Fig.

2D). A CI between 0.8-1.2 indicates the two drugs have additive effects when combined, a CI < 0.8 indicates synergy, and a CI > 1.2 indicates antagonism.

To assess drug-drug synergy between osimertinib and BAY-293 via isobologram analysis, NCI-H1975 cells were cultured under 2D adherent or 3D spheroid conditions for 48 hours, and were treated with varying DEQ combinations of osimertinib:BAY-293 (see Fig. 2B) for four days. Cell viability data was assessed using CellTiter-Glo and EC_{50} values from each DEQ mixture were used to generate isobologram plots and calculate combination indices (Fig. 2E). When cells were cultured under 2D conditions, osimertinib and BAY-293 showed additive effects, as DEQ EC_{50} values fell on the isobole and CI values were between 0.8-1.2. In contrast, when cells were cultured as 3D spheroids, osimertinib and BAY-293 showed significant synergy, as DEQ EC_{50} values were well below the isobole and CI < 0.8.

Bliss independence analysis is an effect-based analysis based on the principle of Bliss additivity, which assumes that two drugs will act independently of each other so that their combined effect can be assessed by assessing the effect of each drug sequentially (Fig. 2F). Unlike isobologram analysis, this method does not require that two drugs being assessed have parallel dose-response curves and can be calculated based as few as three drug treatments, the effect each drug has on its own on the cell population, and the effect of combining the two drug treatments together. By representing the effect of each drug treatment as a probabilistic outcome between 0 (no effect) and 1 (100% effect), we can compare the observed effect of the drug-drug combination to the expected effect if each drug acted independently (Fig. 2E). The ratio of the expected effect to the observed effect is the Bliss Index (BI), where a BI < 1 indicates synergy (Fig. 2G). Alternatively, the magnitude of the difference between the observed and expected result can be reported as the excess over Bliss (Fig. 2H). While excess over Bliss is the most

widely reported synergy metric, the Bliss Index can be directly compared with the combination index in isobologram experiments and should be used when both synergy methods are used to assess a given drug-drug interaction.

To assess drug-drug synergy between osimertinib and BAY-293 via Bliss Independence analysis, NCI-H1975 cells were cultured under 2D adherent or 3D spheroid conditions for 48 hours and were treated with increasing doses of BAY-293, osimertinib, or combinations of the two drugs over a 3-log scale for four days. Cell viability was determined using CellTiter-Glo and overall viability (Fig. 2I), Bliss index (Fig. 2J), and excess over Bliss (Fig. 2K) were represented as heat-maps. Similar to what we observed for isobologram analysis, osimertinib and BAY-293 did not show significant synergy in cells cultured under 2D adherent conditions. In contrast, we observed significant synergy between osimertinib and BAY-293, mostly at dose combinations of osimertinib and BAY-293 falling just below the individual drug EC_{50} values. Overall, the data presented in Fig. 2 indicate that osimertinib and BAY-293 show significant drug-drug synergy in EGFR-mutated H1975 cells, but only in 3D spheroid culture conditions.

To determine whether the SOS1 inhibitor BAY-293 could generally synergize with EGFR-TKIs in EGFR-mutated lung adenocarcinoma cells, we extended our assessment of drug-drug synergy to isobologram analysis (Fig. 3) and Bliss independence analysis (Fig. 4) in six different EGFR-mutated lung adenocarcinoma cell lines. In cells that were sensitive to first-generation EGFR-TKIs (HCC827, PC9, H3255; T790 wild-type), we assess drug-drug synergy between BAY-293 and either a first-generation (gefitinib) or third-generation (osimertinib) EGFR-TKI. In cells that were resistant to first-generation EGFR-TKIs (H1975; PC9-TM, H3255-TM; T790M) we limited our assessment to synergy between BAY-293 and osimertinib. To first determine the individual EC_{50} values for gefitinib, osimertinib, and BAY-293 in each

cell line, cells were cultured as 3D spheroids for 48-72 hours, and then treated with increasing doses of drug for four days followed by assessment of cell viability by CellTiter-Glo (Figure 3-figure supplement 1). In five of six cell lines, the individual dose-response curves for BAY-293, osimertinib, and gefitinib (where appropriate) showed similar maximal effects and Hill coefficients, and were thus appropriate for linear isobologram analysis for each 2-drug combination of BAY-293, osimertinib, and gefitinib (*41*). In contrast, H3255-TM cells were only moderately sensitive to osimertinib, showing at most a 50% reduction in viability at high doses. Therefore, we limited our assessment of drug-drug synergy in H3255-TM cells to Bliss independence analysis. Further, to simplify our assessment of Bliss independence across multiple drugs and cell lines, we limited our drug treatments to 1:2, 1:1, and 2:1 mixtures of each drug combination based on dose equivalence (see Fig. 4A).

For each first-generation EGFR-TKI sensitive cell line (HCC827, PC9, H3255), gefitinib and osimertinib did not show any synergy with each other by either isobologram analysis (Fig. 3) or Bliss Independence analysis (Fig. 4), instead showing additive effects (CI and BI ~ 1) as would be expected for two drugs with the same molecular target. In contrast, BAY-293 showed significant synergy with gefitinib and osimertinib by both isobologram analysis (Fig. 3) and Bliss Independence analysis (Fig. 4), suggesting that SOS1 inhibition can act as a secondary treatment for all EGFR-TKIs. Further, in all three T790M mutated cell lines (H1975, PC9-TM, H3255-TM), BAY-293 again showed synergy with osimertinib. These data suggest that combined SOS1 and EGFR inhibition is a robust therapeutic combination that synergize to inhibit EGFR-mutated lung adenocarcinoma cell growth.

Synergy between BAY-293 and osimertinib is independent of SOS2

We showed that *SOS2* deletion sensitized NCI-H1975 cells to the SOS1 inhibitor BAY-293 (Fig 1F). We wanted to determine whether the synergy we observed between EGFR- and SOS1-inhibition (Fig. 3 and 4) was enhanced by *SOS2* deletion in EGFR-mutated NSCLC cell lines. To examine whether SOS2 deletion alters the synergy between osimertinib and BAY-293 in EGFR (T790M) mutated cells , SOS2 was deleted in H1975, PC9-TM, and H3255-TM cells. For H1975 and PC9-TM cells, *SOS2* KO cells vs NT controls were cultured under 3D spheroid conditions for 48-72 hours, and were then treated with varying DEQ combinations of osimertinib:BAY-293 for four days. Cell viability data was assessed using CellTiter-Glo and EC_{50} values from each DEQ mixture were used to generate Isobologram plots and calculate confidence intervals (Fig. 5A and B). For both cell lines, *SOS2* deletion sensitized cells to BAY-293, decreasing EC_{50} by 5-10-fold compared to NT controls without altering the EC50 to osimertinib treatment alone. However, unlike what we observed in the NT control cells, osimertinib and BAY-293 showed only mild synergy in EGFR-mutated cells where *SOS2* was deleted as assessed by the distance of the interaction points to the isobole and the increased combination index vs. NT controls. Further, when we overlaid the NT and *SOS2* KO isobologram plots at two different scales of BAY-293, the drug combination data points were overlapping between NT and *SOS2* KO cells, suggesting that *SOS2* deletion did not enhance synergy between osimertinib and BAY-293.

Since H3255-TM cells are not appropriate for linear isobologram analysis between BAY-293 and osimertinib, we instead performed Bliss independence analysis to assess potential synergy between osimertinib and BAY-293 in the presence or absence of SOS2. H3255-TM cells where *SOS2* had been deleted vs NT controls were cultured under 3D spheroid conditions for 48-72 hours, and were then treated with increasing doses of osimertinib alone, BAY-293

alone, or mixtures of each drug dose at 1:2, 1:1, and 2:1 mixtures of osimertinib and BAY-293 based on dose equivalence for four days. Cell viability data was assessed using CellTiter-Glo, and the Bliss index was calculated for each drug mixture as shown in Fig. 2C and Fig. 4. As was the case in H1975 and PC9-TM cells, while the *SOS2* deletion sensitized H3255-TM cells to BAY-293 we observed less overall synergy between osimertinib and BAY-293 H3255-TM cells where we had deleted *SOS2* vs NT controls. These data suggest that although osimertinib and BAY-293 synergize to limit viability of EGFR-mutated lung adenocarcinoma cells, the synergy between osimertinib and BAY-293 is independent of SOS2.

BAY-293 and osimertinib synergize to inhibit RAS effector signaling

Mutated EGFR signals through downstream RAF/MEK/ERK and PI3K/AKT effector pathways to promote proliferation, transformation, and survival. Since *SOS2* deletion did not further enhance synergy between BAY-293 and osimertinib, we hypothesized that SOS1 inhibition specifically enhanced EGFR-TKI dependent inhibition of downstream signaling in 3D culture. To perform signaling experiments on 3D cultured spheroids, cells were seeded in 24-well micropatterned low-attachment culture plates (Aggrewell, StemCell) containing ~1200 individual spheroids per condition. To determine the extent to which SOS1 inhibition and/or *SOS2* deletion altered osimertinib-dependent inhibition of downstream effector signaling in 3D culture, H1975 or PC9 cells where *SOS2* was deleted vs. NT controls were cultured as spheroids for 48-72 hrs and then treated with increasing doses of osimertinib +/- BAY-293 prior to spheroid collection, lysis, and Western blotting for phosphorylated ERK and AKT (Fig. 6). In both NT and *SOS2* knockout cells, BAY-293 reduced the dose of osimertinib required to inhibit both ERK and AKT phosphorylation (Fig. 6). For Raf/MEK/ERK signaling, Bliss Independence

analysis of pERK quantitation revealed that either SOS1 inhibition or *SOS2* deletion independently synergized with osimertinib to inhibit Raf/MEK/ERK signaling, and the combination of inhibiting SOS1/2 signaling further enhanced this synergy. In contrast, for PI3K/AKT signaling *SOS2* deletion did not enhance the synergy between osimertinib and BAY-293. While either osimertinib treatment or *SOS2* deletion independently synergized with BAY-293 to inhibit AKT phosphorylation, *SOS2* deletion did not further enhance the ability osimertinib to inhibit PI3K/AKT signaling in the presence or absence of BAY-293. These data strongly suggest that vertical inhibition of EGFR and SOS1 limits call viability by inhibiting activation of both RAF/MEK/ERK and PI3K/AKT effector pathways.

Assessment of Inhibitor Landscape in EGFR-mutated cells lines shows synergy upon inhibition of upstream pathway effectors

Since the most common EGFR-independent resistance mechanisms involve reactivation of RTK/RAS/effector pathways (*7-10*), we wanted to assess whether inhibition of different proteins within the EGFR/RAS signaling pathway could synergize to inhibit 3D survival of EGFR (T790M) mutated cancer cells. To determine drug-drug synergies after inhibition of EGFR-RAS pathway signaling at different levels, we assessed synergy between osimertinib, inhibitors of EGFR signaling intermediates upstream of RAS (BAY-293 for SOS1 and RMC-4450 for SHP2), and inhibitors of the Raf/MEK/ERK (trametinib) and PI3K/AKT (buparlisib) pathways (Fig. 7A). H1975 and PC9-TM cells were treated with each individual inhibitor or 1:1 DEQ mixtures of every drug-drug combination, and the combination index was calculated to assess drug-drug synergy. Since H3255-TM cells are not suitable for isobologram analysis, these cells were treated with full-dose mixtures based on dose equivalence and the Bliss Index was calculated for

each drug-drug combination (Fig. 7B). Intriguingly, all three cell lines showed drug-drug synergy with any combination of EGFR, SOS1, and SHP2 inhibition. In contrast, inhibition of downstream Raf/MEK/ERK or PI3K/AKT pathways failed to consistently synergize with either osimertinib or any other inhibitor (Fig. 7B, top). These data support the premise that combined vertical inhibition of proximal EGFR signaling may constitute an effective strategy to treat EGFR-mutated lung adenocarcinomas.

SHP2 is important for the stabilization of the GRB2:SOS1/2 complexes on EGFR (*42*), and the mechanism of allosteric SHP2 inhibitors depends on SOS1 (*43*), although the contribution of SOS2 to SHP2 inhibitors was not assessed. To determine whether *SOS2* deletion altered the spectrum of drug-drug synergies in EGFR-mutated cells, parallel studies were performed in EGFR-mutated cells where *SOS2* was deleted (Fig. 7B, bottom). Unlike what we observed for synergy between EGFR- and SOS1 inhibition, synergy between SOS1 and SHP2 inhibition was enhanced by *SOS2* deletion. These data suggest that SOS2 plays a role in SHP2-dependent signaling. SOS1 inhibition also synergized with MEK inhibition in *SOS2* KO cells. Given the strong synergy between SOS1 inhibition and SOS2 deletion in inhibiting Raf/MEK/ERK signaling (Fig. 6), these data suggest that deep inhibition of MEK signaling is sufficient to inhibit survival in EGFR-mutated cells.

To further evaluate synergy between inhibitors of proximal EGFR signaling, we examined combinations of EGFR- SOS1- and SPH2 inhibition both by expanded evaluation of each 2-drug combination and by assessing whether combined inhibition of EGFR, SOS1, and SHP2 would be more effective than two drug combinations of these inhibitors. To assess each two-drug combination, H1975 cells cultured under 3D spheroid conditions were treated with dose-equivalent combinations of osimertinib, BAY-293, and RMC-4550, assessed for cell

viability, and subjected to isobologram analysis to assess drug-drug synergy. Each two-drug combination showed synergy at three different DEQ ratios (Fig. 7C), suggesting that inhibition of any two proximal signaling proteins may be an effective therapeutic regimen to treat EGFR-mutated cancer. To assess whether adding a third proximal inhibitor to each two-drug combination would further enhance synergistic inhibition of spheroid survival, each 2-drug combination was mixed at 1:1 ratio, and then a third proximal pathway inhibitor was added to give the indicated 3-drug mixtures (Fig. 7D). Isobologram analysis of these three drug mixtures revealed that addition of a third proximal pathway inhibitor to any 2-drug combination of osimertinib, BAY-293, and RMC-4550 further enhanced synergy above what was observed for each 2-drug combination (Fig. 7D) Finally, comparing the combination index for the three-drug combination at a 1:1:1 ratio when each drug is treated independently versus the two-drug combinations showed marked synergy for the three drug combination, but that this synergy was not significantly enhanced compared to the combination of osimertinib and BAY-293 (Fig. 7E). These data indicate that vertical inhibition of proximal EGFR signaling with the combination of osimertinib and a SOS1 inhibitor may be the most the most effective therapeutic combination to treat *EGFR*-mutated NSCLC.

Discussion

Activating *EGFR* mutations are found in 10-15% of lung adenocarcinomas and are the major cause of lung cancer in never smokers. The third-generation EGFR-TKI osimertinib enhances both progression-free (*44*) and overall survival (*45*) compared to first generation EGFR-TKIs and is now considered first-line treatment in EGFR-mutated NSCLC. Osimertinib resistance often develops via activation of parallel RTK pathways (*7-9*), and broad inhibition RTK signaling may enhance osimertinib efficacy and delay therapeutic resistance. Here, we demonstrate that inhibition of the common RTK signaling intermediate SOS1 using BAY-293 showed marked synergy with osimertinib in 3D spheroid-cultured EGFR-mutated NSCLC cells. Our observations that (i) osimertinib–BAY-293 synergy was only observed in 3D spheroids but not in adherent (2D) cultures and (ii) synergy between RTK-signaling intermediates and osimertinib was not broadly applicable to EGFR downstream signaling components but was limited to proteins upstream of RAS reveal novel insights into pharmacologic studies assessing therapeutics designed to treat NSCLC.

While most studies designed to identify or test therapeutic targets to treat cancer are done in 2D adherent culture, a growing body of evidence suggests that pharmacologic assessment of novel therapeutics must be performed in 3D culture systems (*34*). Here, there are many different 3D model systems available that vary in both ease-of-use and complexity of the system. The simplest systems employ non-scaffold-dependent monoculture of cancer cell lines where spheroids are either generated using hanging-drop methodology, magnetic levitation, or using ultra-low attachment plates. More complex systems include embedding spheroids in an extracellular matrix (Matrigel, collagen, gelatin, or a synthetic hydrogel) either as a cancer cell line monoculture or in combination with cancer-derived fibroblasts, or using specialized

microfluidics or culturing cancer-derived organoids. These methods are have been thoroughly reviewed elsewhere (*22*). In the current study, we use ultra-low attachment plates of monoculture NSCLC cell lines as these have the advantage of recapitulating *in vivo* findings while allowing for dose-response studies done at scale (*46*).

In NSCLC, multiple studies have now revealed the importance of 3D culture systems in order to recapitulate *in vivo* findings. *EGFR*-mutated cells show differential RTK expression and phosphorylation in 3D versus 2D conditions (*27*) and respond more robustly to EGFR-TKIs in 3D cultures compared to 2D settings (Fig. 1 and (*28*)); KRAS-mutated cell lines deemed "KRAS-independent" in 2D culture (*47-51*) still require KRAS for anchorage-independent growth (*52-55*), and some $KRAS^{G12C}$-mutated NSCLC cell lines respond to KRAS(G12C) inhibitors in 3D culture and *in vivo* but not in 2D adherent culture (*35*). The relevance of 3D culture systems extends to the identification of novel therapeutic targets and therapeutic combinations. We recently showed that SOS2 is specifically required for PI3K-dependent protection from anoikis in KRAS-mutated NSCLC cells (*32*) and *SOS2* deletion synergizes with MEK inhibition to kill *KRAS* mutated cells only under 3D culture conditions (*31*). Here, we show marked synergy between vertical inhibition of EGFR and SOS1 in *EGFR* mutated cancer cells, but only under 3D culture conditions (Fig. 2). CRISPR screens performed in spheroid cultures of KRAS- and EGFR-mutated NSCLC cell lines more accurately reproduce *in vivo* findings and identify drivers of oncogenic growth compared to screens performed in 2D cultures (*56*). Intriguingly, in this study SOS1 was essential for 3D spheroid survival but not 2D spheroid growth of both EGFR- and KRAS-mutated cells, and a recently accepted publication assessing a novel SOS1 inhibitor showed that it was more effective in 3D compared to 2D culture (*57*). These data are in complete agreement with our data from Fig. 1 showing the requirement for

SOS1 in 3D transformation but not 2D proliferation, and support our conclusion that SOS1 is an important therapeutic target in *EGFR*-mutated NSCLC. We hypothesize the requirement for SOS1 (and SOS2) to promote oncogenic growth in 3D versus proliferation in 2D culture are due to the requirement for PI3K signaling to promote cell survival in 3D but not 2D. Downstream of EGFR activation, the threshold for Raf/MEK/ERK versus PI3K/AKT pathway activation are drastically different, so small amounts of EFGR signaling (in the presence of either SOS1 or SOS2) promote Raf/MEK/ERK signaling, whereas high levels of EGFR signaling are required to activate the PI3K/AKT pathway (*58*). While this hypothesis remains to be tested, we speculate that depending on the specific oncogenic contexts, either SOS1 or SOS2 inhibition will be sufficient to modulate RTK signaling and change the threshold for PI3K signaling, thereby affecting oncogenic growth. These data suggest that future studies assessing novel therapeutics to treat lung adenocarcinomas must be performed in a 3D setting, and that SOS1 and SOS2 might be ubiquitous therapeutic targets in RTK-driven tumors.

Osimertinib resistant can occur via oncogenic shift to alternative RTKs including c-MET (*11*), HER2 and/or HER3 (*7-9*), IGF1R (*12*), and AXL (*13-16*). The variety of RTK bypass pathways that can lead to osimertinib resistance suggests that broad inhibition of RTK signaling may be a more effective therapeutic strategy than any individual RTK inhibitor to limit osimertinib resistance, whereas once resistance via oncogenic shift to an alternative RTK occurs then inhibition of the upregulated RTK would have therapeutic benefit. Toward this end, Phase I and II clinical trials are currently examining whether combining osimertinib with inhibitors of AXL (DS-1205c, NCT03255083) or c-MET (teponitib, NCT03940703; savolitinib, NCT03778229) are effective in patients who have progressed on osimertinib treatment.

Combining osimertinib with a MEK inhibitor can enhance osimertinib efficacy (*10, 17, 20, 59, 60*) and Phase II clinical trials are currently underway to assess combining osimertinib with the MEK inhibitor selumetinib in EGFR-mutated NSCLC (NCT03392246), although resistance to combined osimertinib and MEK inhibition still occurs (*17*). In a recent study designed to understand resistance to combined osimertinib and MEK inhibition, Kurppa et al. (2020) show that combining osimertinib with the MEK inhibitor trametinib results in *EGFR*-mutated cells entering a senescent state that is dependent on the activation of the Hippo pathway effector YAP and its transcription factor binding partner TEAD (*61*). Inhibition of YAP/TEAD signaling overcame this senescence and enhanced killing of EGFR-mutated cells (*61*). EGFR-signaling drives YAP nuclear translocation and transcriptional regulation through PI3K-PDK1 signaling (*62-64*). This suggest that therapeutic combinations able to synergistically inhibit both Raf/MEK/ERK and PI3K/AKT effector signaling should overcome YAP-dependent senescence and treat *EGFR*-mutated NSCLC.

Here, we show that osimertinib does not broadly synergize with inhibitors of downstream EGFR/RAS/RAS effector signaling. Instead, we found that synergy was limited to combinations of osimertinib with inhibitors of proximal EGFR signaling intermediates SOS1 and SHP2 (Fig. 7). Further, SOS1 inhibition significantly enhanced osimertinib-dependent inhibition of both Raf/MEK/ERK and PI3K/AKT signaling (Fig. 6), whereas inhibition of individual downstream Raf/MEK/ERK or PI3K/AKT effector pathways did not synergize with osimertinib (Fig. 7) to inhibit 3D spheroid growth. We hypothesize that these two findings are inexorably linked, so that any potential therapeutic must synergize with osimertinib to inhibit all downstream RAS effector signaling to show drug-drug synergy in 3D culture. In support of this idea, previous studies showed inhibition of SRC family kinases (SFK) potentiated osimertinib to a much greater

extent than either MEK or PI3K inhibition (*20*), and that SFK inhibition synergized with osimertinib to inhibit both Raf/MEK/ERK and PI3K/AKT signaling (*20, 65*).

There remain several open questions regarding SOS1 inhibition as a therapeutic strategy to limit osimertinib resistance. First, does SOS1 inhibition enhance osimertinib efficacy *in vivo* using xenograft studies? While BAY-293 shows tremendous specificity toward SOS1 (Fig. 1, Fig. S2, and (*33*)) and is a very useful tool compound for *in vitro* studies, it has limited bioavailability making it unsuitable for *in vivo* use. Thus, new SOS1 inhibitors that can be used *in vivo* are needed to move SOS1 forward as a therapeutic target. Intriguingly, while this paper was under review Boehringer Ingelheim reported two orally available SOS1 inhibitors suitable for in vivo studies (*57*). They found that SOS1 inhibition could overcome MEK inhibitor resistance in *KRAS*-mutated cell lines and that the combination of SOS1 and MEK inhibition showed marked show efficacy in *KRAS*-mutated cell lines and xenograft models. They are now moving one of these compounds into Phase I safety trials for *KRAS* mutated solid tumors (BI-1701963, NCT04111458). It will be exciting to assess whether these new SOS1 inhibitors work in combination with osimertinib to limit the growth *EGFR*-mutated tumors. Further, these studies will be necessary to translate SOS1-targeted therapies for use in *EGFR*-mutated lung adenocarcinoma. Second, does SOS1 inhibition actually limit the development of osimertinib resistance? While outside the scope of the current paper, it will be intriguing to use in vitro models of EGFR-TKI resistance (*17*) to assess whether SOS1 inhibition can block the development of osimertinib resistance. Third, while we have focused on the RAF/MEK/ERK and PI3K/AKT effector pathways as the major contributors to mutant *EGFR*-driven NSCLC, there are many different effector pathways downstream of RAS that may be SOS1-dependent and contribute to the oncogenic phenotype. Here, and unbiased approach at understanding the

individual and combined effects of osimertinib and SOS1 inhibition on RAS activation (to validate relatively new SOS1 inhibitors) and RAS effector signaling would provide valuable insight into how these therapies alter EGFR-driven signaling in NSCLC.

Overall, our data suggest that inhibitors of proximal signaling may be the most efficacious therapeutics to combine with osimertinib to treat EGFR-mutated tumors. Toward this end, Phase I trials are currently underway assessing the combination of osimertinib and the SRC inhibitor dasatinib (NCT02954523) in *EGFR*-mutated NSCLC, and recently developed SOS1 (BI-1701963, NCT04111458) and SHP2 (JAB-3068, NCT03565003; RMC-4630, NCT03634982) inhibitors have entered Phase I safety trials. Our study provides a framework for the systematic, preclinical assessment of therapeutic combinations designed to treat EGFR-mutated cancer cells. We show both how to use basic pharmacologic principles to assess drug-drug synergy and that these combinations must be assessed under 3D culture conditions. Using this framework, we show that the combination of osimertinib and the SOS1 inhibitor BAY-293 shows marked efficacy in 3D spheroid culture and should be pursued as a therapeutic option to treat EGFR-mutated lung adenocarcinoma.

Acknowledgments:

We thank Udayan Guha for NCI-H1975, HCC827, PC9, H3255 and H3255-TM cells and for helpful discussions throughout the project. We thank Julian Downward for PC9-TM cells.

Funding: This work was supported by grants from the Congressionally Directed Medical Research Program to R.L.K. (LC160222 and LC180213). **Competing interests**: The authors declare they have no competing interests. **Data and materials availability**: All data needed to evaluate the conclusions in the paper are present in the paper or the Supplementary Materials. Materials are available upon request from R.L.K.

Materials and Methods

Key Resources Table				
Reagent type (species) or resource	**Designation**	**Source or reference**	**Identifiers**	**Additional information**
cell line (*Homo-sapiens*)	Lung; adenocarcinoma; non-small cell lung cancer	Obtained from Udayan Guha, available at ATCC	NCI-H1975 CRL-5908 RRID:CVCL_UE30	
cell line (*Homo-sapiens*)	Lung; adenocarcinoma; epithelial	Obtained from Udayan Guha, available at ATCC	HCC827 CRL-2868 **RRID:CVCL_DH92**	
cell line (*Homo-sapiens*)	Lung; adenocarcinoma; non-small cell lung cancer	Obtained from Udayan Guha, available at NCI-DTP or ATCC	**NCI-H3255 CRL-2882NCI-DTP Cat# NCI-H3255, RRID:CVCL_6831**	
cell line (*Homo-sapiens*)	Lung; adenocarcinoma; non-small cell lung cancer	(*38*)	NCI-H3255TM	
cell line (*Homo-sapiens*)	Dermal fibroblast (normal, Adult)	Obtained from Udayan Guha, available at Millipore Sigma or BCRJ	PC9 #90071810 **BCRJ Cat# 0331, RRID:CVCL_B260**	
cell line (*Homo-sapiens*)	Lung; adenocarcinoma; non-small cell lung cancer	(*39*)	PC9-TM	

cell line (*Homo-sapiens*)	Kidney; epithelial fibroblast (fetus)	ATCC	HEK-293T ATCC Cat# CRL-3216, RRID:CVCL_0063	
Other	TransIT-Lenti	Mirus	Catalogue # MIR 6605	Lentiviral transduction reagent
Other	MISSION Lentiviral packaging mix	Millipore Sigma	Catalogue # SHP001	
Other	Bovine Serum Albumin	Millipore Sigma	Catalogue # A8022	Cell culture reagent for ACL-4 media
Other	apo-Transferrin (human)	Millipore Sigma	Catalogue # T5391	Cell culture reagent for ACL-4 media
Other	Sodium Selenite	Millipore Sigma	Catalogue # S9133	Cell culture reagent for ACL-4 media
Other	Hydrocortisone	Millipore Sigma	Catalogue # H0135	Cell culture reagent for ACL-4 media
Other	Ethanolamine	Millipore Sigma	Catalogue # E0135	Cell culture reagent for ACL-4 media
Other	O-Phosphorylethanolamine	Millipore Sigma	Catalogue # P0503	Cell culture reagent for ACL-4 media

Other	3,3',5-Triiodo-L-thyronine [T3]	Millipore Sigma	Catalogue # T5516	Cell culture reagent for ACL-4 media
Other	Sodium Pyruvate	Millipore Sigma	Catalogue # P4562	Cell culture reagent for ACL-4 media
Other	HEPES	Invitrogen	Catalogue # 15630-080	Cell culture reagent for ACL-4 media
Other	Epidermal Growth Factor [EGF]	Millipore Sigma	Catalogue # E4127	Cell culture reagent for ACL-4 media
Other	Recombinant Human Insulin	Millipore Sigma	Catalogue # I9278	Cell culture reagent for ACL-4 media
Other	AggreWell 400 low-attachment culture plates	Stem Cell	Catalogue # 34415	
Other	ultra-low attachment 96-well round bottomed plates	Corning Corstar	Catalogue # 7007	
Other	Nunc Nucleon Sphera microplates	ThermoFisher	Catalogue # 174929	
Other	coated 96-well white-walled	Perken Elmer	Catalogue # 6005688	

	CulturePlates			
antibody	anti-Sos 1 Antibody (C-23): sc-256, rabbit polyclonal	Santa Cruz	sc-256	(1:500)
antibody	anti-SOS2 antibody (C-19): sc-258, rabbit polyclonal	Santa Cruz	sc-258	(1:500)
antibody	anti-β-actin antibody AC15, mouse monoclonal	Millipore Sigma	#A1978	(1:5000)
antibody	anti-Phospho-EGF Receptor (Tyr1068) (D7A5) XP® Rabbit mAb #3777	Cell Signaling Technology	#3777	(1:1000)
antibody	anti-phospho p44/42 MAPK (Erk1/2) (Thr202/Tyr204) (D13.14.4E) XP® Rabbit mAb #4370	Cell Signaling Technology	#4370	(1:1000)
antibody	anti-p44/42 MAPK (Erk1/2) (L34F12) Mouse mAb #4696	Cell Signaling Technology	#4696	(1:1000)
antibody	anti- Phospho-Akt (Ser473) (D9E) XP® Rabbit mAb #4060	Cell Signaling Technology	#4060	(1:1000)
antibody	anti- Akt (pan) (40D4) Mouse mAb #2920	Cell Signaling Technology	#2920	(1:1000)

antibody	anti-HSP 90α/β Antibody (H-114): sc-7947	Santa Cruz	#sc-7947	(1:1000)
antibody	anti-EGF Receptor (D38B1) XP® Rabbit mAb #4267	Cell Signaling Technology	#4267	(1:1000)
Recombinant DNA Reagent	pLentiCrispr v2	(*66*)		
Other	CellTiter-Glo® 2.0	Promega	G9243	
Recombinant DNA reagent	pLentiCrispr. NT	(*31*)	NT	sgRNA: CCATATCGGGGCGAGACATG
Recombinant DNA reagent	pLentiCrispr. SOS2-9	(*31*)	SOS2-9	sgRNA: GAGAACAGTCCGAAATGGCG
Recombinant DNA reagent	pLentiCrispr. SOS1-1	This manuscript	SOS1-1	sgRNA: GGGCAGCTGCTGCGCCTGCA
Recombinant DNA reagent	pLentiCrispr. SOS1-2	This manuscript	SOS1-2	sgRNA: GCATCCTTTCCAGTGTACTC
Recombinant DNA reagent	pLentiCrispr. SOS1-3	This manuscript	SOS1-3	sgRNA: TATTCTGCATTGCTAGCACC
Recombinant DNA reagent	pLentiCrispr. SOS1-4	This manuscript	SOS1-4	sgRNA: AGTGGCATATAAGCAGACCT

Recombinant DNA reagent	pLentiCrispr. SOS1-5	This manuscript	SOS1-5	sgRNA: ATTGCAAGA GACAATGGA CC
Recombinant DNA reagent	pLentiCrispr. SOS1-6	This manuscript	SOS1-6	sgRNA: GCTTATATG CCACTCAAC TG
Recombinant DNA reagent	pLentiCrispr. SOS1-7	This manuscript	SOS1-7	sgRNA: GAAGGAACT CTTACACGT GT
Recombinant DNA reagent	pLentiCrispr. SOS1-8	This manuscript	SOS1-8	sgRNA: CTATTGGGT GTAAGGTGA GC

Cell culture. Cell lines were cultured at 37°C and 5% CO_2. HCC827, NCI-H1975, PC9, and PC9-TM cells were maintained in Roswell Park Memorial Institute medium (RPMI), each supplemented with 10% fetal bovine serum and 1% penicillin-streptomycin. Cell lines were authenticated by STR profiling and confirmed as mycoplasma negative. EGFR mutations were confirmed by Sanger sequencing. H3255 and H3255-TM were maintained in ACL4 medium formulated in DMEM:F-12 including: Bovine Serum Albumin 0.5% (w/v) (Sigma cat no. A8022), apo-Transferrin (human) (Sigma cat no. T5391) 0.01 mg/mL, Sodium Selenite (Sigma cat no. S9133) 25nM, Hydrocortisone (Sigma cat no. H0135) 50nM, Ethanolamine (Sigma cat no. E0135) 0.01mM, O-Phosphorylethanolamine (Sigma cat no. P0503) 0.01mM, 3,3',5-Triiodo-L-thyronine [T3] (Sigma cat no. T5516) 100pM, Sodium Pyruvate (Sigma cat no. P4562), HEPES (Invitrogen cat no 15630-080) 10mM, Epidermal Growth Factor [EGF] 1ng/mL, Recombinant Human Insulin (Sigma cat no. I9278) 0.02mg/mL, and 1% penicillin-streptomycin.

For signaling experiments, cells were seeded in 24-well micropatterned AggreWell 400 low-attachment culture plates (Stem Cell # 34415) at 1.2×10^6 cells/well in 2 mL of medium. 24 h post-plating, half of the media was carefully replaced with fresh media to not disturb the spheroids. At 48 hours, 1 mL media was removed and replaced with 2 x inhibitor. Cells were treated with inhibitor for 6 hrs and then collected for cell lysis and western blot analysis.

Cell lysis and Western blot analysis. Cells were lysed in RIPA buffer (1% NP-40, 0.1% SDS, 0.1% Na-deoxycholate, 10% glycerol, 0.137 M NaCl, 20 mM Tris pH [8.0], protease (Biotool #B14002) and phosphatase (Biotool #B15002) inhibitor cocktails) for 20 minutes at 4°C and spun at 10,000 RPM for 10 minutes. Clarified lysates were boiled in SDS sample buffer containing 100 mM DTT for 10 minutes prior to Western blotting. Proteins were resolved by sodium dodecyl sulfate-polyacrylamide (Criterion TGX precast) gel electrophoresis and transferred to nitrocellulose membranes. Western blots were developed by multiplex Western blotting using anti-SOS1 (Santa Cruz sc-256; 1:500), anti-SOS2 (Santa Cruz sc-258; 1:500), anti-β-actin (Sigma AC-15; 1:5,000), anti-pEGFR (Cell Signaling 3777; 1:1000), anti-EGFR (Cell Signaling 4267; 1:1000), anti-pERK1/2 (Cell Signaling 4370; 1:1,000), anti-ERK1/2 (Cell Signaling 4696; 1:1000), anti-pAKT Ser^{473} [Cell Signaling 4060; 1:1000]), anti-AKT (Cell Signaling 2920; 1:1000), anti-HSP90 (Santa Crux sc-7947, 1:1000), primary antibodies. Anti-mouse and anti-rabbit secondary antibodies conjugated to IRDye680 or IRDye800 (LI-COR; 1:10,000) were used to probe primary antibodies. Western blot protein bands were detected and quantified using the Odyssey system (LI-COR). For quantification of SOS1 and SOS2 abundance, samples were normalized to either β-actin or HSP90. For quantification of pERK

and pAKT, samples were normalized to a weighted average of HSP90, β-actin, total ERK1/2, total AKT, and total EGFR (*67*).

Proliferation Studies. For 2D proliferation assays, 5×10^2 cells were seeded on cell culture-coated 96-well white-walled CulturePlates (Perkin Elmer #6005688). Cells were lysed with CellTiter-Glo® 2.0 Reagent (Promega), and luminescence was read using a Bio-Tek Cytation 5 multi-mode plate reader. Cell number was assessed 24 hours after plating to account for any discrepancies in plating (Day 1), and then on days 3, 5, and 7. Data were analyzed as an increase in luminescence over Day 1.

Transformation Studies. H3255 and H3255-TM cells were seeded in 0.32% Nobel agar at 2×10^4 cells per 35-mm dish to assess anchorage-independent. Soft agar colonies were counted 28 days after seeding. For all other cell lines spheroid growth assessed in ultra-low attachment 96-well round bottomed plates (Corning Costar #7007), cells were seeded at 500 cells per well. Images were taken 24 hours after plating to assess initial spheroid size, and then 7, 14, and 21 days later to assess transformation. Cell number was assessed in parallel plates at 0, 7, 14, and 21 days using CellTiter-Glo® 2.0 reagent.

sgRNA studies. A non-targeting (NT) single guide RNA (sgRNA), a SOS2-targeted sgRNA (*31*), and 8 potential SOS1-targeted sgRNAs previously used to target SOS1 in a genome-wide CRISPR screen (*37*) were each cloned into pLentiCRISPRv2 as previously described (*66*). SOS1-2 was chosen as the SOS1 sgRNA for the study, and SOS2-9 was chosen as previously

described (*31*). For studies in Fig. 1, cells were infected lentivirus to express the given sgRNA with Cas9, and cells were selected for 10 days with puromycin prior to Western blotting. Cell lysates were probed for SOS1 or SOS2, and only cell populations showing grater that 80% SOS deletion within the overall population were used. Importantly, cell clones were not used, rather cell populations where >80% of cells showed SOS deletion were used to minimize clonal effects. Independent infections were used for each experiment.

construct	sgRNA
NT	CCATATCGGGGCGAGACATG
SOS2-9	GAGAACAGTCCGAAATGGCG
SOS1-1	GGGCAGCTGCTGCGCCTGCA
SOS1-2	GCATCCTTTCCAGTGTACTC
SOS1-3	TATTCTGCATTGCTAGCACC
SOS1-4	AGTGGCATATAAGCAGACCT
SOS1-5	ATTGCAAGAGACAATGGACC
SOS1-6	GCTTATATGCCACTCAACTG
SOS1-7	GAAGGAACTCTTACACGTGT
SOS1-8	CTATTGGGTGTAAGGTGAGC

Production of recombinant lentiviruses. Lentiviruses were produced by co-transfecting MISSION lentiviral packaging mix (Sigma) into 293T cells using Mirus *Trans*IT®-Lenti transfection reagent (Mirus Bio # MIR6605) in Opti-MEM (Thermo Scientific #31-985-062). At 48 h post-transfection, viral supernatants were collected and filtered. Viral supernatants were then either stored at −80°C or used immediately to infect cells in combination with polybrene at 8 μg/mL. 48 hours post-infection, cells were selected in 4 μg/mL Puromycin (Invitrogen). Twelve days after selection, cells were analyzed for SOS1 and SOS2 expression and plated for proliferation and transformation assays.

Inhibitor Studies

- 2D adherent studies – Cells were seeded at 500-1,000 cells per well in 100 μL in the inner-60 wells of 96-well white-walled culture plates (Perkin Elmer) and allowed to

attach for 48 hours prior to drug treatment. Cells were treated with drug for 72 hours prior to assessment of cell viability using CellTiter-Glo® 2.0.

- 3D adherent studies – Cells were seeded at 500-1,000 cells per well in 100 μL in the inner-60 wells of 96-well ultra-low attachment round bottomed plates (Corning #7007) or Nunc Nucleon Sphera microplates (ThermoFisher # 174929) and allowed to coalesce as spheroids for 48-72 hours prior to drug treatment. Cells were treated with drug for 96 hours prior to assessment of cell viability using CellTiter-Glo® 2.0.

For all studies, outer wells (rows A and H, columns 1 and 12) were filled with 200 μL of PBS to buffer inner cells from temperature and humidity fluctuations. Triplicate wells of cells were then treated with increasing concentrations 100 μL of 2× inhibitor at either a semilog (single drug dose response curves to determine EC_{50}) or a 1/3-log scale (isobologram and Bliss independence experiments) for 72 (adherent cultures) or 96 (spheroids) hours. Cell viability was assessed using CellTiter-Glo® 2.0 (30 μL/well). Luminescence was assessed using a Bio-Tek Cytation 5 multi-mode plate reader. Data were normalized to the maximum luminescence reading of untreated cells, and individual drug EC_{50} values were calculated using Prism 8 by non-linear regression using log(inhibitor) vs. response with a variable slope (four parameters) to assess for differences in the Hill Coefficient between different drug treatments. For all drug-treatment studies, the untreated sample for each cell line was set to 100%. This would mask any differences in 3D cell proliferation seen between cell lines.

Isobologram Analysis

Dose equivalence was first determined by assessing individual-drug EC_{50} values; individual-drug Hill Coefficients were determined to assure that the two drugs could be assessed for synergy by

Lowe additivity. To generate dose-equivalent dose-response curves, the dose for each drug closest to the EC_{50} on a 1/3-log scale was set as equivalent, and 10-point dose response curves were generated for each individual drug on either side of the equivalent dose to ensure the top (no drug effect) and bottom (maximal drug effect) were represented on the dose-response curve. 100 μL of drug each drug dose was added as outlined above. To generate dose-equivalent mixtures for isobologram analysis, equivalent doses of the two drugs were mixed at different ratios so that the total dose (100 μL) would be expected to have an equivalent effect on the cells if the two drugs were additive. Drugs were mixed at either five (4:1, 2:1, 1:1, 1:2, and 1:4) or three (2:1, 1:1, and 1:2) different drug mixtures depending on the experiment. Cells were treated and EC_{50} values for each individual drug or drug mixture based on each drug's dosing were determined for as outlined above. To generate an isobologram plot, the EC_{50} of each individual drug was plotted as the x- or y-intercept, and the calculated contribution of each drug to the overall EC_{50} for each DEQ mix is plotted as a single point ($EC_{50,A}$, $EC_{50,B}$) on the graph.

$$\text{Combination Index} = \frac{EC_{50}\,A_{mix}}{EC_{50}\,A_{alone}} + \frac{EC_{50}\,B_{mix}}{EC_{50}\,B_{alone}}$$

To calculate the combination index for each dose equivalent mixture, the calculated contribution of each drug to the overall EC_{50} were used in the equation:

As an example, we will show data for one trial analyzing the combination of osimertinib and BAY-293 in 3D spheroid cultured H1975 cells in Fig. 2B. The EC_{50} values for each individual drug were first determined: -8.57 for osimertinib and -5.73 for BAY-293. Based on these EC_{50} values, the dose equivalence was set at -8.67 for osimertinib -5.67 for BAY-293 (**approximated EC_{50} for each drug in bold**), and the following 10-point dose response curves were generated:

osimertinib	-11	-10.67	-10.33	-10	-9.67	-9.33	-9	**-8.67**	-8.33	-8
BAY-293	-8	-7.67	-7.33	-7	-6.67	-6.33	-6	**-5.67**	-5.33	-5

Cells were then treated with the following volumes of each drug to generate seven dose-equivalent dose response curves:

		4:1 mixture	2:1 mixture	1:1 mixture	1:2 mixture	1:4 mixture	
osimertinib	100 μL	80 μL	66 μL	50 μL	34 μL	20 μL	0 μL
BAY-293	0 μL	20 μL	34 μL	50 μL	66 μL	80 μL	100 μL

EC_{50} values for each dose-response curve were then determined based on each drug's dosing:

	OSM alone	4:1 mixture	2:1 mixture	1:1 mixture	1:2 mixture	1:4 mixture	BAY alone
osimertinib EC_{50} (nM)	2.62	0.84	0.70	0.92	1.49	1.19	2.40
BAY-293 EC_{50} (μM)	2.14	1.01	0.83	1.09	1.49	1.04	1.82

EC_{50} values were then adjusted based on the amount of each drug that was put in the mixture to determine the contribution of each drug in the mixture to the overall EC_{50}. For example, the 4:1 mixture was 80% osimertinib, so the osimertinib EC50 for that mixture is multiplied by 0.8. The corresponding corrected EC_{50} values and combination indices were:

	OSM alone	4:1 mixture	2:1 mixture	1:1 mixture	1:2 mixture	1:4 mixture	BAY alone
osimertinib EC_{50} (nM)	2.62	0.67	0.45	0.46	0.52	0.24	0
BAY-293 EC_{50} (μM)	0	0.20	0.29	0.54	0.97	0.84	1.82
Combination Index		0.40	0.34	0.44	0.65	0.46	

Bliss Independence Analysis

Unlike Isobologram analysis, individual drug doses are not reduced for drug-drug combinations when performing Bliss independence analysis. For data in Fig. 2, wells were treated with a full dose of each individual drug or drug combination in a 10 × 10 matrix of dose

combinations for osimertinib and BAY-293 on a 1/3-log scale. Data were normalized to the maximum luminescence reading of untreated cells, and a heat-map depicting cell viability was generated using Prism 8. The Bliss index was calculated by first converting viability (on a scale of 0 to 1) for each treatment to the effect of each drug or drug combination, where 0 represents no effect and 1 represents 100% effect (no viable cells).

$$\text{effect} = 1 - \text{viability}$$

From the effect data, the expected effect for each drug combination is calculated:

$$\text{Expected effect} = E_A + E_B * (1 - E_A)$$

$$\text{Expected effect} = E_A + E_B - E_A * E_B$$

The Bliss Index is the ratio of the expected effect / actual effect:

$$\text{Bliss Index} = (\text{expected effect}) / (\text{actual effect})$$

$$\text{Bliss Index} = (E_A + E_B - E_A * E_B) / (E_{A+B\ MIX})$$

A Bliss Index of 1 indicates that the actual and expected effects are equivalent, and the effects of the two drugs are additive. Bliss Index < 1 indicates increasing synergy, whereas Bliss Index >1 indicates antagonism.

Excess over Bliss is calculated by determining how much greater the actual effect of the drug combination is versus the expected effect, and is calculated as:

$$\text{Excess over Bliss} = 100 * [\text{actual effect} - \text{expected effect}]$$

$$\text{Excess over Bliss} = 100 * [\ E_{A+B\ MIX} - (E_A + E_B - E_A * E_B)\ ]$$

An excess over Bliss of 0 indicates that the actual and expected effects are equivalent, and the effects of the two drugs are additive; values > 0 indicate increasing synergy, whereas values < 0 indicate antagonism.

Since synergy occurred at drug combinations at or just below the EC_{50} values for each individual drug, Bliss experiments in Figs. 4 and 5, drug mixtures were limited to 3 × 10 drug mixtures based on dose equivalence with mixtures at approximately 2:1, 1:1, and 1:2 mixes of the two drugs based on dose equivalence. Here, the doses used for one drug were held constant, and the second drug dose wash shifted by 1/3 log up or down to generate 2:1 and 1:2 mixtures. For example, for the combination of osimertinib and BAY-293 in H1975 cells, the following drug doses were used:

Osimertinib (1:2 ratio of OSM:BAY)	-11.33	-11	-10.67	-10.33	-10	-9.67	-9.33	-9	-8.67	-8.33
Osimertinib (1:1 ratio of OSM:BAY)	-11	-10.67	-10.33	-10	-9.67	-9.33	-9	-8.67	-8.33	-8
Osimertinib (2:1 ratio of OSM:BAY)	-10.67	-10.33	-10	-9.67	-9.33	-9	-8.67	-8.33	-8	-7.67
BAY-293 (constant)	-8	-7.67	-7.33	-7	-6.67	-6.33	-6	-5.67	-5.33	-5

3-drug Isobologram analysis

For three-drug isobologram studies with osimertinib (EC_{50} = -8.57), BAY-293 (EC_{50} = -5.74), and RCM-4550 (EC_{50} = -6.84), drugs were again mixed based on dose equivalency. The dose-equivalent 10-point dose-response curves for these drugs in 3D cultured H1975 cells were (**approximated EC_{50} for each drug in bold**):

osimertinib	-11	-10.67	-10.33	-10	-9.67	-9.33	-9	**-8.67**	-8.33	-8
BAY-293	-8	-7.67	-7.33	-7	-6.67	-6.33	-6	**-5.67**	-5.33	-5
RMC-4550	-9	**-8.67**	-8.33	-8	-7.67	-7.33	-7	**-6.67**	-6.33	-6

Each two-drug combination was set as a single "drug mixture" at a 1:1 ratio, and the third drug was combined with this drug mixture at 2:1, 1:1, and 1:2 drug ratios. To generate the proper two and three-drug mixtures for analysis, 21 total dose response curves were generated. The five dose-response curves on the right represent the mixtures used to generate the isobologram plots in Fig. 7D. The other two two-drug mixtures in **bold** (2-drug 2:1 and 1:2 mixtures) were used to generate the isobologram plots in Fig. 7CCombination indices were calculated based on whether addition of the third drug to each 2-drug 1:1 mixture further enhanced synergy when added to the two-drug mixture.

[osimertinib:BAY-293] mixture vs. RCM-4550

	OSM:BAY 2:1	**OSM:BAY 1:2**	OSM:BAY 1:1	(1+1):1 2:1 mixture	(1+1):2 1:1 mixture	(1+1):4 1:2 mixture	RCM alone
osimertinib	**66 µL**	**34 µL**	50 µL	33 µL	25 µL	17 µL	0 µL
BAY-293	**34 µL**	**66 µL**	50 µL	33 µL	25 µL	17 µL	0 µL
RMC-4550	**0 µL**	**0 µL**	0 µL	34 µL	50 µL	66 µL	100 µL

$$\text{Combination Index} = \frac{EC_{50}\ \text{OSM+BAY}_{\text{3-drug mix}}}{EC_{50}\ \text{OSM+BAY}_{50:50}} + \frac{EC_{50}\ \text{RCM}_{\text{3-drug mix}}}{EC_{50}\ \text{RCM}_{\text{alone}}}$$

[osimertinib:RCM-4550] mixture vs. BAY-293:

	OSM:RCM 2:1	**OSM:RCM 1:2**	OSM:RCM 1:1	(1+1):1 2:1 mixture	(1+1):2 1:1 mixture	(1+1):4 1:2 mixture	RCM alone
osimertinib	**66 µL**	**34 µL**	50 µL	33 µL	25 µL	17 µL	0 µL
BAY-293	**0 µL**	**0 µL**	0 µL	34 µL	50 µL	66 µL	100 µL
RMC-4550	**34 µL**	**66 µL**	50 µL	33 µL	25 µL	17 µL	0 µL

$$\text{Combination Index} = \frac{EC_{50}\ \text{OSM+RCM}_{\text{3-drug mix}}}{EC_{50}\ \text{OSM+RCM}_{50:50}} + \frac{EC_{50}\ \text{BAY}_{\text{3-drug mix}}}{EC_{50}\ \text{BAY}_{\text{alone}}}$$

[BAY-293:RCM-4550] mixture vs. osimertinib

	BAY:RCM 2:1	**BAY:RCM 1:2**	BAY:RCM 1:1	(1+1):1 2:1 mixture	(1+1):2 1:1 mixture	(1+1):4 1:2 mixture	RCM alone
osimertinib	**0 µL**	**0 µL**	0 µL	34 µL	50 µL	66 µL	100 µL
BAY-293	**66 µL**	**34 µL**	50 µL	33 µL	25 µL	17 µL	0 µL
RMC-4550	**34 µL**	**66 µL**	50 µL	33 µL	25 µL	17 µL	0 µL

$$\text{Combination Index} = \frac{EC_{50}\ \text{BAY+RCM}_{\text{3-drug mix}}}{EC_{50}\ \text{BAY+RCM}_{50:50}} + \frac{EC_{50}\ \text{OSM}_{\text{3-drug mix}}}{EC_{50}\ \text{OSM}_{\text{alone}}}$$

To calculate the three-drug combination index where each drug was considered independently (Fig. 7E), the following equation was used:

$$\text{Combination Index} = \frac{EC_{50}\ \text{OSM}_{\text{3-drug mix}}}{EC_{50}\ \text{OSM}_{\text{alone}}} + \frac{EC_{50}\ \text{BAY}_{\text{3-drug mix}}}{EC_{50}\ \text{BAY}_{\text{alone}}} + \frac{EC_{50}\ \text{RCM}_{\text{3-drug mix}}}{EC_{50}\ \text{RCM}_{\text{alone}}}$$

Figure legends

Figure 1. *SOS1* deletion inhibits anchorage-dependent (3D) transformation in EGFR-mutated NSCLC cell lines.
(A) Dose-response curves of EGFR-mutated HCC827 (Δex19) (left) or NCI-H1975 (L858R/T790M) (right) cells treated with gefitinib or osimertinib under 2D anchorage-dependent (gray diamonds) or 3D spheroid (black squares) culture conditions.
(B-C) 2D proliferation (left) or 3D spheroid growth (right) in pooled populations of **(B)** HCC827 or **(C)** NCI-H1975 cells where *SOS1* or *SOS2* has been deleted using CRISPR/Cas9 vs NT controls. 10x images of representative spheroids at day 0 and 21 are shown, scale bar=250 mm.
(D) 3D transformation in pooled populations of the indicated EGFR-mutated NSCLC cell lines where *SOS1* or *SOS2* has been deleted using CRISPR/Cas9 vs NT controls.
(E) Dose-response curve cells of NCI-H1975 cells treated with the SOS1 inhibitor BAY-293 under 2D anchorage-dependent (gray diamonds) or 3D spheroid (black squares) culture conditions. Data are represented as cell # versus untreated for each individual cell line.
(F) Dose-response curves of NCI-H1975 cells where *SOS1* (red circles) or *SOS2* (blue triangles) has been deleted using CRISPR/Cas9 vs NT controls (black squares) treated with BAY-293 under 3D spheroid culture conditions. For each condition, the untreated sample was set to 100%, and drug-treated samples were compared to untreated for each cell line.
Dose-response curves and 2D proliferation are presented as mean +/- s.d. from a least three independent experiments. For transformation studies, data are from four independent experiments. Each individual experiment was performed using populations (not clones) of independently CRISPR'd cells. For each experiment, three technical replicates were assessed.
Statistical significance was determined by ANOVA using Tukey's method for multiple comparisons. * $p<0.05$, ** $p<0.01$, *** $p<0.001$ vs. NT cells. # $p<0.05$, ## $p<0.01$ vs. *SOS1* KO cells.

Figure 2. SOS1 inhibition synergizes with the EGFR-TKI inhibitor osimertinib to inhibit cell survival under anchorage-independent (3D) culture conditions.
(A-D) Isobologram analysis examines drug-drug synergy by comparing dose equivalent (DEQ) mixtures of two drugs based on their EC_{50} values to treatment with either drug alone **(A and B)**. From the dose-response curves of the DEQ mixtures, plotting the fractional EC_{50} for each drug in the combination (purple) relative to the individual drug EC_{50} values (blue, red) on an isobologram plot **(C)** and calculation of the combination index (CI, **D and E**) allows assessment of drug-drug synergy. Additive effects occur on the dashed lines of the isobologram plot and have a CI 0.8-1.2 (gray box), whereas synergistic interactions fall below the dashed lines and have a CI < 0.8.
(E) Isobologram plots and CI from dose-equivalent treatments of H1975 EGFR-mutated NSCLC cells treated with DEQ combinations of osimertinib and BAY-293. Isobologram and CI data are presented as mean +/- s.d. from three independent experiments.
(F) Bliss additivity evaluates whether the overall effect of an individual drug combination ($E_{A+B\ mix}$) is greater than should be expected for two drugs with independent effects on the overall population ($E_A + E_B - E_A * E_B$).
(G) The Bliss Index compares the ratio of the expected effect to the actual effect. Synergistic interactions have a Bliss Index < 0.85.
(H) Excess over Bliss evaluates the magnitude of the difference between the actual and expected effects. Increasingly synergistic interactions show an excess over Bliss Index > 0.
(I) Heat map of H1975 cells treated with the indicated doses of osimertinib and/or BAY-293 grown in either 2D (adherent) culture conditions or as 3D spheroids. Green indicates more cells, red indicates fewer cells. EC_{50} values for each individual drug are indicated by an *.
(J) Heat map of Bliss Index assessing drug-drug synergy between osimertinib and BAY-293 at each dose combination from **D**.
(K) Heat map of excess over Bliss assessing drug-drug synergy between osimertinib and BAY-293 at each dose combination from **D**.
Bliss Index and excess-over Bliss are presented as the mean from three independent experiments. For each experiment, three technical replicates were assessed.

Figure 3. Isobologram analysis showing that SOS1 inhibition synergizes with EGFR-TKI treatment to inhibit survival in multiple EGFR-mutated NSCLC cell lines.
Isobologram analysis and Combination Index (CI) from dose-equivalent treatments of the indicated EGFR-mutated gefitinib-sensitive (L858R or Dex19, top) or gefitinib-resistant (T790M, bottom) NSCLC cell lines with combinations of gefitinib, osimertinib, and BAY-293. Additive effects occur on the dashed lines of the isobologram plot and have a CI 0.8-1.2 (gray box), whereas synergistic interactions fall below the dashed lines and have a CI < 0.8.
Data are presented as mean +/- s.d. from three independent experiments.
For each experiment, three technical replicates were assessed.

Figure 4. Bliss Independence analysis showing that SOS1 inhibition synergizes with EGFR-TKI treatment to inhibit survival in multiple EGFR-mutated NSCLC cell lines.
(A) Bliss Index heatmap from 3D spheroid cultured NCI-H1975 cells Fig. 2A (left) and horizontal projections of Bliss Indices of drug treatments at 2:1, 1:1, and 1:2 ratios of osimertinib:BAY-293 based on dose equivalencies (right). Increasingly synergistic interactions (Bliss index < 0.85) are indicated by the corresponding heat map. The concentration of BAY-293 (held constant, bottom) and of osimertinib (above each horizontal projection) are given. The IC_{50} for each individual drug are shown (*).
(B) Bliss Index heatmaps based on A for the indicated gefitinib-sensitive and gefitinib-resistant cell lines at 2:1, 1:1, and 1:2 ratios of osimertinib, gefitinib, and BAY-293 based on dose equivalencies. Data for NCI-H1975 cells are the same as in A.
Data are presented as the mean from three independent experiments.
For each experiment, three technical replicates were assessed.

Figure 5. *SOS2* deletion does not enhance the synergistic interaction between SOS1 inhibition and EGFR-TKI treatment.
(A-B) Isobologram analysis (left) and Combination Index (right) from dose-equivalent treatments of osimertinib and BAY-293 in H1975 (**A**) or PC9-TM (**B**) cells where *SOS2* has been deleted (blue) versus NT controls (black). Overlay plots on two different BAY-293 dosing scales are shown below the individual isobologram plots. Additive effects occur on the dashed lines of the isobologram plot and have a CI 0.8-1.2 (gray box), whereas synergistic interactions fall below the dashed lines and have a CI < 0.8.
(C) Bliss Index heatmaps for H3255-TM cells where *SOS2* has been deleted versus NT controls treated at at 1:2, 1:1, and 2:1 ratios of osimertinib and BAY-293 based on dose equivalencies.
Data are presented as mean +/- s.d. from three independent experiments.
For each experiment, three technical replicates were assessed.

Figure 6. SOS1 inhibition synergizes with mutant EGFR inhibition to inhibit downstream effector signaling.
Western blots **(A, D)**, pERK and pAKT quantitation **(B, E)**, and Bliss Indices **(C, F)** of WCLs of NCI-H1975 cells (A-C, top) or PC9-TM cells (D-F, bottom) cultured under 3D spheroid conditions for 48 hours and then treated with the indicated concentrations of the EGFR-TKI osimertinib and/or the SOS1 inhibitor BAY-293 for 6 hours. Western blots are for pEGFR, EGFR, pAKT, AKT, pERK1/2, ERK1/2, HSP90, and β-actin. pERK and pAKT quantifications were calculated using a weighted average of total protein western blots. Combination Indices are based on pERK / Total protein and pAKT / Total protein quantitations. Increasingly synergistic combinations are indicated in yellow, orange, red, or purple.
Phosphoprotein quantitations are presented as mean +/- s.d. from three independent experiments.
Bliss indices are presented as mean from three independent experiments.
For each experiment, three technical replicates were assessed.

Figure 7. Assessment of the EGFR/RAS pathway 'inhibitor landscape' suggests that combination therapies inhibiting mutated EGFR, SOS1, and SHP2 have therapeutic potential in EGFR-mutated NSCLC.
(A) Signaling diagram showing EGFR/RAS pathway inhibitors that were assessed for pairwise synergy by isobologram analysis using 50:50 dose-equivalent mixes of each drug pair.
(B) Heat map of Combination Indices from isobologram analyses of the indicated drug-drug combinations in NT and *SOS2* KO NSCLC cell lines. Synergistic combinations are indicated in yellow, orange, or red. Data are presented as the mean from three independent experiments.
(C-D) Isobologram analysis and Combination Index (CI) from dose-equivalent treatments of 3D spheroid cultured NCI-H1975 cells treated with the indicated 2-drug **(C)** or 3-drug **(D)** combinations of osimertinib (black), RMC-4550 (purple), and BAY-293 (red). For three drug combination, the two drugs indicated on the y-axis were held at a 1:1 ratio, and then mixed at dose equivalent ratiow with the third drug. CI values indicate enhanced synergy beyond the two drug combination on the y-axis of the isobologram plot and are calculated based on the y-axis drug combination calculated a s single drug treatment. Additive effects occur on the dashed lines of the isobologram plot and have a CI 0.8-1.2 (gray box), whereas synergistic interactions fall below the dashed lines and have a CI < 0.8.
(E) Combination indices from 2-drug combinations of osimertinib (black), RMC-4550 (purple), and BAY-293 (red) mixed at 2:1, 1:1, or 1:2 ratios or the three drug combination at a 1:1:1 ratio (grey). CI are calculated based on three individual drug treatments.
(F) Signaling model based on data from Figs. 1-7 showing that combined targeting of mutated EGFR and SOS1 provides sufficient vertical inhibition of upstream signaling to inhibit RAS effector signaling and block oncogenic transformation. This synergistic inhibition can be further enhanced by SHP2 inhibition, providing multiple potential drug combinations for therapeutic intervention in EGFR-mutated NSCLC.
Isobologram and CI data are presented as mean +/- s.d. from three independent experiments. For each experiment, three technical replicates were assessed.

Figure 1-figure supplement 1. **Deletion of SOS1 using CRISPR/Cas9.**
293T cells were transduced with lentiviruses expressing Cas9 and either a non-targeting sgRNA (NT) or one of eight different sgRNAs targeting SOS1. Whole cell lysates (WCLs) were analyzed by Western blotting with antibodies specific for SOS1 or β-actin. SOS1 sgRNA constructs #1, #2, and #8 consistently showed >90% reduction in total SOS1 protein abundance. SOS1-2 was used for experiments in Fig. 1.

Figure 1-figure supplement 2. **The SOS1 inhibitor BAY-293 is specific for SOS1 and is enhanced by *SOS2* deletion in EGFR (T790M) mutated NSCLC cell lines.**
A-C. Dose-response curves of NCI-H1975 (A), PC9-TM (B), or H3255-TM (C) cells where *SOS1* (red circles) or *SOS2* (blue triangles) has been deleted using CRISPR/Cas9 vs NT controls (black squares) treated with BAY-293 under 3D spheroid culture conditions. For each condition, the untreated sample was set to 100%, and drug-treated samples were compared to untreated for each cell line.
Data are presented as mean +/- s.d. from at least three independent experiments.
Data are represented as cell # versus untreated for each individual cell line.
For each experiment, three technical replicates were assessed.

Figure 3-figure supplement 1. **EGFR mutated NSCLC cell lines are responsive to osimertinib, BAY-293, and gefitinib in 3D spheroid cultures.**
A-F. Dose-response curves of 3D spheroid cultured HCC827 (A), NCI-H1975 (B), PC9 (C), PC9-TM (D), H3255 (E), or H3255-TM (F) cells to osimertinib (black squares), BAY-293 (red circles) or gefitinib (grey diamonds). Hill coefficients +/- s.d. are shown to the right.
Data are presented as mean +/- s.d. from at least three independent experiments.
For each experiment, three technical replicates were assessed.

References

1. N. Cancer Genome Atlas Research, Comprehensive molecular profiling of lung adenocarcinoma. *Nature* **511**, 543-550 (2014).

2. T. S. Mok *et al.*, Gefitinib or carboplatin-paclitaxel in pulmonary adenocarcinoma. *N Engl J Med* **361**, 947-957 (2009).

3. J. J. Yang *et al.*, A phase III randomised controlled trial of erlotinib vs gefitinib in advanced non-small cell lung cancer with EGFR mutations. *Br J Cancer* **116**, 568-574 (2017).

4. D. A. Eberhard *et al.*, Mutations in the epidermal growth factor receptor and in KRAS are predictive and prognostic indicators in patients with non-small-cell lung cancer treated with chemotherapy alone and in combination with erlotinib. *J Clin Oncol* **23**, 5900-5909 (2005).

5. P. A. Janne *et al.*, AZD9291 in EGFR inhibitor-resistant non-small-cell lung cancer. *N Engl J Med* **372**, 1689-1699 (2015).

6. D. A. Cross *et al.*, AZD9291, an irreversible EGFR TKI, overcomes T790M-mediated resistance to EGFR inhibitors in lung cancer. *Cancer Discov* **4**, 1046-1061 (2014).

7. M. Mancini *et al.*, An oligoclonal antibody durably overcomes resistance of lung cancer to third-generation EGFR inhibitors. *EMBO Mol Med* **10**, 294-308 (2018).

8. D. Romaniello *et al.*, A Combination of Approved Antibodies Overcomes Resistance of Lung Cancer to Osimertinib by Blocking Bypass Pathways. *Clin Cancer Res* **24**, 5610-5621 (2018).

9. S. La Monica *et al.*, Trastuzumab emtansine delays and overcomes resistance to the third-generation EGFR-TKI osimertinib in NSCLC EGFR mutated cell lines. *J Exp Clin Cancer Res* **36**, 174 (2017).

10. C. A. Eberlein *et al.*, Acquired Resistance to the Mutant-Selective EGFR Inhibitor AZD9291 Is Associated with Increased Dependence on RAS Signaling in Preclinical Models. *Cancer Res* **75**, 2489-2500 (2015).

11. P. Shi *et al.*, Met gene amplification and protein hyperactivation is a mechanism of resistance to both first and third generation EGFR inhibitors in lung cancer treatment. *Cancer Lett* **380**, 494-504 (2016).

12. J. H. Park *et al.*, Activation of the IGF1R pathway potentially mediates acquired resistance to mutant-selective 3rd-generation EGF receptor tyrosine kinase inhibitors in advanced non-small cell lung cancer. *Oncotarget* **7**, 22005-22015 (2016).

13. D. Kim *et al.*, AXL degradation in combination with EGFR-TKI can delay and overcome acquired resistance in human non-small cell lung cancer cells. *Cell Death Dis* **10**, 361 (2019).

14. H. Taniguchi *et al.*, AXL confers intrinsic resistance to osimertinib and advances the emergence of tolerant cells. *Nat Commun* **10**, 259 (2019).

15. T. Jimbo *et al.*, DS-1205b, a novel selective inhibitor of AXL kinase, blocks resistance to EGFR-tyrosine kinase inhibitors in a non-small cell lung cancer xenograft model. *Oncotarget* **10**, 5152-5167 (2019).

16. K. Namba *et al.*, Activation of AXL as a Preclinical Acquired Resistance Mechanism Against Osimertinib Treatment in EGFR-Mutant Non-Small Cell Lung Cancer Cells. *Mol Cancer Res* **17**, 499-507 (2019).

17. E. M. Tricker *et al.*, Combined EGFR/MEK Inhibition Prevents the Emergence of Resistance in EGFR-Mutant Lung Cancer. *Cancer Discov* **5**, 960-971 (2015).

18. K. Jacobsen *et al.*, Convergent Akt activation drives acquired EGFR inhibitor resistance in lung cancer. *Nat Commun* **8**, 410 (2017).

19. B. M. Ku *et al.*, Acquired resistance to AZD9291 as an upfront treatment is dependent on ERK signaling in a preclinical model. *PLoS One* **13**, e0194730 (2018).

20. E. Ichihara *et al.*, SFK/FAK Signaling Attenuates Osimertinib Efficacy in Both Drug-Sensitive and Drug-Resistant Models of EGFR-Mutant Lung Cancer. *Cancer research* **77**, 2990-3000 (2017).

21. A. S. Nunes, A. S. Barros, E. C. Costa, A. F. Moreira, I. J. Correia, 3D tumor spheroids as in vitro models to mimic in vivo human solid tumors resistance to therapeutic drugs. *Biotechnol Bioeng* **116**, 206-226 (2019).

22. S. A. Langhans, Three-Dimensional in Vitro Cell Culture Models in Drug Discovery and Drug Repositioning. *Front Pharmacol* **9**, 6 (2018).

23. H. X. Hao *et al.*, Tumor Intrinsic Efficacy by SHP2 and RTK Inhibitors in KRAS-Mutant Cancers. *Mol Cancer Ther* **18**, 2368-2380 (2019).

24. J. W. Kim, W. J. Ho, B. M. Wu, The role of the 3D environment in hypoxia-induced drug and apoptosis resistance. *Anticancer Res* **31**, 3237-3245 (2011).

25. A. Riedl *et al.*, Comparison of cancer cells in 2D vs 3D culture reveals differences in AKT-mTOR-S6K signaling and drug responses. *J Cell Sci* **130**, 203-218 (2017).

26. G. G. Jones *et al.*, SHOC2 phosphatase-dependent RAF dimerization mediates resistance to MEK inhibition in RAS-mutant cancers. *Nat Commun* **10**, 2532 (2019).

27. J. E. Ekert *et al.*, Three-dimensional lung tumor microenvironment modulates therapeutic compound responsiveness in vitro--implication for drug development. *PLoS One* **9**, e92248 (2014).

28. N. Jacobi *et al.*, Organotypic three-dimensional cancer cell cultures mirror drug responses in vivo: lessons learned from the inhibition of EGFR signaling. *Oncotarget* **8**, 107423-107440 (2017).

29. D. Vigil, J. Cherfils, K. L. Rossman, C. J. Der, Ras superfamily GEFs and GAPs: validated and tractable targets for cancer therapy? *Nat Rev Cancer* **10**, 842-857 (2010).

30. H. H. Jeng, L. J. Taylor, D. Bar-Sagi, Sos-mediated cross-activation of wild-type Ras by oncogenic Ras is essential for tumorigenesis. *Nat Commun* **3**, 1168 (2012).

31. E. Sheffels *et al.*, Oncogenic RAS isoforms show a hierarchical requirement for the guanine nucleotide exchange factor SOS2 to mediate cell transformation. *Sci Signal* **11**, (2018).

32. E. Sheffels, N. E. Sealover, P. L. Theard, R. L. Kortum, Anchorage-independent growth conditions reveal a differential SOS2 dependence for transformation and survival in RAS-mutant cancer cells. *Small GTPases*, 1-12 (2019).

33. R. C. Hillig *et al.*, Discovery of potent SOS1 inhibitors that block RAS activation via disruption of the RAS-SOS1 interaction. *Proc Natl Acad Sci U S A* **116**, 2551-2560 (2019).

34. A. S. Nunes, A. S. Barros, E. C. Costa, A. F. Moreira, I. J. Correia, 3D tumor spheroids as in vitro models to mimic in vivo human solid tumors resistance to therapeutic drugs. *Biotechnology and Bioengineering* **116**, 206-226 (2019).

35. M. R. Janes *et al.*, Targeting KRAS Mutant Cancers with a Covalent G12C-Specific Inhibitor. *Cell* **172**, 578-589 e517 (2018).

36. N. Jacobi *et al.*, Organotypic three-dimensional cancer cell cultures mirror drug responses in vivo: lessons learned from the inhibition of EGFR signaling. *Oncotarget* **8**, 107423-107440 (2017).

37. D. M. Munoz *et al.*, CRISPR Screens Provide a Comprehensive Assessment of Cancer Vulnerabilities but Generate False-Positive Hits for Highly Amplified Genomic Regions. *Cancer Discov* **6**, 900-913 (2016).

38. E. C. de Bruin *et al.*, Reduced NF1 expression confers resistance to EGFR inhibition in lung cancer. *Cancer Discov* **4**, 606-619 (2014).

39. J. A. Engelman *et al.*, Allelic dilution obscures detection of a biologically significant resistance mutation in EGFR-amplified lung cancer. *J Clin Invest* **116**, 2695-2706 (2006).

40. K. R. Roell, D. M. Reif, A. A. Motsinger-Reif, An Introduction to Terminology and Methodology of Chemical Synergy-Perspectives from Across Disciplines. *Front Pharmacol* **8**, 158 (2017).

41. R. J. Tallarida, Quantitative methods for assessing drug synergism. *Genes & Cancer* **2**, 1003-1008 (2011).

42. M. Dance, A. Montagner, J.-P. Salles, A. Yart, P. Raynal, The molecular functions of Shp2 in the Ras/Mitogen-activated protein kinase (ERK1/2) pathway. *Cell Signal* **20**, 453-459 (2008).

43. R. J. Nichols *et al.*, RAS nucleotide cycling underlies the SHP2 phosphatase dependence of mutant BRAF-, NF1- and RAS-driven cancers. *Nat Cell Biol* **20**, 1064-1073 (2018).

44. J. C. Soria *et al.*, Osimertinib in Untreated EGFR-Mutated Advanced Non-Small-Cell Lung Cancer. *N Engl J Med* **378**, 113-125 (2018).

45. S. S. Ramalingam *et al.*, Overall Survival with Osimertinib in Untreated, EGFR-Mutated Advanced NSCLC. *N Engl J Med* **382**, 41-50 (2020).

46. F. Mittler *et al.*, High-Content Monitoring of Drug Effects in a 3D Spheroid Model. *Front Oncol* **7**, 293 (2017).

47. O. A. Balbin *et al.*, Reconstructing targetable pathways in lung cancer by integrating diverse omics data. *Nat Commun* **4**, 2617 (2013).

48. A. Singh *et al.*, A gene expression signature associated with "K-Ras addiction" reveals regulators of EMT and tumor cell survival. *Cancer Cell* **15**, 489-500 (2009).

49. A. Singh *et al.*, TAK1 inhibition promotes apoptosis in KRAS-dependent colon cancers. *Cell* **148**, 639-650 (2012).

50. C. Scholl *et al.*, Synthetic lethal interaction between oncogenic KRAS dependency and STK33 suppression in human cancer cells. *Cell* **137**, 821-834 (2009).

51. S. Lamba *et al.*, RAF suppression synergizes with MEK inhibition in KRAS mutant cancer cells. *Cell Rep* **8**, 1475-1483 (2014).

52. S. Fujita-Sato *et al.*, Enhanced MET Translation and Signaling Sustains K-Ras-Driven Proliferation under Anchorage-Independent Growth Conditions. *Cancer research* **75**, 2851-2862 (2015).

53. A. Rotem *et al.*, Alternative to the soft-agar assay that permits high-throughput drug and genetic screens for cellular transformation. *Proc Natl Acad Sci U S A* **112**, 5708-5713 (2015).

54. Z. Zhang, G. Jiang, F. Yang, J. Wang, Knockdown of mutant K-ras expression by adenovirus-mediated siRNA inhibits the in vitro and in vivo growth of lung cancer cells. *Cancer Biol Ther* **5**, 1481-1486 (2006).

55. F. McCormick, KRAS as a Therapeutic Target. *Clin Cancer Res* **21**, 1797-1801 (2015).

56. K. Han *et al.*, CRISPR screens in cancer spheroids identify 3D growth-specific vulnerabilities. *Nature* **ePub March 11, 2020**, (2020).

57. M. H. Hofmann *et al.*, BI-3406, a potent and selective SOS1::KRAS interaction inhibitor, is effective in KRAS-driven cancers through combined MEK inhibition. *Cancer Discovery*, provisionary acceptance (2020).

58. A. Fortian, A. Sorkin, Live-cell fluorescence imaging reveals high stoichiometry of Grb2 binding to the EGF receptor sustained during endocytosis. *J Cell Sci* **127**, 432-444 (2014).

59. P. Shi *et al.*, Overcoming Acquired Resistance to AZD9291, A Third-Generation EGFR Inhibitor, through Modulation of MEK/ERK-Dependent Bim and Mcl-1 Degradation. *Clin Cancer Res* **23**, 6567-6579 (2017).

60. C. M. Della Corte *et al.*, Antitumor Efficacy of Dual Blockade of EGFR Signaling by Osimertinib in Combination With Selumetinib or Cetuximab in Activated EGFR Human NCLC Tumor Models. *J Thorac Oncol* **13**, 810-820 (2018).

61. K. J. Kurppa *et al.*, Treatment-Induced Tumor Dormancy through YAP-Mediated Transcriptional Reprogramming of the Apoptotic Pathway. *Cancer Cell* **37**, 104-122 e112 (2020).

62. R. Fan, N. G. Kim, B. M. Gumbiner, Regulation of Hippo pathway by mitogenic growth factors via phosphoinositide 3-kinase and phosphoinositide-dependent kinase-1. *Proc Natl Acad Sci U S A* **110**, 2569-2574 (2013).

63. H. Xia *et al.*, EGFR-PI3K-PDK1 pathway regulates YAP signaling in hepatocellular carcinoma: the mechanism and its implications in targeted therapy. *Cell Death Dis* **9**, 269 (2018).

64. K. Tumaneng *et al.*, YAP mediates crosstalk between the Hippo and PI(3)K-TOR pathways by suppressing PTEN via miR-29. *Nat Cell Biol* **14**, 1322-1329 (2012).

65. S. Watanabe *et al.*, T790M-Selective EGFR-TKI Combined with Dasatinib as an Optimal Strategy for Overcoming EGFR-TKI Resistance in T790M-Positive Non-Small Cell Lung Cancer. *Mol Cancer Ther* **16**, 2563-2571 (2017).

66. N. E. Sanjana, O. Shalem, F. Zhang, Improved vectors and genome-wide libraries for CRISPR screening. *Nat Methods* **11**, 783-784 (2014).

67. K. A. Janes, An analysis of critical factors for quantitative immunoblotting. *Sci Signal* **8**, rs2 (2015).

Figure 1

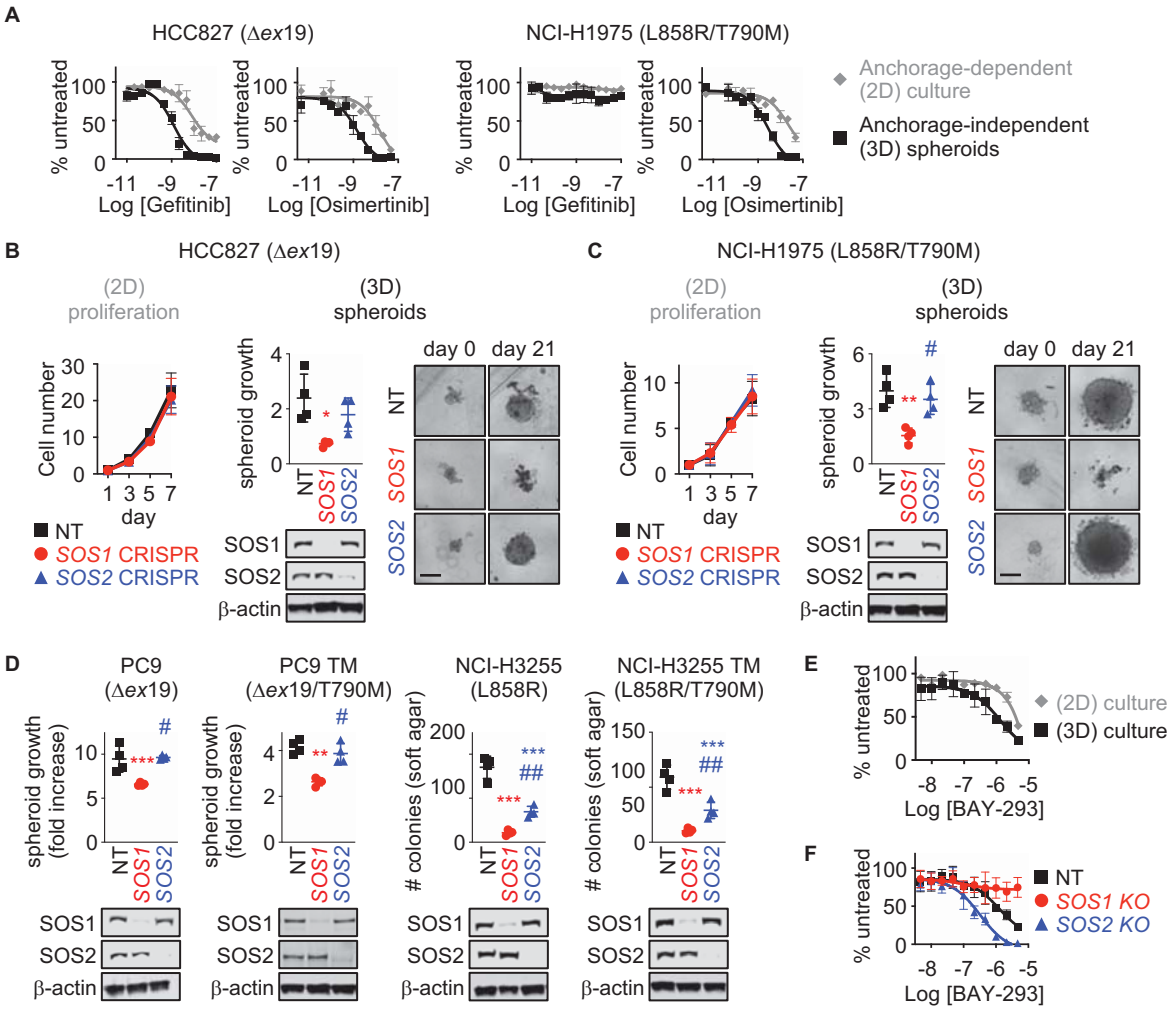
A
HCC827 (Δex19)
NCI-H1975 (L858R/T790M)
% untreated
Log [Gefitinib]
Log [Osimertinib]
Anchorage-dependent (2D) culture
Anchorage-independent (3D) spheroids
B
HCC827 (Δex19)
(2D) proliferation
(3D) spheroids
Cell number
day
spheroid growth
day 0
day 21
NT
SOS1 CRISPR
SOS2 CRISPR
SOS1
SOS2
β-actin
C
NCI-H1975 (L858R/T790M)
D
PC9 (Δex19)
PC9 TM (Δex19/T790M)
NCI-H3255 (L858R)
NCI-H3255 TM (L858R/T790M)
spheroid growth (fold increase)
colonies (soft agar)
E
(2D) culture
(3D) culture
Log [BAY-293]
F
SOS1 KO
SOS2 KO

Figure 2

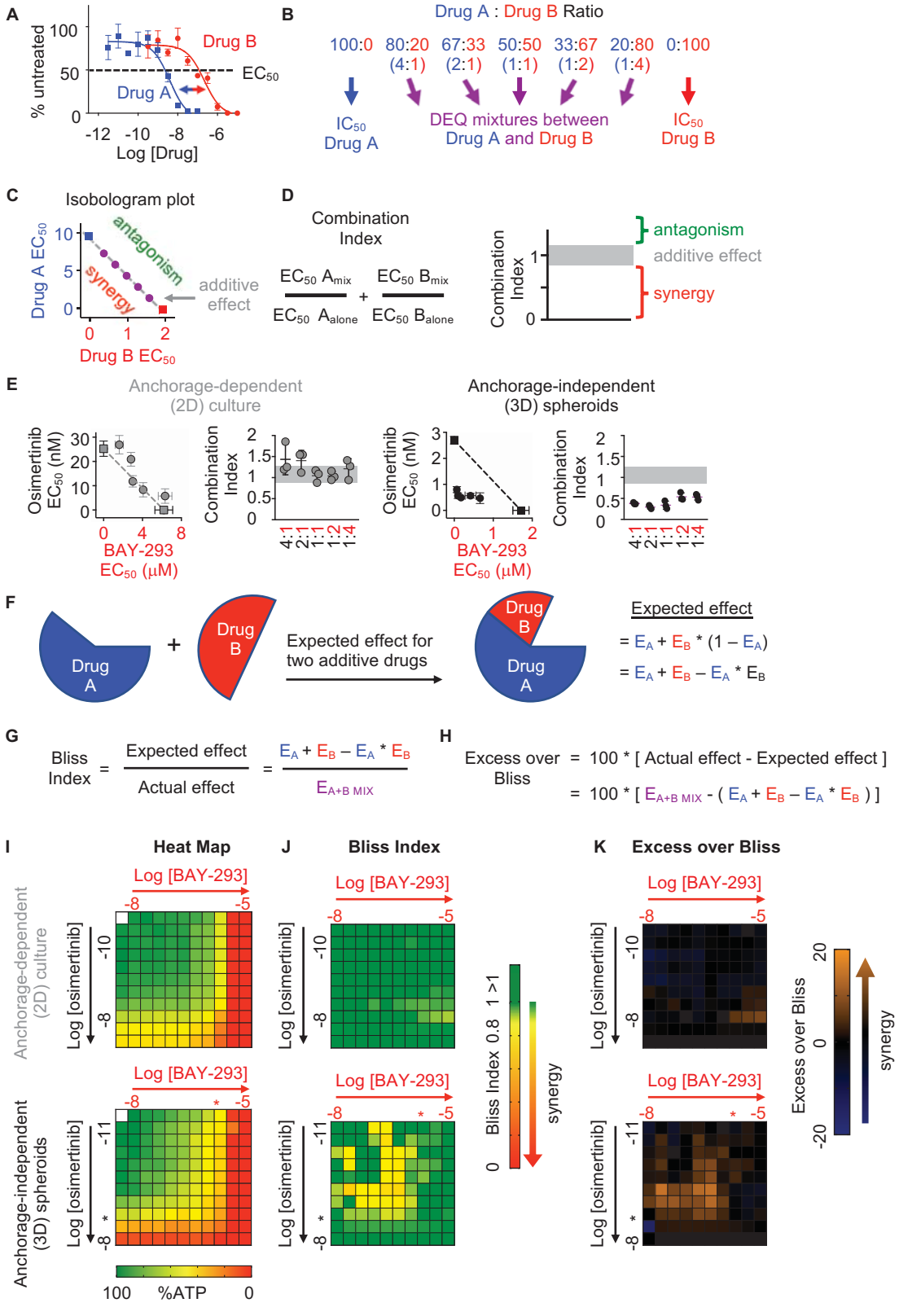
A
% untreated
100
50
0
Drug B
EC50
Drug A
-12 -10 -8 -6
Log [Drug]
B
Drug A : Drug B Ratio
100:0
80:20 (4:1)
67:33 (2:1)
50:50 (1:1)
33:67 (1:2)
20:80 (1:4)
0:100
IC50 Drug A
DEQ mixtures between Drug A and Drug B
IC50 Drug B
C
Isobologram plot
Drug A EC50
10
5
0
antagonism
synergy
additive effect
0 1 2
Drug B EC50
D
Combination Index
EC50 Amix / EC50 Aalone + EC50 Bmix / EC50 Balone
Combination Index
1
0
antagonism
additive effect
synergy
E
Anchorage-dependent (2D) culture
Anchorage-independent (3D) spheroids
Osimertinib EC50 (nM)
30
20
10
0
0 4 8
BAY-293 EC50 (μM)
Combination Index
2
1.5
1
0.5
0
4:1 2:1 1:1 1:2 1:4
Osimertinib EC50 (nM)
3
2
1
0
0 1 2
BAY-293 EC50 (μM)
Combination Index
2
1.5
1
0.5
0
4:1 2:1 1:1 1:2 1:4
F
Drug A
+
Drug B
Expected effect for two additive drugs
Drug B
Drug A
Expected effect
= EA + EB * (1 – EA)
= EA + EB – EA * EB
G
Bliss Index = Expected effect / Actual effect = EA + EB – EA * EB / EA+B MIX
H
Excess over Bliss = 100 * [Actual effect - Expected effect]
= 100 * [EA+B MIX - (EA + EB – EA * EB)]
I
Heat Map
Anchorage-dependent (2D) culture
Log [BAY-293]
-8 -5
Log [osimertinib]
-10 -8
Anchorage-independent (3D) spheroids
Log [BAY-293]
-8 * -5
Log [osimertinib]
-11 -8 *
100 %ATP 0
J
Bliss Index
Log [BAY-293]
-8 -5
Log [osimertinib]
-10 -8
Log [BAY-293]
-8 * -5
Log [osimertinib]
-11 -8 *
Bliss Index 0.8 1 >1
0
synergy
K
Excess over Bliss
Log [BAY-293]
-8 -5
Log [osimertinib]
-10 -8
Log [BAY-293]
-8 * -5
Log [osimertinib]
-11 -8 *
Excess over Bliss
20
0
-20
synergy

Figure 3

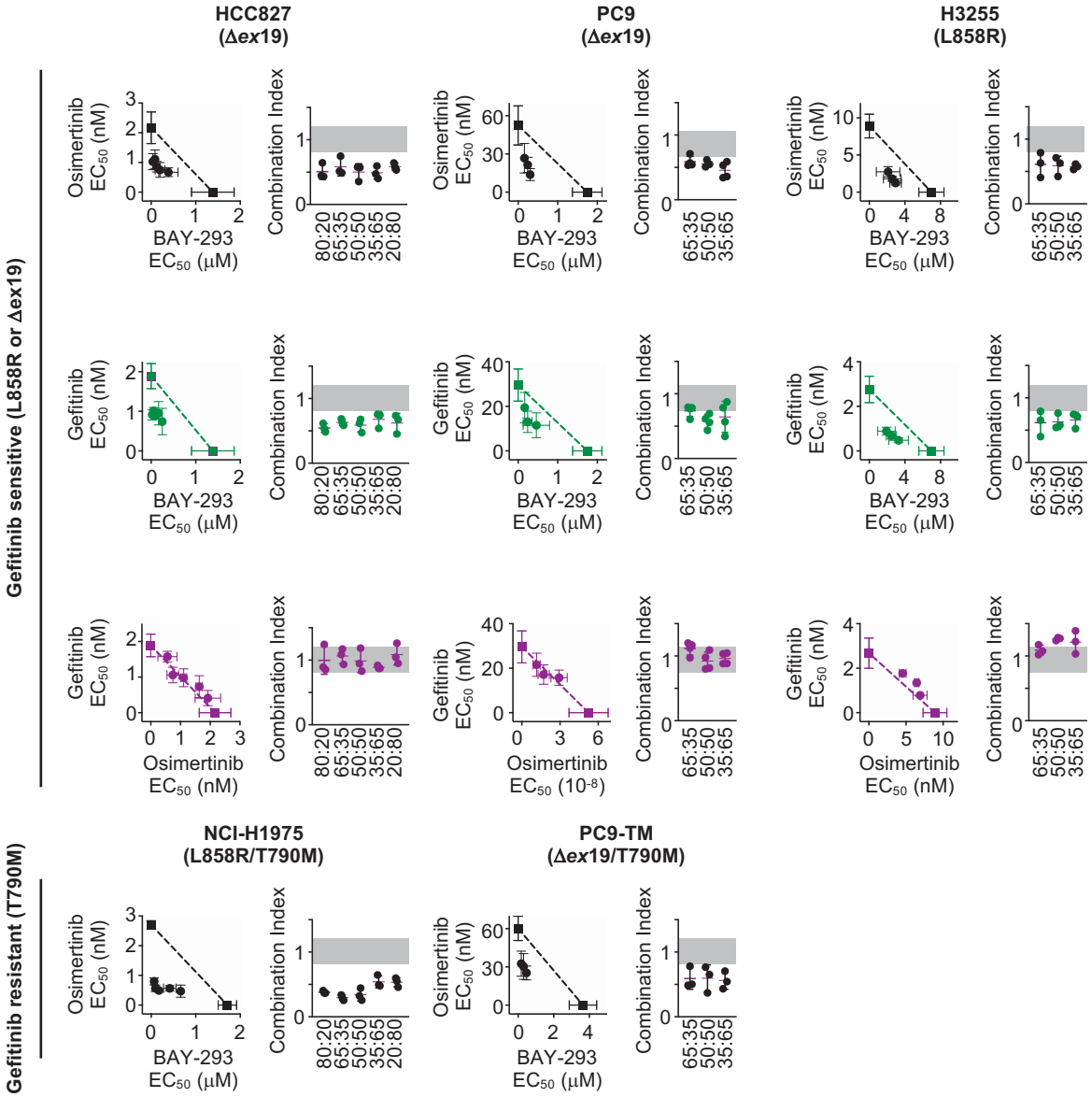
HCC827 (Δex19)
PC9 (Δex19)
H3255 (L858R)
NCI-H1975 (L858R/T790M)
PC9-TM (Δex19/T790M)
Gefitinib sensitive (L858R or Δex19)
Gefitinib resistant (T790M)
Osimertinib EC50 (nM)
Gefitinib EC50 (nM)
BAY-293 EC50 (μM)
Osimertinib EC50 (10-8)
Combination Index
80:20
65:35
50:50
35:65
20:80

Figure 4

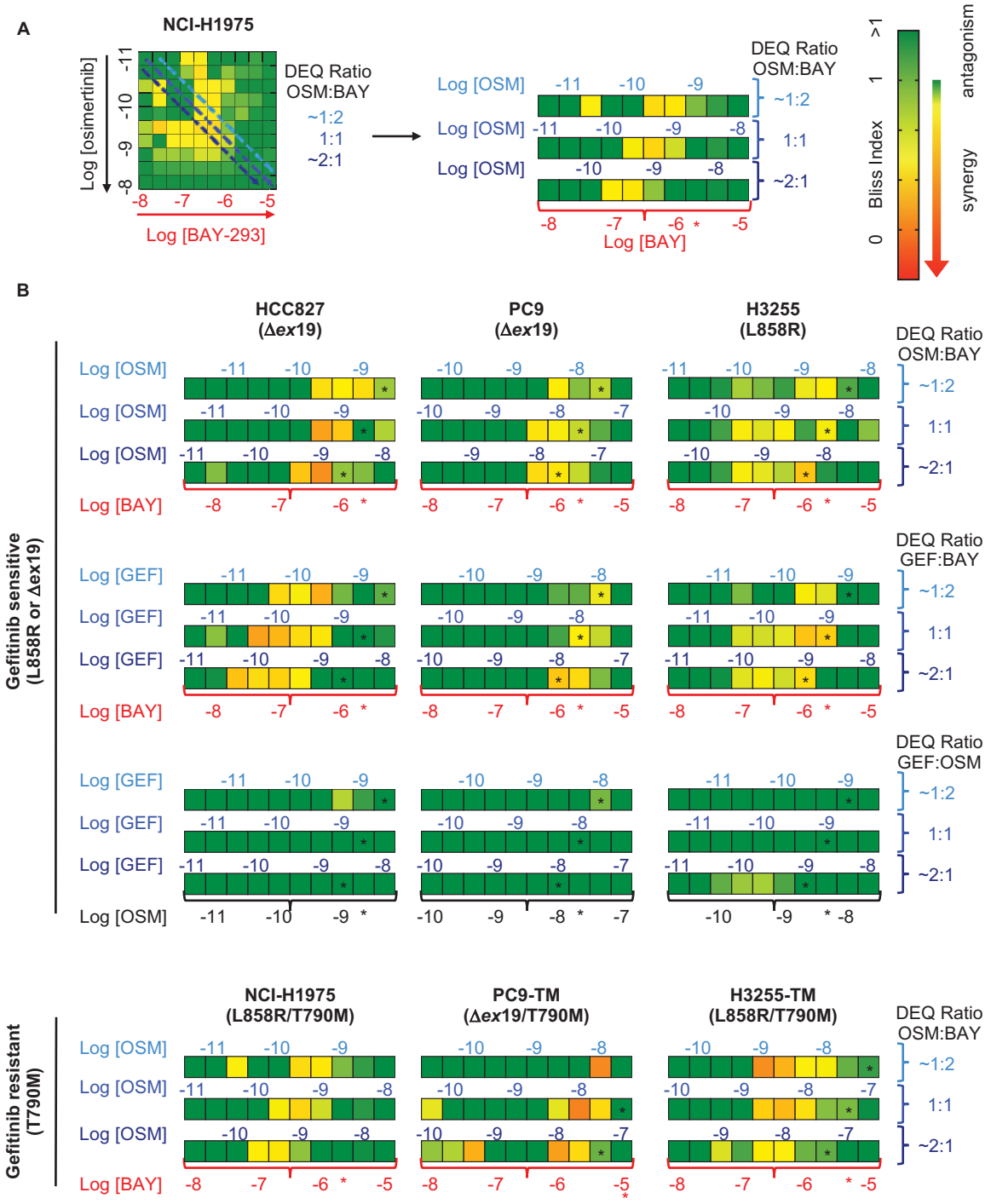
A
NCI-H1975
Log [osimertinib]
Log [BAY-293]
DEQ Ratio
OSM:BAY
~1:2
1:1
~2:1
Log [OSM]
Log [BAY]
Bliss Index
antagonism
synergy
B
HCC827
(Δex19)
PC9
(Δex19)
H3255
(L858R)
Gefitinib sensitive
(L858R or Δex19)
Log [GEF]
DEQ Ratio
GEF:BAY
DEQ Ratio
GEF:OSM
NCI-H1975
(L858R/T790M)
PC9-TM
(Δex19/T790M)
H3255-TM
(L858R/T790M)
Gefitinib resistant
(T790M)

Figure 5

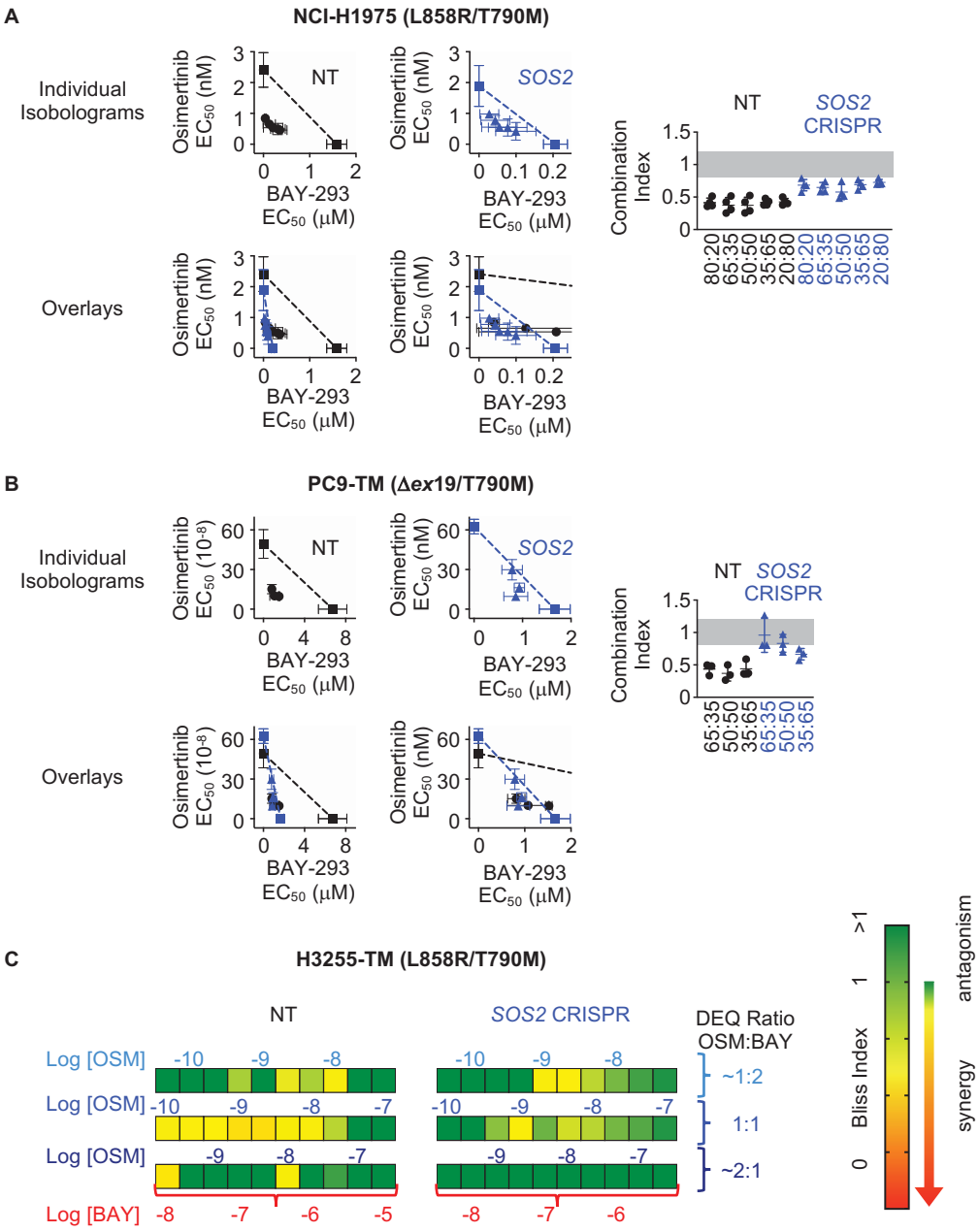
A
NCI-H1975 (L858R/T790M)
Individual Isobolograms
Overlays
Osimertinib EC50 (nM)
BAY-293 EC50 (μM)
NT
SOS2
Combination Index
SOS2 CRISPR
80:20
65:35
50:50
35:65
20:80
B
PC9-TM (Δex19/T790M)
Osimertinib EC50 (10-8)
C
H3255-TM (L858R/T790M)
Log [OSM]
Log [BAY]
DEQ Ratio OSM:BAY
~1:2
1:1
~2:1
Bliss Index
antagonism
synergy

Figure 6

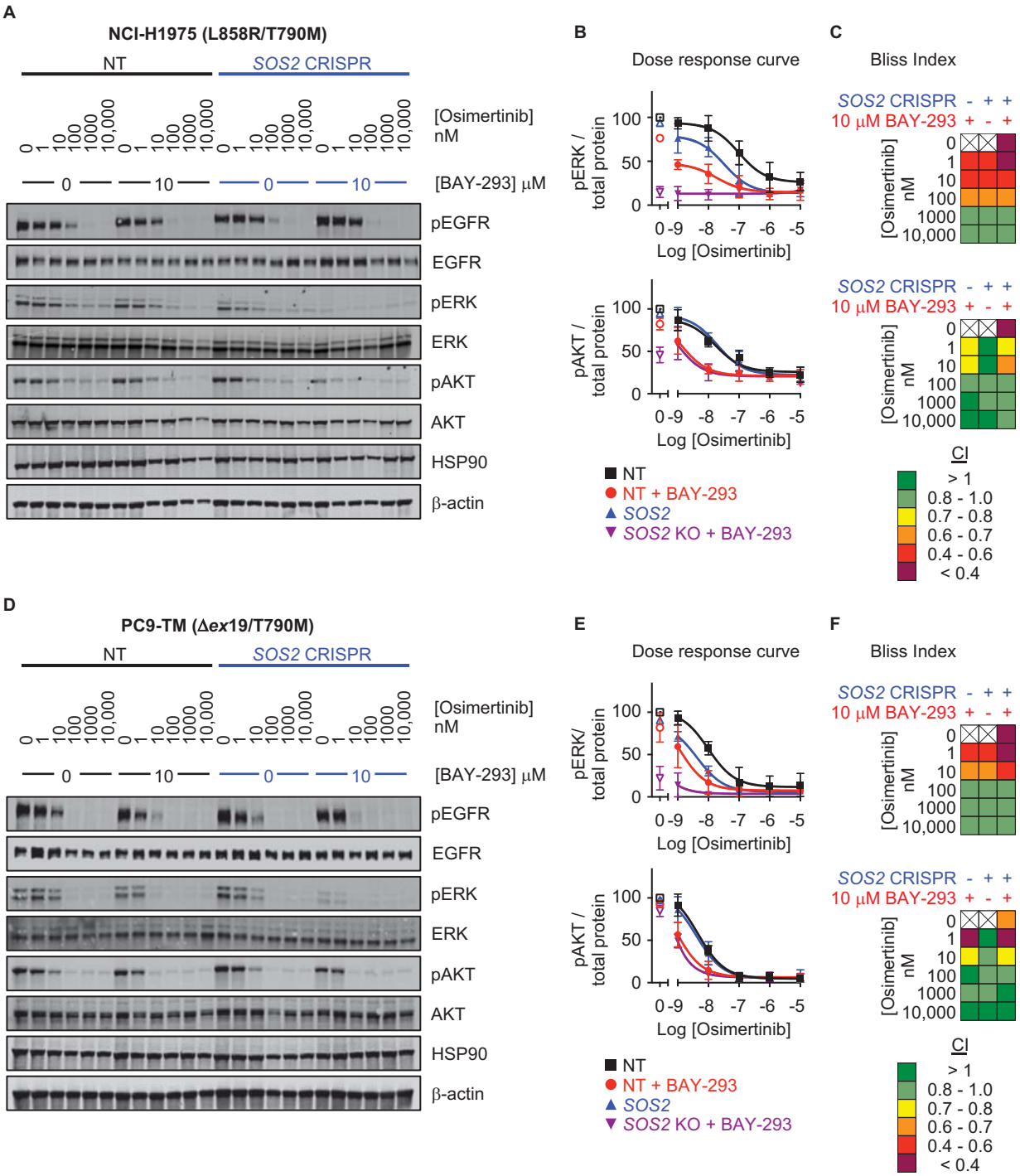
A
NCI-H1975 (L858R/T790M)
NT
SOS2 CRISPR
[Osimertinib] nM
[BAY-293] μM
pEGFR
EGFR
pERK
ERK
pAKT
AKT
HSP90
β-actin
B
Dose response curve
pERK / total protein
pAKT / total protein
Log [Osimertinib]
NT
NT + BAY-293
SOS2
SOS2 KO + BAY-293
C
Bliss Index
SOS2 CRISPR
10 μM BAY-293
[Osimertinib] nM
CI
> 1
0.8 - 1.0
0.7 - 0.8
0.6 - 0.7
0.4 - 0.6
< 0.4
D
PC9-TM (Δex19/T790M)
E
F

Figure 7

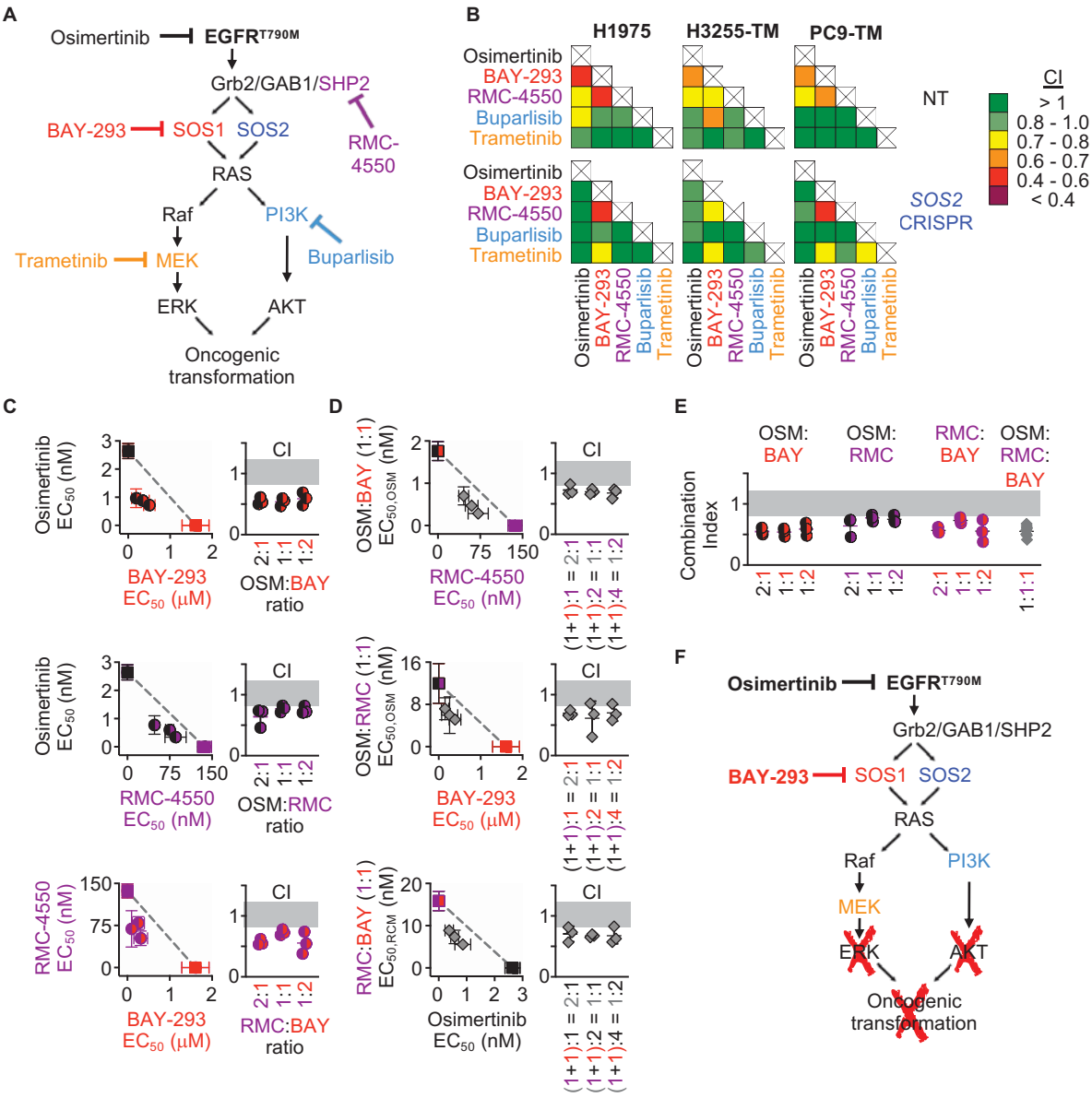
A
Osimertinib
EGFR T790M
Grb2/GAB1/SHP2
BAY-293
SOS1
SOS2
RMC-4550
RAS
Raf
PI3K
Trametinib
MEK
Buparlisib
ERK
AKT
Oncogenic transformation
B
H1975
H3255-TM
PC9-TM
Osimertinib
BAY-293
RMC-4550
Buparlisib
Trametinib
NT
SOS2 CRISPR
CI
> 1
0.8 - 1.0
0.7 - 0.8
0.6 - 0.7
0.4 - 0.6
< 0.4
C
Osimertinib EC50 (nM)
BAY-293 EC50 (μM)
CI
OSM:BAY ratio
RMC-4550 EC50 (nM)
OSM:RMC ratio
RMC-4550 EC50 (nM)
RMC:BAY ratio
D
OSM:BAY (1:1) EC50,OSM (nM)
RMC-4550 EC50 (nM)
OSM:RMC (1:1) EC50,OSM (nM)
BAY-293 EC50 (μM)
RMC:BAY (1:1) EC50,RCM (nM)
Osimertinib EC50 (nM)
(1+1):1 = 2:1
(1+1):2 = 1:1
(1+1):4 = 1:2
E
OSM: BAY
OSM: RMC
RMC: BAY
OSM: RMC: BAY
Combination Index
2:1
1:1
1:2
1:1:1
F
Osimertinib
EGFR T790M
Grb2/GAB1/SHP2
BAY-293
SOS1
SOS2
RAS
Raf
PI3K
MEK
ERK
AKT
Oncogenic transformation

Figure 1-Figure Supplement 1

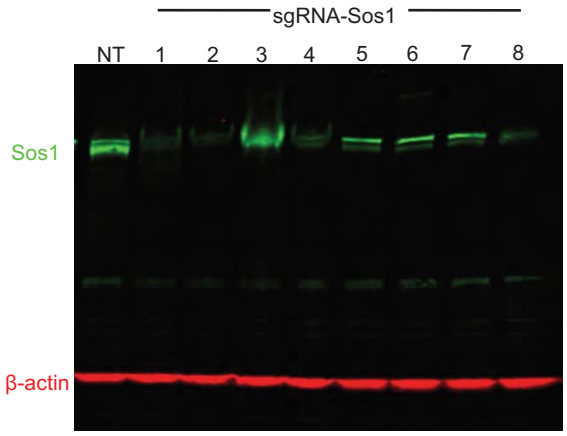

Figure 1-Figure Supplement 2

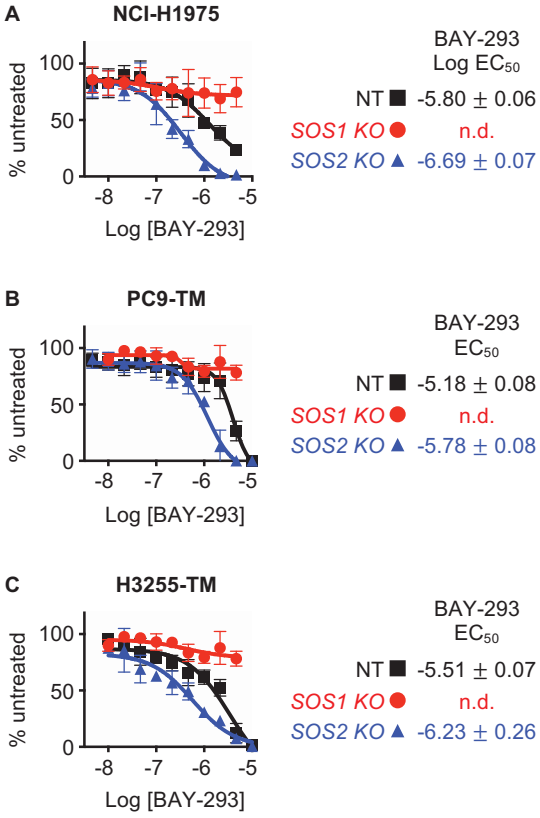

Figure 3-Figure Supplement 1

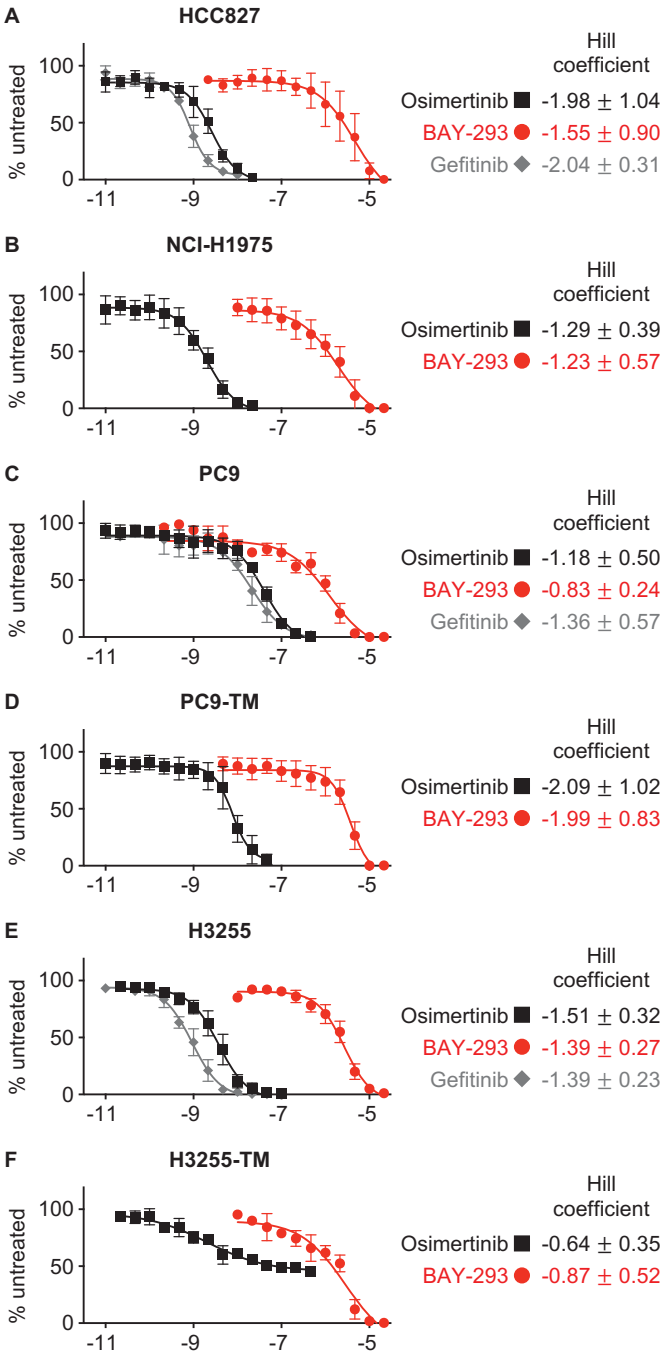

Article

Molecular Cell

Distinct Binding Preferences between Ras and Raf Family Members and the Impact on Oncogenic Ras Signaling

Graphical Abstract

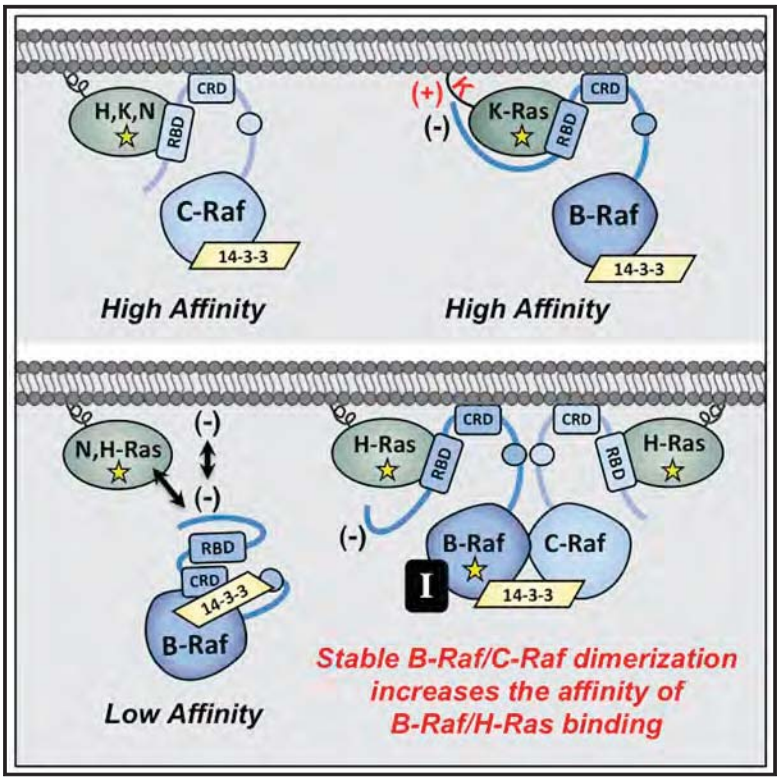

Highlights

- C-Raf binds all Ras proteins equivalently, but B-Raf exhibits selectivity for K-Ras
- Raf N-terminal segments and Ras HVR sequences determine binding preferences
- C-Raf is critical for downstream transmission of H-Ras-driven signaling
- Events that increase B-Raf/C-Raf dimerization augment the B-Raf/H-Ras interaction

Authors

Elizabeth M. Terrell, David E. Durrant, Daniel A. Ritt, ..., John F. Hancock, Robert L. Kortum, Deborah K. Morrison

Correspondence

morrisod@mail.nih.gov

In Brief

The Raf kinases bind to active Ras proteins and function to transmit signals that control cell growth and tumorigenesis. The study by Terrell et al. reveals distinct binding preferences between individual Ras and Raf family members and identifies events that can alter these interactions to upregulate Ras-driven cancer signaling.

Terrell et al., 2019, Molecular Cell *76*, 872–884
December 19, 2019
https://doi.org/10.1016/j.molcel.2019.09.004

CellPress

CellPress

Molecular Cell
Article

Distinct Binding Preferences between Ras and Raf Family Members and the Impact on Oncogenic Ras Signaling

Elizabeth M. Terrell,[1] David E. Durrant,[1] Daniel A. Ritt,[1] Nancy E. Sealover,[2] Erin Sheffels,[2] Russell Spencer-Smith,[1] Dominic Esposito,[3] Yong Zhou,[4] John F. Hancock,[4] Robert L. Kortum,[2] and Deborah K. Morrison[1,5,*]

[1]Laboratory of Cell and Developmental Signaling, NCI-Frederick, Frederick, MD 21702, USA

[2]Department of Pharmacology and Molecular Therapeutics, Uniformed Services University of the Health Sciences, Bethesda, MD 20814, USA

[3]NCI-Ras Initiative, Cancer Research Technology Program, Frederick National Laboratory for Cancer Research, Leidos Biomedical Research, Frederick, MD 21702, USA

[4]Department of Integrative Biology and Pharmacology, McGovern Medical School, University of Texas Health Science Center at Houston, Houston, TX 77030, USA

[5]Lead Contact

*Correspondence: morrisod@mail.nih.gov

https://doi.org/10.1016/j.molcel.2019.09.004

SUMMARY

The Ras GTPases are frequently mutated in human cancer, and, although the Raf kinases are essential effectors of Ras signaling, the tumorigenic properties of specific Ras-Raf complexes are not well characterized. Here, we examine the ability of individual Ras and Raf proteins to interact in live cells using bioluminescence resonance energy transfer (BRET) technology. We find that C-Raf binds all mutant Ras proteins with high affinity, whereas B-Raf exhibits a striking preference for mutant K-Ras. This selectivity is mediated by the acidic, N-terminal segment of B-Raf and requires the K-Ras polybasic region for high-affinity binding. In addition, we find that C-Raf is critical for mutant H-Ras-driven signaling and that events stabilizing B-Raf/C-Raf dimerization, such as Raf inhibitor treatment or certain B-Raf mutations, can allow mutant H-Ras to engage B-Raf with increased affinity to promote tumorigenesis, thus revealing a previously unappreciated role for C-Raf in potentiating B-Raf function.

INTRODUCTION

Ras proteins are membrane-associated, small GTPases that function to transmit a multitude of cellular signals (Pylayeva-Gupta et al., 2011). All Ras family members, which include H-Ras, K-Ras4A/4B, and N-Ras, can relay signals received by cell surface receptors due to their ability to cycle between a GDP-bound "off" state and a GTP-bound "on" state (Cox and Der, 2010; Simanshu et al., 2017). Typically, receptor engagement results in the recruitment of guanine nucleotide exchange factors (GEFs) to the cell surface where they facilitate the GTP-loading of Ras and, in turn, the interaction of Ras with downstream effectors. Following signal transmission, Ras cycles back to its inactive state as a result of GTPase-activating proteins (GAPs) that stimulate the intrinsic GTPase activity of Ras (Bos et al., 2007).

Consistent with its central role in cell signaling, dysregulation of Ras cycling can promote human disease states, with somatic mutations in the *Ras* genes being prominent drivers of tumorigenesis and *Ras* germline mutations contributing to a group of related developmental disorders known as the RASopathies (Fernández-Medarde and Santos, 2011; Schubbert et al., 2007). Importantly, disease-associated mutations tend to render Ras insensitive to GAP stimulation and reduce its intrinsic GTPase activity, leaving Ras in a constitutively active state that promotes pathway activation in an unregulated manner (Prior et al., 2012).

One of the essential effector cascades required for Ras signaling is the ERK cascade, comprised of the Raf, MEK, and ERK protein kinases (Lavoie and Therrien, 2015). All Raf family members, which include A-Raf, B-Raf, and C-Raf, possess a conserved Ras-binding domain (RBD) that resides in the Raf N-terminal regulatory domain. In quiescent cells, the Rafs exist as autoinhibited monomers in the cytosol (Nan et al., 2013). However, when growth signals are received, the Raf kinases are recruited by Ras to the plasma membrane where they become activated through an allosteric mechanism that requires dimerization of the C-terminal Raf kinase domains (Hu et al., 2013). In normal Ras-dependent signaling, B-Raf/C-Raf heterodimers predominate (Freeman et al., 2013) and function to initiate the phosphorylation cascade that results in MEK and ERK activation. Once activated, ERK plays a critical role in the forward transmission of signals but also participates in the attenuation of Ras signaling through the phosphorylation of upstream pathway components, which, in the case of the Rafs, inhibit both Ras/Raf binding and Raf dimerization (Dougherty et al., 2005; Ritt et al., 2010).

Despite being one of the most frequently mutated signaling pathways in human cancer, various aspects of Ras biology are still poorly understood. For example, even though it is well

known that the C-terminal hypervariable region (HVR) of the Ras proteins results in differential lipid processing and membrane localization (Prior and Hancock, 2012), the extent to which these differences influence Ras signaling and/or effector interactions is not clear. Moreover, a puzzling aspect of Ras-induced tumorigenesis is that, although the Ras proteins are highly conserved and rather ubiquitously expressed, their mutational frequency can vary significantly among cancer types, with *K-Ras* mutations being the predominant driver among all Ras-associated tumors but other family members being the primary driver in select tumor types. Therefore, given the central role of the Raf kinases in Ras signaling, studies examining the Ras/Raf interaction in live cells could reveal valuable information needed to tease apart unique tumorigenic properties of individual Ras members and may prove helpful in the pursuit of more effective therapeutic strategies.

Here, we examine the Ras/Raf interaction utilizing bioluminescence resonance energy transfer (BRET), a technique that allows quantitative measurements to be obtained under conditions that preserve crucial features of Ras and Raf regulation, including lipid processing, intracellular trafficking, membrane microdomain targeting, and protein phosphorylation. Strikingly, we find that different Ras and Raf family members exhibit distinct binding preferences and that these differences have important implications for disease-associated Ras signaling.

RESULTS

Live-Cell BRET Analysis of the Ras/Raf Interaction

Bioluminescence resonance energy transfer (BRET) was used to investigate the requirements for Ras/Raf binding in live cells (Pfleger and Eidne, 2006). In this system, a BRET signal is generated when a protein tagged with an energy donor comes in close proximity and can transfer energy to a protein tagged with an energy acceptor. Donor, acceptor, and BRET signals are each monitored individually, providing internal controls for protein expression and producing a sensitive ratiometric readout that is independent of cell number. Quantitative data regarding the interaction can also be obtained by generating a saturation curve in which expression of the energy donor remains constant, while expression of the energy acceptor increases. In this type of analysis, a specific interaction will generate a hyperbolic curve, with $BRET_{max}$ being reflective of the total number of binding pairs that can form and $BRET_{50}$ being a relative measure of binding affinity.

For our analysis, the Raf members functioned as the energy donor, tagged at a conserved C-terminal position with the Rluc8 enzyme, and the Ras proteins served as the energy acceptor, tagged at the N terminus with the Venus fluorophore. It should be noted that our initial studies were performed using proteins that encode the entire Raf regulatory domain (Raf^{Reg}) but lack the kinase domain. This approach was taken in order to mitigate any indirect effects on Ras/Raf binding that might be caused by dimerization of the Raf kinase domains or due to inhibitory feedback loops generated by Raf catalytic activation. As shown in Figure 1A, a strong BRET signal was observed when wild-type (WT) C-Raf^{Reg} was co-expressed with the Q61R mutant of K-Ras4B (hereon referred to as K-Ras). However, if the RBD of C-Raf^{Reg} contained an arginine to leucine (R > L) mutation known to disrupt the Ras/Raf interaction (Fabian et al., 1994), the BRET signal was dramatically reduced. In addition, when the C-terminal CAAX motif of K-Ras^{Q61R} was mutated to prevent the lipid processing and membrane localization of K-Ras (K-$Ras^{Q61R/C>A}$), the BRET signal was significantly compromised as was the GTP loading of Ras (Figures 1A and 1B). In co-immunoprecipitation assays, WT-C-Raf^{Reg}, but not the R > L mutant, was strongly detected in K-Ras^{Q61R} complexes, and only faint levels of WT-C-Raf^{Reg} were observed in K-$Ras^{Q61R/C>A}$ complexes (Figure 1B). Moreover, live-cell imaging studies verified the cytosolic localization of K-$Ras^{Q61R/C>A}$ and showed that K-Ras^{Q61R} could recruit WT-C-Raf to the cell surface but not the R > L mutant (Figure 1C). Thus, these findings confirm that the Ras and Raf proteins generated for use in the BRET assay exhibit their expected subcellular localization and protein binding properties.

Next, each Raf family member was evaluated for binding interactions with a panel of K-Ras mutants. As shown in Figure 1D, a BRET signal was detected for all the Raf^{Reg}/K-Ras pairings, with the highest binding affinity (represented by lower $BRET_{50}$ values) and highest $BRET_{max}$ observed with C-Raf, followed by A-Raf, and then B-Raf. For each individual Raf^{Reg} protein, $BRET_{50}$ values were similar for all the K-Ras mutants, indicating a comparable binding affinity (Figure 1E). Interestingly, the highest $BRET_{max}$ signals were observed with K-Ras proteins containing mutations in the Q61 site, likely reflecting the reported increased GTP occupancy of Q61 mutants (Buhrman et al., 2011; Hunter et al., 2015) and an increase in the number of K-Ras proteins available for pairing with the Rafs. Finally, incorporation of the RBD R > L mutation into each Raf member disrupted the Ras/Raf interaction in both the BRET and co-immunoprecipitation assays (Figures 1D–1F).

BRET Analysis Reveals Binding Preferences between Ras and Raf Family Members

To determine whether any of the Raf or Ras family members display preferential binding to one another in live cells, the ability of each Raf^{Reg} protein to interact with G12V or Q61R mutants of H-Ras, N-Ras, or K-Ras was monitored (Figures 2A and S1A). Surprisingly, differences in the $BRET_{max}$ and $BRET_{50}$ values were observed among the different pairings, revealing that the Rafs do not bind the Ras family members equivalently. For A-Raf and B-Raf, the highest $BRET_{max}$ and lowest $BRET_{50}$ values were observed when they were paired with mutant K-Ras. In contrast, when C-Raf was paired with mutant K-Ras, the $BRET_{max}$ signals were lower than those observed with mutant H-Ras or N-Ras; however, all the C-Raf/Ras pairings were of similar high affinity ($BRET_{50}$ values ranging from 0.165–0.172). As expected, the RBD R > L mutation significantly disrupted all Ras/Raf interactions (Figure 2A).

In co-immunoprecipitation assays (Figures 2B and S1B), C-Raf^{Reg} was detected at nearly equivalent levels in all the mutant Ras complexes. A-Raf^{Reg} was also observed in all Ras complexes, but binding to K-Ras was increased. Strikingly, B-Raf^{Reg} was found to co-immunoprecipitate almost exclusively with activated K-Ras. Of note, the observed co-immunoprecipitation

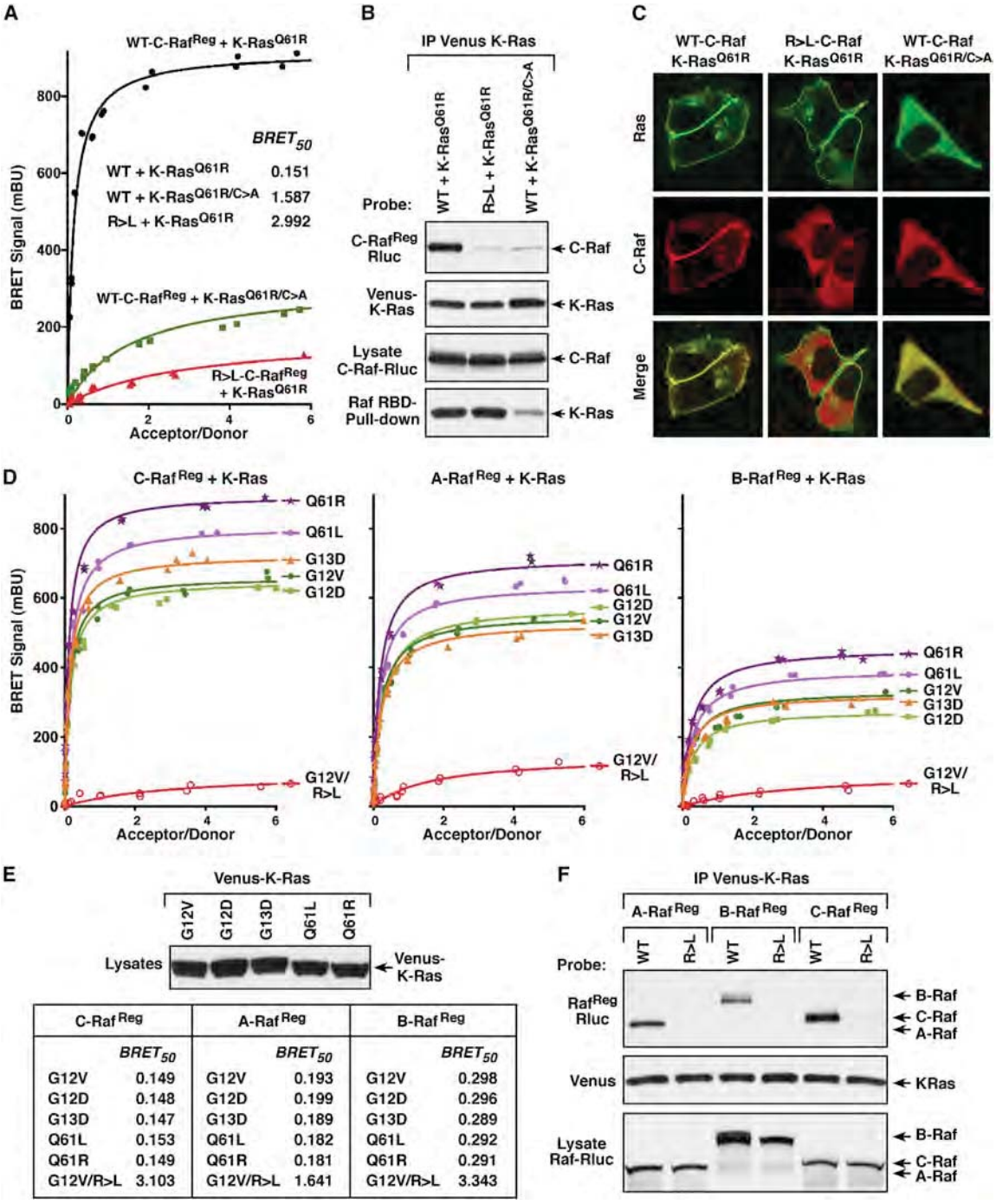

C-Raf^{Reg}		A-Raf^{Reg}		B-Raf^{Reg}	
	$BRET_{50}$		$BRET_{50}$		$BRET_{50}$
G12V	0.149	G12V	0.193	G12V	0.298
G12D	0.148	G12D	0.199	G12D	0.296
G13D	0.147	G13D	0.189	G13D	0.289
Q61L	0.153	Q61L	0.182	Q61L	0.292
Q61R	0.149	Q61R	0.181	Q61R	0.291
G12V/R>L	3.103	G12V/R>L	1.641	G12V/R>L	3.343

Figure 1. Analysis of Raf-Binding Interactions with Activated K-Ras Mutants

(A) BRET saturation curves are shown examining the interaction of WT or RBD mutant (R > L) C-Raf^{Reg}-Rluc proteins with Venus-K-Ras^{Q61R} and the interaction of WT C-Raf^{Reg}-Rluc with the CAAX mutant (C185A) Venus-K-Ras$^{Q61R/C>A}$. $BRET_{50}$ values are listed.

(B) K-Ras and C-Raf proteins analyzed in (A) were examined in co-immunoprecipitation assays. Venus-K-Ras proteins were also evaluated for GTP loading in Raf-RBD pull-down assays.

(C) Live-cell imaging shows the intracellular localization of the indicated K-Ras and C-Raf proteins.

(D) BRET saturation curves are shown examining the interaction of WT or R > L Raf^{Reg}-Rluc proteins with the indicated Venus-K-Ras mutants.

(E) $BRET_{50}$ values from (D) are listed and the expression level of the K-Ras mutants is shown.

(F) WT and R > L Raf^{Reg}-Rluc proteins were examined in co-immunoprecipitation assays for binding to Venus-K-Ras^{Q61R}. Lysates were also monitored for Raf^{Reg}-Rluc expression, and all experiments were conducted in 293FT cells.

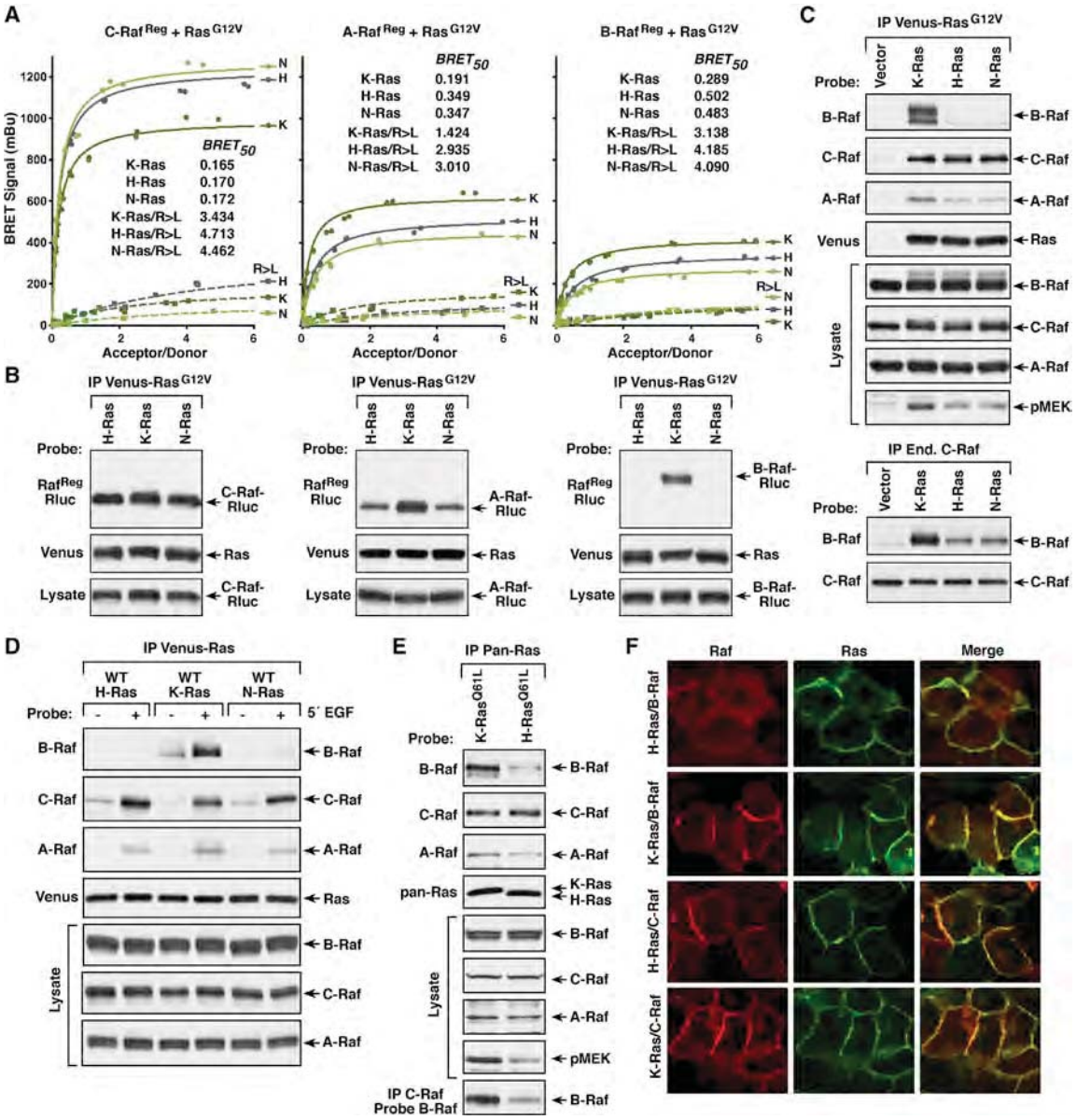

Figure 2. Binding Preferences between Ras and Raf Family Members

(A) BRET saturation curves examining the interaction of WT or R > L Raf^{Reg}-Rluc proteins with the Venus-Ras^{G12V} proteins are shown, and the BRET$_{50}$ values are listed.

(B) WT Raf^{Reg}-Rluc proteins were examined in co-immunoprecipitation assays for binding to the Venus-Ras^{G12V} proteins.

(C) Immunoprecipitated Venus-Ras^{G12V} complexes were probed for the presence of endogenous B-Raf, C-Raf, or A-Raf and Venus-Ras. Lysates were also examined for B-Raf, C-Raf, A-Raf, and pMEK levels (upper). Endogenous C-Raf complexes were isolated from cells expressing the indicated Venus-Ras^{G12V} proteins and examined for dimerization with B-Raf (lower).

(D) HeLa cells expressing WT Venus-Ras proteins were treated or not with EGF prior to lysis. Immunoprecipitated Venus-Ras complexes were probed for the presence of endogenous B-Raf, C-Raf, or A-Raf and Venus-Ras. Lysates were also examined for Raf levels.

(E) Ras complexes were immunoprecipitated from Ras-deficient MEFs re-expressing either K-Ras^{Q61L} or H-Ras^{Q61L} and probed for the presence of endogenous B-Raf, C-Raf, or A-Raf and Ras. Endogenous C-Raf was also isolated from the MEF lines and examined for dimerization with B-Raf. Lysates were examined for B-Raf, C-Raf, A-Raf, and pMEK levels.

(F) MCF10A cells stably expressing Halo-tagged K-Ras^{G12V} or H-Ras^{G12V} and B-Raf-Cherry or C-Raf-Cherry were examined by live-cell imaging to visualize recruitment of the Rafs to the plasma membrane. Experiments shown in (A)–(C) were conducted in 293FT cells.

See also Figure S1.

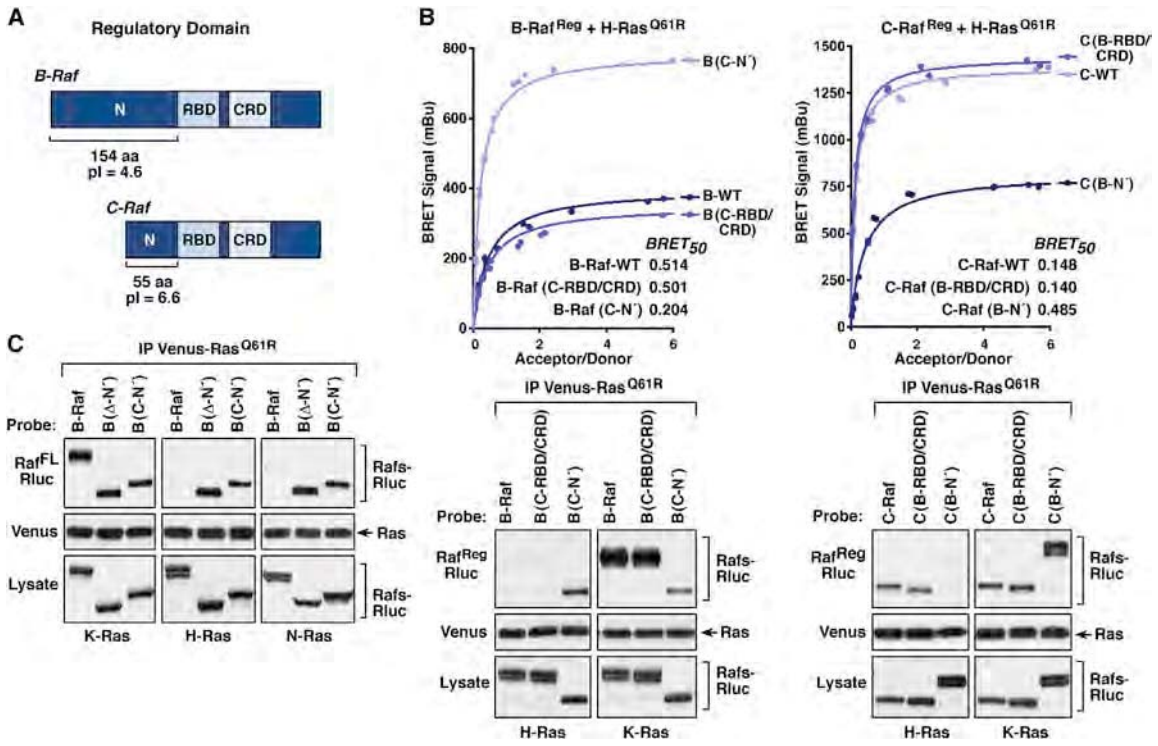

Figure 3. Raf N-Terminal Segment Determines the Ras Binding Selectivity

(A) Schematic depiction of the B-Raf and C-Raf regulatory domains with the RBD, CRD, and N′-segment indicated.

(B) Raf^{Reg}-Rluc proteins were generated in which the RBD/CRD or N′-segment of B-Raf and C-Raf were exchanged. BRET (upper) and co-immunoprecipitation assays (lower) were performed examining the interaction of WT or domain-exchanged Raf^{Reg}-Rluc proteins with Venus-tagged H-Ras^{Q61R} or K-Ras^{Q61R}. $BRET_{50}$ values are listed.

(C) WT full-length B-Raf^{FL}-Rluc or B-Raf^{FL}-Rluc proteins lacking the N′-segment (Δ-N′) or containing the N′-segment of C-Raf (C-N′) were examined for their ability to interact with the indicated Venus-Ras^{Q61R} proteins in co-immunoprecipitation assays. Lysates were also monitored for Raf-Rluc expression in (B and C), and all experiments were conducted in 293FT cells.

See also Figure S2.

results appear to align more closely with the $BRET_{50}$ values, which are reflective of the affinity of the interaction and are consistent with the fact that binding interactions detected in co-immunoprecipitation assays must be of sufficient strength to withstand detergent-based cell lysis and immunopurification.

Similar Ras binding preferences were observed when the endogenous Raf kinases were evaluated for their ability to co-immunoprecipitate with constitutively active Ras mutants or with growth-factor-activated WT Ras proteins (Figures 2C and 2D and S1C). Preferential binding of B-Raf to activated K-Ras was further confirmed in co-immunoprecipitation assays using Ras-deficient mouse embryonic fibroblasts (MEFs) (Drosten et al., 2010) reconstituted to express untagged H-Ras^{Q61L} or K-Ras^{Q61L} at endogenous levels (Figure 2E). Moreover, in live-cell imaging studies using MCF10A cell lines that stably express Halo-tagged H-Ras^{G12V} or K-Ras^{G12V} and Cherry-tagged B-Raf or C-Raf, the plasma membrane recruitment of B-Raf was significantly increased in cells expressing K-Ras^{G12V}, whereas strong membrane localization of C-Raf was observed in both cell lines (Figure 2F). Consistent with the preferred binding of B-Raf to K-Ras, mutant K-Ras was found to be the strongest driver of endogenous B-Raf/C-Raf dimer formation as well as downstream MEK activation (Figures 2C and 2E). Taken together, these findings indicate that C-Raf and K-Ras can bind with high affinity to all Ras or Raf family members respectively, whereas H-Ras displays preferential binding to C-Raf, and B-Raf exhibits a striking selectivity for K-Ras.

Role of the Raf N-Terminal Segment in Determining Ras Binding Selectivity

Given that B-Raf and C-Raf were found to exhibit the most divergent binding to Ras members, experiments were conducted to determine which regions of the Rafs might account for these differences. The Raf regulatory domain contains two conserved areas: the RBD and the membrane-binding cysteine-rich domain (CRD) (Hekman et al., 2002; Williams et al., 2000). However, preceding the RBD, there lies an N-terminal segment (N′-segment) that varies significantly among the Rafs (Figure 3A). In particular, the N′-segment of B-Raf is comprised of 154 amino acids and has an acidic isoelectric point (pI) of 4.6, whereas the C-Raf N′-segment contains 55 amino acids and has a more neutral pI of 6.6. Of note, the A-Raf N′-segment also has a neutral pI (6.9) and is 18 amino acids in length.

Therefore, B-Raf and C-Raf constructs were generated in which the N′-segments were exchanged, and the resulting proteins were evaluated in BRET and co-immunoprecipitation assays for binding interactions with activated H-Ras or K-Ras. As shown in Figure 3B, when the B-Raf N′-segment was replaced with that of C-Raf (B-Raf$^{(C\text{-}N')}$), the B-Raf/H-Ras interaction was significantly increased as $BRET_{max}$ signals were higher, $BRET_{50}$ values were lower, and B-Raf$^{(C\text{-}N')}$ could be detected in H-Ras immunoprecipitates. In contrast, replacing the C-Raf N′-segment with that of B-Raf (C-Raf$^{(B\text{-}N')}$) greatly reduced the C-Raf/H-Ras interaction. Consistent with the ability of K-Ras to engage all Raf kinases with high affinity, exchange of the Raf N′-segments had no significant effect on the affinity of K-Ras binding in either co-immunoprecipitation or BRET assays (Figures 3B and S2). Exchange of the conserved RBD-CRD domains was also evaluated and found to have little effect on Ras/Raf interactions.

The role of the N′-segment in determining the Ras binding selectivity of B-Raf was further confirmed in co-immunoprecipitation assays using full-length B-Raf proteins in which the N′-segment was either deleted (Δ-N′) or replaced with that of C-Raf (C-N′). As shown in Figure 3C, all B-Raf proteins were detected in K-Ras^{Q61R} complexes; however, only proteins lacking the B-Raf N′-segment were present in H-Ras or N-Ras complexes, suggesting that the B-Raf N′-segment may impede or obstruct high-affinity binding to H-Ras and N-Ras.

Contribution of the Ras Hypervariable Region to the Ras/Raf Interaction

Next, we sought to identify the region of the Ras proteins that likewise determines the Raf binding preferences. Members of the Ras family are highly conserved and diverge primarily at the C-terminal hypervariable region (HVR) (Figure 4A), which contains distinct signals for lipid processing and membrane attachment (Parker and Mattos, 2015; Prior and Hancock, 2012). All Ras proteins end with a CAAX motif, which is processed to yield a C-terminal farnesylated cysteine residue that is carboxymethylated. The H-Ras and N-Ras HVRs contain additional cysteine residues that are palmitoylated and function with the farneysl group to mediate plasma membrane attachment. In contrast, the K-Ras4B HVR uniquely contains a lysine-rich polybasic region (PBR) that aids in membrane binding.

To investigate whether the Ras HVRs might also contribute to the Raf binding preferences, Ras proteins were analyzed in which the HVRs of mutant K-Ras4B (amino acids 165–188) and H-Ras (amino acids 165–189) were exchanged. As shown in Figure 4B, placing the K-Ras4B HVR sequences onto H-Ras^{Q61R} increased the binding of B-Raf^{Reg} such that the $BRET_{max}$ signals and $BRET_{50}$ values were similar to those observed with K-Ras^{Q61R}. Conversely, exchanging the K-Ras4B HVR with that of H-Ras reduced the K-Ras^{Q61R}/B-Raf^{Reg} interaction to levels observed with H-Ras^{Q61R}. Moreover, B-Raf^{Reg} and endogenous B-Raf were only able to co-immunoprecipitate with Ras proteins that contained the K-Ras4B HVR (Figures 4B and S3A).

Consistent with the high-affinity binding of C-Raf to all Ras members, C-Raf^{Reg} and endogenous C-Raf were detected in all of the mutant Ras complexes, and all C-Raf^{Reg} pairings exhibited high-affinity $BRET_{50}$ values (Figures 4B and S3A). However, the highest $BRET_{max}$ signals were observed with proteins that contained the H-Ras HVR, suggesting that the H-Ras HVR sequence itself or the localization of these Ras proteins allows more C-Raf binding pairs to form. In addition, the K-Ras4A splice variant, whose HVR contains a palmitoylated cysteine residue instead of the PBR, interacted with the Rafs in a manner similar to H-Ras and N-Ras, as only C-Raf proteins could bind with sufficient affinity to co-immunoprecipitate with K-Ras4A^{Q61R} (Figures 4C and S3B).

The above findings suggest that the PBR-containing HVR of K-Ras4B also contributes to the B-Raf selectivity, and by utilizing a panel of previously characterized K-Ras^{G12V} PBR mutants (Zhou et al., 2017), we further found that the positive charge of the PBR was critical for high-affinity B-Raf binding. As shown in Figure 4D, substitution of each individual PBR lysine residue to an uncharged glutamine reduced binding of B-Raf^{Reg} but had little effect on C-Raf^{Reg} binding. Moreover, the reduction in B-Raf^{Reg} binding was equivalent for all the PBR mutants, correlating with an equivalent reduction in the net basic charge of the PBR. In addition, replacing all six lysine residues with similarly charged arginine residues (6R) had minimal effect on B-Raf^{Reg} binding; however, mutation of the serine phosphorylation site adjacent to the PBR to a phosphomimetic acidic residue (S181D) reduced the B-Raf^{Reg} interaction, whereas mutation of the site to a neutral alanine residue had little effect (Figure 4D). Similar results were obtained when a subset of these mutants was evaluated for binding to endogenous B-Raf or C-Raf or when they were assessed in BRET assays (Figures S3D and S3E).

Finally, to investigate whether the positively charged K-Ras PBR might interact with the negatively charged B-Raf N′-segment, several cancer-associated mutations that alter acidic residues in the B-Raf N′-segment were analyzed in co-immunoprecipitation assays (Figure 4E). Strikingly, the E46K mutation resulted in reduced binding of B-Raf^{Reg} to mutant K-Ras but increased binding to mutant H-Ras. Collectively, these findings support a model whereby the PBR contributes to the B-Raf/K-Ras interaction by engaging the B-Raf N′-segment, thus disrupting its inhibitory effect to facilitate high-affinity RBD contact.

Dimerization with C-Raf Can Influence the Affinity of the B-Raf/H-Ras^{Q61R} Interaction

B-Raf and C-Raf are known to form heterodimers, and, given that C-Raf exhibits high-affinity binding to all Ras proteins, experiments were initiated to determine whether B-Raf/C-Raf dimerization might alter the ability of B-Raf to interact with Ras members that lack the PBR. For these studies, full-length B-Raf proteins containing well-characterized mutations in the Raf dimer interface were utilized: dimerization-deficient R509H-B-Raf and dimerization-enhanced E586K-B-Raf. These mutants and WT-B-Raf were then evaluated in BRET and co-immunoprecipitation assays for binding to activated H-Ras or K-Ras. As indicated by the $BRET_{50}$ values, full-length WT-B-Raf (B-Raf^{FL}) exhibited a similar binding affinity to mutant H-Ras, as did the B-Raf^{Reg} protein, and showed little ability to co-immunoprecipitate with H-Ras (Figures 5A and 2A). The R509H mutant also displayed low-affinity binding to H-Ras, whereas E586K-B-Raf exhibited an increased binding affinity and co-immunoprecipitated with mutant H-Ras in a manner that correlated with its increased

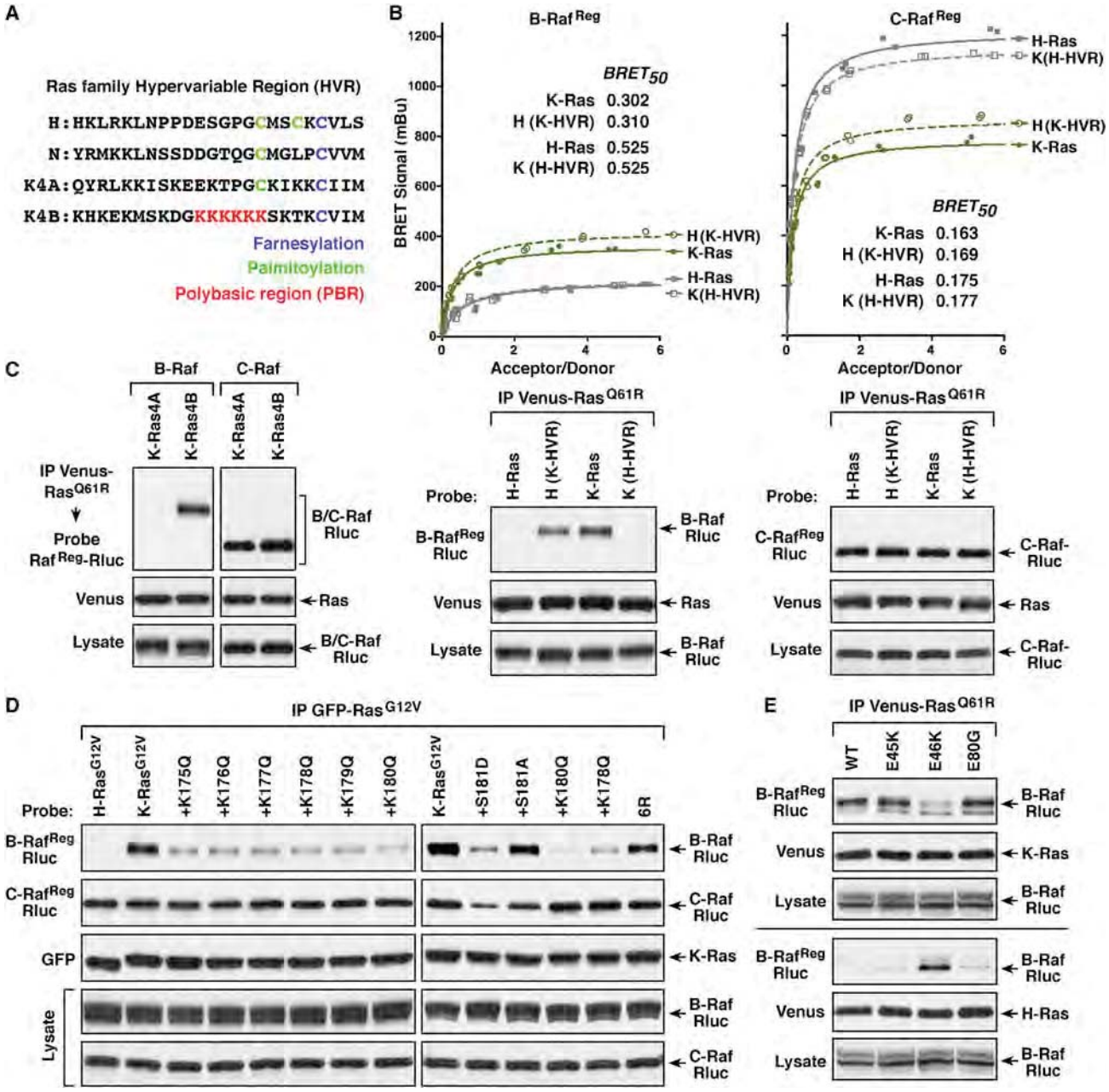

Figure 4. The Ras HVRs Contribute to the Ras/Raf Binding Preferences

(A) Shown are the HVR sequences of the various Ras proteins.

(B) Venus-Ras^{Q61R} proteins were generated in which the HVRs of H-Ras and K-Ras4B were exchanged. BRET (upper) and co-immunoprecipitation assays (lower) were performed examining the interaction of B-Raf^{Reg} or C-Raf^{Reg}-Rluc with WT or HVR-exchanged Venus-Ras^{Q61R} proteins. $BRET_{50}$ values are listed.

(C) Co-immunoprecipitation assays were performed examining the interaction of B-Raf^{Reg} or C-Raf^{Reg}-Rluc with Venus-tagged K-Ras4A^{Q61R} or K-Ras4B^{Q61R}.

(D) Cells co-expressing the indicated GFP-Ras^{G12V} proteins and B-Raf^{Reg} or C-Raf^{Reg}-Rluc were lysed, and GFP-Ras complexes were immunoprecipitated from the cell lysates and examined for Raf^{Reg}-Rluc binding.

(E) WT or N′-segment mutant B-Raf^{Reg}-Rluc proteins were examined in co-immunoprecipitation assays for binding to Venus-tagged K-Ras^{Q61R} or H-Ras^{Q61R}. Lysates were monitored for the indicated proteins in (B–E), and all experiments were conducted in 293FT cells.

See also Figure S3.

ability to dimerize with C-Raf (Figure 5A). As expected, all of the B-Raf^{FL} proteins bound mutant K-Ras with a similar high affinity (Figure S4A).

Further supporting the model that dimerization with C-Raf can facilitate the interaction between B-Raf and H-Ras, stabilizing B-Raf/C-Raf dimers by mutation of the ERK-mediated feedback

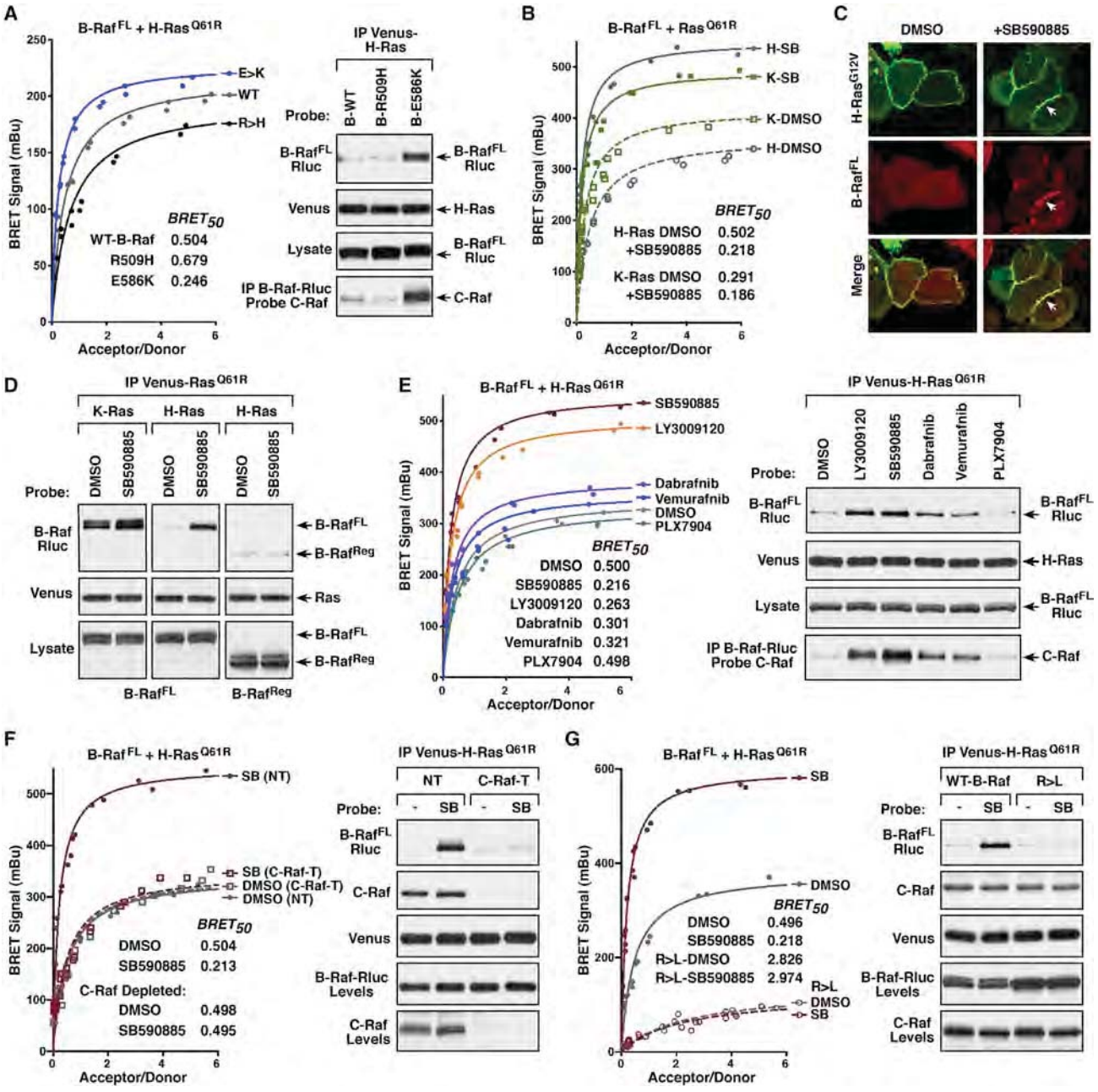

Figure 5. B-Raf/C-Raf Dimerization Can Modulate the B-Raf/H-Ras^{Q61R} Interaction

(A) BRET (left) and co-immunoprecipitation assays (right) are shown examining the interaction of WT, R509H (dimer-defective), or E586K (dimer-enhanced) B-Raf^{FL}-Rluc proteins with Venus-H-Ras^{Q61R}. The B-Raf^{FL}-Rluc proteins were also monitored for dimerization with C-Raf.

(B) BRET saturation curves were performed examining the effect of 1 h DMSO or Raf inhibitor SB590885 (SB) treatment on the interaction of B-Raf^{FL}-Rluc with Venus-tagged H-Ras^{Q61R} or K-Ras^{Q61R}. $BRET_{50}$ values are listed.

(C) MCF10A cells stably expressing Halo-H-Ras^{G12V} and B-Raf^{FL}-Cherry were treated for 1 h with DMSO or SB590885 prior to live-cell imaging. Recruitment of B-Raf to the plasma membrane in SB590885-treated cells is indicated by white arrows.

(D) 293FT cells expressing B-Raf^{FL}-Rluc with Venus-H-Ras^{Q61R} or Venus-K-Ras^{Q61R} or expressing B-Raf^{Reg}-Rluc with Venus-H-Ras^{Q61R} were treated for 1 h with DMSO or SB590885 prior to lysis. Immunoprecipitated Venus-Ras complexes were probed for B-Raf-Rluc and Venus-Ras.

(E) BRET (left) and co-immunoprecipitation (right) assays were performed examining the effect of various Raf inhibitors on the interaction of B-Raf^{FL}-Rluc with Venus-H-Ras^{Q61R}. $BRET_{50}$ values are listed. B-Raf^{FL}-Rluc proteins were also examined for dimerization with C-Raf.

(F) BRET (left) and co-immunoprecipitation (right) assays were performed examining the effect of SB590885 treatment on the interaction of B-Raf^{FL}-Rluc and Venus-H-Ras^{Q61R} in control (NT) or C-Raf-depleted (C-Raf-T) 293FT cells. $BRET_{50}$ values are listed. Co-immunoprecipitation of endogenous C-Raf with Venus-H-Ras^{Q61R} is also shown.

(legend continued on next page)

phosphorylation sites (which function to disrupt Raf dimerization) also resulted in increased B-Raf/H-Ras binding (Figure S4B). Of note, Ras proteins have also been proposed to dimerize; however, a mutation (D154Q) reported to impair Ras dimer formation (Ambrogio et al., 2018) was found to have little effect on Ras/Raf binding in either the BRET or co-immunoprecipitation assays (Figure S4C).

Stable B-Raf/C-Raf dimer formation can also be driven by treatment of cells with ATP-competitive Raf inhibitors (Durrant and Morrison, 2018). Therefore, we next used a B-Raf inhibitor known to strongly promote Raf dimerization, SB590885, to determine whether inhibitor treatment would alter B-Raf interactions (Figures 5B–5D). In the BRET system, SB590885 treatment resulted in a dramatic increase in binding of B-Raf^{FL} to mutant H-Ras, as evidenced by increased BRET$_{max}$ signals and reduced BRET$_{50}$ values (Figure 5B). SB590885 treatment also allowed B-Raf^{FL} to stably co-immunoprecipitate with mutant H-Ras (Figure 5D) and resulted in a significant increase in the membrane localization of B-Raf-Cherry in MCF10A cells expressing Halo-H-Ras^{G12V} (Figure 5C). Binding between B-Raf^{FL} and mutant K-Ras was also enhanced in SB590885-treated cells; however, the increases were not as pronounced (Figures 5B, 5D, and S5A). Importantly, the enhancing effect of SB590885 treatment required binding of the inhibitor to the B-Raf kinase domain as SB590885 treatment had no effect on the interaction of H-Ras and the B-Raf^{Reg} protein, which lacks the kinase domain that mediates Raf dimerization (Figures 5D and S5B).

When a panel of Raf inhibitors was evaluated, we found that all of the inhibitors tested, with the exception of the second-generation ''paradox-breaker'' inhibitor PLX7904 (Zhang et al., 2015), increased the level and affinity of the B-Raf^{FL}/H-Ras interaction and that the increased affinity correlated with the degree to which the inhibitors promoted B-Raf/C-Raf dimerization (Figure 5E). Further establishing C-Raf as a mediator of the upregulated interaction between B-Raf and H-Ras, depletion of endogenous C-Raf prevented SB590885 from increasing the B-Raf/H-Ras interaction in BRET or co-immunoprecipitation assays (Figure 5F). Finally, our findings suggest that inhibitor-stabilized B-Raf/C-Raf dimerization impacts the ability of B-Raf to directly contact H-Ras, as no increased binding to H-Ras was observed in SB590885-treated cells if the B-Raf^{FL} protein contained the RBD R > L mutation (Figure 5G).

Co-occurrence of B-Raf and H-Ras Mutations

Although H-Ras is not a prevalent driver of human cancer, 85% of Ras mutations in bladder cancer occur in *H-Ras,* and genomic analysis of metadata from cBioPortal and COSMIC databases indicates that mutations in *H-Ras* co-occur with *B-Raf* mutations at a statistically significant level (p value = 0.003). Strikingly, the majority of the co-occurring *B-Raf* mutations cause alterations in the B-Raf kinase domain that are known to promote increased dimerization with C-Raf (Yao et al., 2017). When a panel of these mutants was compared against WT-B-Raf^{FL} in the BRET and co-immunoprecipitation assays, all of the kinase domain mutants exhibited an increased affinity for H-Ras^{Q61R} that correlated with the extent to which the mutations augmented B-Raf/C-Raf dimerization (Figures 6A and S6A). In these cells, MEK activation was also increased, indicating enhanced H-Ras-driven signaling (Figures 6A and S6A). As was observed for Raf inhibitor treatment, the increased B-Raf/H-Ras interaction was dependent on C-Raf in that co-immunoprecipitation of the G466V- and D594G-B-Raf mutants with H-Ras^{Q61R} was reduced to background levels in C-Raf-depleted cells (Figure 6B). Moreover, the interaction with C-Raf again appeared to promote direct binding of G466V-B-Raf to H-Ras, as no increase in B-Raf/H-Ras co-immunoprecipitation was observed if G466V-B-Raf contained the RBD R > L mutation (Figure S6B).

Importance of C-Raf in H-Ras-Driven Signaling

Given that H-Ras binds C-Raf with the highest affinity and that C-Raf can promote increased B-Raf/H-Ras binding through B-Raf/C-Raf dimer formation, it is possible that C-Raf may be required for efficient transmission of H-Ras-mediated signals. To test this hypothesis, we first monitored the transformation potential of mutant H-Ras in focus-forming assays using NIH 3T3 cells that were depleted or not of endogenous C-Raf. As shown in Figure 6C, the number of foci induced by H-Ras^{G12V} expression was dramatically reduced (~80%) in cells lacking C-Raf, suggesting a dependence on C-Raf. In comparison, K-Ras^{G12V}-induced focus formation was only modestly affected by C-Raf loss (15%–20% reduction), and the effect of C-Raf depletion on H-Ras- and K-Ras-mediated transformation could be reversed by exchanging the C′-terminal HVR sequences (Figure 6C), further demonstrating the role of the Ras HVR in determining Raf engagement.

Next, we examined the effect of C-Raf depletion on the transformation potential and proliferative growth of two human cancer cell lines expressing mutant H-Ras proteins: T24 bladder carcinoma cells and the RL95-2 endometrial carcinoma line. Using the CRISPR/Cas9 system to individually deplete each of the Raf kinases or H-Ras, loss of C-Raf was found to reduce the 2D proliferative and 3D spheroid growth of T24 and RL95-2 cells to a similar extent as did H-Ras depletion, whereas loss of A-Raf or B-Raf had minimal effect (Figure 6D). When a similar analysis was performed on cancer lines expressing mutant K-Ras proteins, H358 lung carcinoma cells and the SW480 colorectal line, individually depleting each Raf member was found to have little effect on 2D proliferation. Spheroid growth could be reduced by depletion of either B-Raf or C-Raf; however, the effect was not as great as that observed for K-Ras depletion (Figure S6C). Taken together, the above depletion experiments demonstrate that C-Raf is critical for H-Ras-mediated transformation.

Finally, the cancer cell lines were utilized to further validate the effects of Raf inhibitor treatment on Ras/Raf binding. For these studies, previously characterized Ras antibodies (Waters et al., 2017) were used to selectively immunoprecipitate the

(G) BRET (left) and co-immunoprecipitation (right) assays were performed examining the effect of SB590885 treatment on the interaction of WT or R > L B-Raf^{FL}-Rluc with Venus-H-Ras^{Q61R}. BRET$_{50}$ values are listed. Co-immunoprecipitation of endogenous C-Raf with Venus-H-Ras^{Q61R} is also shown. Lysates were monitored for the indicated protein levels in (A, D, and E–G).
See also Figures S4 and S5.

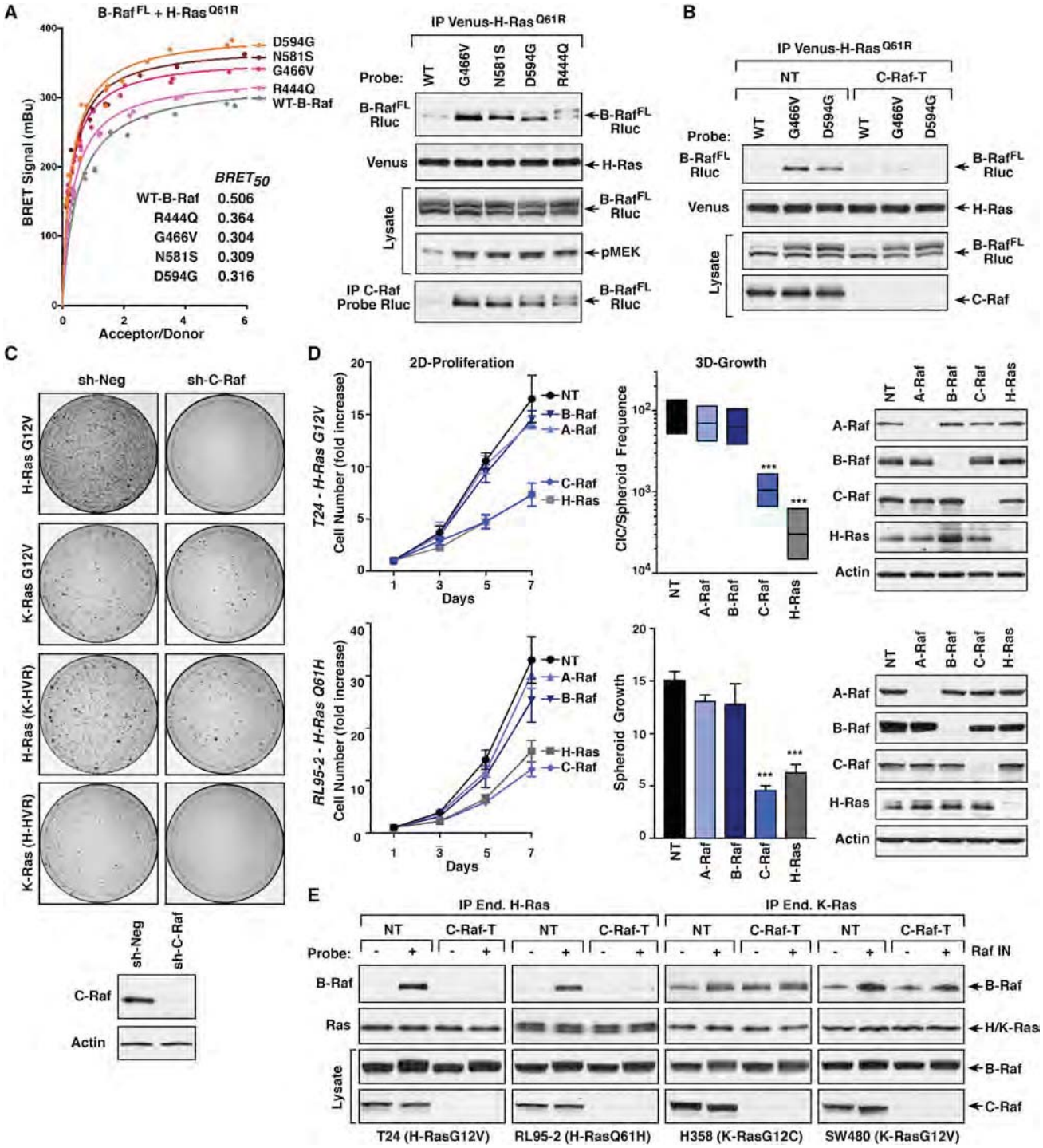

Figure 6. Co-occurring B-Raf and H-Ras Mutations in Cancer

(A) BRET (left) and co-immunoprecipitation assays (right) were performed comparing the interaction of WT and mutant B-Raf^{FL}-Rluc proteins with Venus-H-Ras^{Q61R}. $BRET_{50}$ values are listed. Endogenous C-Raf was also examined for dimerization with the B-Raf^{FL}-Rluc mutants. Lysates were monitored for pMEK and B-Raf-Rluc levels.

(B) Control (NT) or C-Raf-depleted (C-Raf-T) 293FT cells expressing WT, G466V, or D594G B-Raf^{FL}-Rluc with Venus-H-Ras^{Q61R} were examined in co-immunoprecipitation assays for binding of B-Raf^{FL}-Rluc to Venus-H-Ras^{Q61R}.

(C) Control (sh-Neg) or C-Raf-depleted (sh-C-Raf) NIH 3T3 cells were infected with retroviruses expressing the indicated Ras proteins. After two weeks of culture, focus formation was visualized by methylene blue staining. Shown are focus plates from a representative experiment.

(legend continued on next page)

endogenous mutant Ras proteins from cells that had been depleted or not of C-Raf (Figures 6E and S6D and S6E). In the mutant K-Ras lines, H358 and SW480, co-immunoprecipitation of B-Raf and mutant K-Ras was observed in the presence or absence of Raf inhibitor treatment, and depletion of C-Raf had no significant effect on the B-Raf/K-Ras interaction. However, for the mutant H-Ras lines, T24 and RL95-2, B-Raf was only detected in H-Ras immunoprecipitates from cells that had been treated with Raf inhibitor, and this interaction was reduced to background levels by C-Raf depletion (Figure 6E). These findings further support the model that B-Raf/C-Raf dimerization can allow mutant H-Ras to engage B-Raf with increased affinity and may provide an explanation for why melanoma patients treated with Raf inhibitors often developed secondary cancers driven by activating *H-Ras* mutations.

DISCUSSION

The Raf kinases are essential effectors of Ras signaling, and, although it has been over 20 years since they were first shown to possess a Ras-binding domain, whether these kinases differ in their ability to interact with an individual Ras family member in live cells has been unclear. In this study, we have utilized BRET technologies to further investigate the interactions of the Raf kinases with Ras members. In contrast to *in vitro* Ras/Raf binding studies, the BRET system allows for this important interaction to be monitored in the context of the plasma membrane and under conditions where post-translational modifications and lipid processing still occur, events that can strongly influence protein binding as well as signal progression. Despite the highly conserved nature of the Ras effector domains and the Raf RBDs, our findings reveal pronounced binding preferences between the Ras and Raf family members.

For all Ras proteins, C-Raf was found to exhibit the highest level and affinity of binding, followed by A-Raf, and then B-Raf, which surprisingly demonstrated a strong selectivity for K-Ras. These findings were further supported in co-immunoprecipitation studies, where the ability of the Ras/Raf interaction to withstand detergent cell lysis and immunopurification was found to correlate with lower $BRET_{50}$ values, which are indicative of higher binding affinities. The preferential binding of B-Raf to activated K-Ras was also observed in live-cell imaging experiments as well as in co-immunoprecipitation assays examining the ability of endogenous B-Raf to bind Ras members in cells overexpressing Venus-tagged Ras proteins, in Ras-deficient MEFs reconstituted to express untagged mutant H-Ras or K-Ras proteins at endogenous levels, and in human cancer cell lines harboring H-Ras or K-Ras mutant alleles.

Through the generation of various chimeric Ras and Raf proteins, we found that the B-Raf N′-segment and polybasic residues (PBR) in the K-Ras HVR account for the K-Ras binding selectivity of B-Raf. With regard to Ras members that lack the PBR, the B-Raf N′-segment, which carries an acidic charge and is 100–150 amino acids larger than the N′-segment of C-Raf or A-Raf, appears to act in an inhibitory manner as removal of the N′-segment allowed B-Raf to bind all Ras members with high affinity. It should be noted that our findings differ from a previous study where B-Raf was reported to bind with high affinity to farnesylated, GTP-bound H-Ras in surface plasmon resonance (SPR) assays (Fischer et al., 2007). However, in the SPR studies, B-Raf was coupled to the biosensor chip via a GST tag that was fused to the N′-segment, likely causing conformation changes or steric constraints that may have abrogated the inhibitory effect of the B-Raf N′-segment. In addition, the absence of crucial cellular components, including 14-3-3 dimers that stabilize the Raf autoinhibited state, and the lack of an authentic membrane environment, features which are preserved in the BRET system, may also contribute to the observed differences.

Nevertheless, through BRET, co-immunoprecipitation, and live-cell imaging experiments, all of our results indicate that the B-Raf N′-segment results in reduced binding to Ras proteins that lack the PBR. For these Ras members (H-Ras, N-Ras, and K-Ras4A), it is possible that the B-Raf N′-segment, with its increased size and acidic charge, might occlude the RBD or act to repel B-Raf from the negatively charged plasma membrane such that contact with the RBD cannot be established. However, for K-Ras, our findings suggest that basic residues in the PBR may engage acidic residues in the B-Raf N′-segment to disrupt its inhibitory effect and facilitate high-affinity RBD binding (model depicted in Figure 7). Support for this model comes from the observations that reducing the basic charge of the PBR as well as reversing the charge of an acidic residue in the B-Raf N′-segment could reduce the affinity of the B-Raf/K-Ras interaction. Although further studies are needed to fully define the points of contact between B-Raf and K-Ras, these findings indicate the existence of other interactions, in addition to RBD binding, that uniquely contribute to the B-Raf/K-Ras interaction.

The distinct binding properties of the various Ras and Raf proteins also suggest that certain Raf kinases may play a more important role in cancers driven by a specific Ras family member. For example, our results implicate C-Raf as being required for H-Ras-driven transformation in that depletion of C-Raf, but not B-Raf or A-Raf, could suppress cell proliferation and the spheroid growth of two human cancer cell lines expressing mutant H-Ras alleles, T24 and RL95-2. Moreover, in NIH 3T3 focus-forming assays, C-Raf depletion severely reduced the transformation potential of $H\text{-}Ras^{G12V}$, whereas it had only a modest effect on $K\text{-}Ras^{G12V}$-mediated transformation. Notably, C-Raf was also found to impact the H-Ras/B-Raf interaction as B-Raf mutations or drug treatments stabilizing B-Raf/C-Raf

(D) T24 and RL95-2 cells were infected with lentiviruses expressing Cas9 and either a non-targeting sgRNA (NT) or sgRNAs targeting *A-Raf*, *B-Raf*, *C-Raf*, or *H-Ras*. Cells were assessed for 2D proliferation (left), 3D growth (middle), and expression of A-Raf, B-Raf, C-Raf, or H-Ras proteins (right). Data are represented as mean ± SD. ***$p < 0.001$.

(E) Control (NT) or C-Raf-depleted (C-Raf-T) lines were serum-starved for 18 h and then treated for 1 h with DMSO or SB590885 prior to lysis. Endogenous mutant H-Ras proteins from T24 and RL95-2 cells and endogenous mutant K-Ras proteins from H358 and SW480 were immunoprecipitated and examined for the presence of endogenous B-Raf. Lysates were monitored for the indicated protein levels in (A–E).

See also Figure S6.

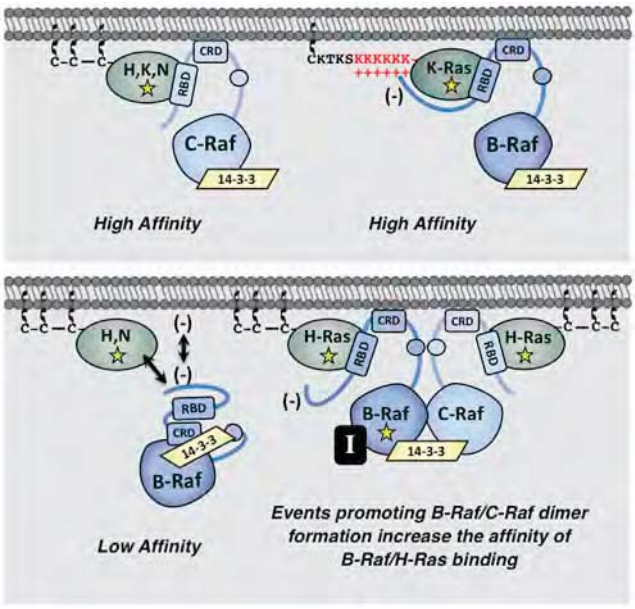

Figure 7. Model for Ras/Raf Binding Preferences

The C-Raf kinase exhibits high-affinity binding to all Ras family members. In contrast, B-Raf, whose N-terminal segment is larger and possesses an overall acidic charge, only binds with high affinity to mutant K-Ras, whose HVR contains a series of polybasic lysine residues (upper). In the context of H-Ras or N-Ras, the B-Raf N′-segment might occlude the RBD or act to repel B-Raf from the negatively charged plasma membrane. However, events that promote stable B-Raf/C-Raf dimer formation, such as B-Raf mutations (depicted as yellow star) or treatment with B-Raf inhibitors (black box containing the letter I), allow mutant H-Ras to engage B-Raf with increased affinity to upregulate ERK cascade signaling (lower).

dimerization significantly increased the affinity of B-Raf/H-Ras binding in a manner that required C-Raf (Figure 7). It is unclear whether dimerization with C-Raf alters the conformation of the B-Raf N-terminal domain or facilitates B-Raf localization at the membrane such that binding of H-Ras to the B-Raf RBD can occur. Nevertheless, augmented dimer formation with C-Raf appears to promote direct contact between B-Raf and mutant H-Ras, as no increase in H-Ras binding was observed if B-Raf contained the RBD R > L mutation.

Finally, our results indicate that the ability of C-Raf to facilitate the binding of B-Raf to non-PBR-containing Ras proteins may have important biological consequences. In particular, these findings likely explain why melanoma patients treated with the B-Raf inhibitors vemurafenib and dabrafenib often developed secondary cancers driven by *H-Ras* mutations (Boussemart et al., 2016; Oberholzer et al., 2012; Su et al., 2012). In this case, inhibitor-stabilized B-Raf/C-Raf dimerization would allow mutant H-Ras to engage B-Raf with increased affinity, thus upregulating ERK cascade signaling to levels that promote tumorigenesis. Likewise, B-Raf mutations that increase B-Raf/C-Raf dimerization and co-occur with oncogenic mutations in non-PBR-containing Ras members may be functionally relevant, acting to augment the signaling potential of these Ras mutants in human cancer. In conclusion, our study highlights the importance of elucidating the distinct roles of individual Ras and Raf family members in cell signaling and tumorigenesis and may aid in the design of new therapeutic strategies.

STAR★METHODS

Detailed methods are provided in the online version of this paper and include the following:

- KEY RESOURCES TABLE
- LEAD CONTACT AND MATERIALS AVAILABILITY
- EXPERIMENTAL MODEL AND SUBJECT DETAILS
  - Cell Lines and Culture Conditions
- METHOD DETAILS
  - DNA Constructs
  - BRET Assay
  - Transfection, Lysis, and Co-immunoprecipitation
  - Live-cell Imaging
  - Raf-RBD Pull-down Assays
  - shRNA and CRISPR/Cas9 Vectors
  - Recombinant Lentiviruses and Cell Infection
  - NIH 3T3 Focus Formation Assay
  - Cell Proliferation Assay
  - Transformation and Spheroid Growth Assays
- QUANTIFICATION AND STATISTICAL ANALYSIS
- DATA CODE AND AVAILABILITY

SUPPLEMENTAL INFORMATION

Supplemental Information can be found online at https://doi.org/10.1016/j.molcel.2019.09.004.

ACKNOWLEDGMENTS

We thank Linda Miller (LCDS) and Vanessa Wall (FNLCR Protein Expression Laboratory) for technical support. This project has been funded by federal funds from the National Cancer Institute, United States under project number ZIA BC 010329 (D.K.M.) and contract number HHSN261200800001E (D.E.), by federal funds from the National Institutes of Health, United States under grant number R01 GM124233 (J.F.H.), and from the Congressionally Directed Medical Research Program, United States LC160222 (R.L.K.).

AUTHOR CONTRIBUTIONS

E.M.T., R.L.K., and D.K.M. conceived the project, designed the experiments, and interpreted the data. E.M.T. performed the majority of the experiments (BRET and co-immunoprecipitation assays) with crucial help from D.E.D., D.A.R., and R.S.-S. (live-cell imaging, co-immunoprecipitation, and transformation assays); N.E.S. and E.S. (2D and 3D growth assays); and D.E., Y.Z., and J.F.H. (generation and analysis of critical reagents). E.M.T. and D.K.M. wrote the manuscript.

DECLARATION OF INTERESTS

The authors declare no competing interests.

Received: October 8, 2018
Revised: July 22, 2019
Accepted: September 5, 2019
Published: October 9, 2019

REFERENCES

Ambrogio, C., Köhler, J., Zhou, Z.W., Wang, H., Paranal, R., Li, J., Capelletti, M., Caffarra, C., Li, S., Lv, Q., et al. (2018). KRAS Dimerization Impacts MEK

Inhibitor Sensitivity and Oncogenic Activity of Mutant KRAS. Cell *172*, 857–868.e15.

Bos, J.L., Rehmann, H., and Wittinghofer, A. (2007). GEFs and GAPs: critical elements in the control of small G proteins. Cell *129*, 865–877.

Boussemart, L., Girault, I., Malka-Mahieu, H., Mateus, C., Routier, E., Rubington, M., Kamsu-Kom, N., Thomas, M., Tomasic, G., Agoussi, S., et al. (2016). Secondary Tumors Arising in Patients Undergoing BRAF Inhibitor Therapy Exhibit Increased BRAF-CRAF Heterodimerization. Cancer Res. *76*, 1476–1484.

Buhrman, G., Kumar, V.S., Cirit, M., Haugh, J.M., and Mattos, C. (2011). Allosteric modulation of Ras-GTP is linked to signal transduction through RAF kinase. J. Biol. Chem. *286*, 3323–3331.

Cox, A.D., and Der, C.J. (2010). Ras history: The saga continues. Small GTPases *1*, 2–27.

Dougherty, M.K., Müller, J., Ritt, D.A., Zhou, M., Zhou, X.Z., Copeland, T.D., Conrads, T.P., Veenstra, T.D., Lu, K.P., and Morrison, D.K. (2005). Regulation of Raf-1 by direct feedback phosphorylation. Mol. Cell *17*, 215–224.

Drosten, M., Dhawahir, A., Sum, E.Y., Urosevic, J., Lechuga, C.G., Esteban, L.M., Castellano, E., Guerra, C., Santos, E., and Barbacid, M. (2010). Genetic analysis of Ras signalling pathways in cell proliferation, migration and survival. EMBO J. *29*, 1091–1104.

Durrant, D.E., and Morrison, D.K. (2018). Targeting the Raf kinases in human cancer: the Raf dimer dilemma. Br. J. Cancer *118*, 3–8.

Fabian, J.R., Vojtek, A.B., Cooper, J.A., and Morrison, D.K. (1994). A single amino acid change in Raf-1 inhibits Ras binding and alters Raf-1 function. Proc. Natl. Acad. Sci. USA *91*, 5982–5986.

Fernández-Medarde, A., and Santos, E. (2011). Ras in cancer and developmental diseases. Genes Cancer *2*, 344–358.

Fischer, A., Hekman, M., Kuhlmann, J., Rubio, I., Wiese, S., and Rapp, U.R. (2007). B- and C-RAF display essential differences in their binding to Ras: the isotype-specific N terminus of B-RAF facilitates Ras binding. J. Biol. Chem. *282*, 26503–26516.

Freeman, A.K., Ritt, D.A., and Morrison, D.K. (2013). Effects of Raf dimerization and its inhibition on normal and disease-associated Raf signaling. Mol. Cell *49*, 751–758.

Hekman, M., Hamm, H., Villar, A.V., Bader, B., Kuhlmann, J., Nickel, J., and Rapp, U.R. (2002). Associations of B- and C-Raf with cholesterol, phosphatidylserine, and lipid second messengers: preferential binding of Raf to artificial lipid rafts. J. Biol. Chem. *277*, 24090–24102.

Hu, Y., and Smyth, G.K. (2009). ELDA: extreme limiting dilution analysis for comparing depleted and enriched populations in stem cell and other assays. J. Immunol. Methods *347*, 70–78.

Hu, J., Stites, E.C., Yu, H., Germino, E.A., Meharena, H.S., Stork, P.J.S., Kornev, A.P., Taylor, S.S., and Shaw, A.S. (2013). Allosteric activation of functionally asymmetric RAF kinase dimers. Cell *154*, 1036–1046.

Hunter, J.C., Manandhar, A., Carrasco, M.A., Gurbani, D., Gondi, S., and Westover, K.D. (2015). Biochemical and Structural Analysis of Common Cancer-Associated KRAS Mutations. Mol. Cancer Res. *13*, 1325–1335.

Inouye, K., Mizutani, S., Koide, H., and Kaziro, Y. (2000). Formation of the Ras dimer is essential for Raf-1 activation. J. Biol. Chem. *275*, 3737–3740.

Lavoie, H., and Therrien, M. (2015). Regulation of RAF protein kinases in ERK signalling. Nat. Rev. Mol. Cell Biol. *16*, 281–298.

Nan, X., Collisson, E.A., Lewis, S., Huang, J., Tamgüney, T.M., Liphardt, J.T., McCormick, F., Gray, J.W., and Chu, S. (2013). Single-molecule superresolution imaging allows quantitative analysis of RAF multimer formation and signaling. Proc. Natl. Acad. Sci. USA *110*, 18519–18524.

Oberholzer, P.A., Kee, D., Dziunycz, P., Sucker, A., Kamsukom, N., Jones, R., Roden, C., Chalk, C.J., Ardlie, K., Palescandolo, E., et al. (2012). RAS mutations are associated with the development of cutaneous squamous cell tumors in patients treated with RAF inhibitors. J. Clin. Oncol. *30*, 316–321.

Parker, J.A., and Mattos, C. (2015). The Ras-Membrane Interface: Isoform-specific Differences in The Catalytic Domain. Mol. Cancer Res. *13*, 595–603.

Pfleger, K.D., and Eidne, K.A. (2006). Illuminating insights into protein-protein interactions using bioluminescence resonance energy transfer (BRET). Nat. Methods *3*, 165–174.

Prior, I.A., and Hancock, J.F. (2012). Ras trafficking, localization and compartmentalized signalling. Semin. Cell Dev. Biol. *23*, 145–153.

Prior, I.A., Lewis, P.D., and Mattos, C. (2012). A comprehensive survey of Ras mutations in cancer. Cancer Res. *72*, 2457–2467.

Pylayeva-Gupta, Y., Grabocka, E., and Bar-Sagi, D. (2011). RAS oncogenes: weaving a tumorigenic web. Nat. Rev. Cancer *11*, 761–774.

Ritt, D.A., Monson, D.M., Specht, S.I., and Morrison, D.K. (2010). Impact of feedback phosphorylation and Raf heterodimerization on normal and mutant B-Raf signaling. Mol. Cell. Biol. *30*, 806–819.

Sanjana, N.E., Shalem, O., and Zhang, F. (2014). Improved vectors and genome-wide libraries for CRISPR screening. Nat. Methods *11*, 783–784.

Schubbert, S., Shannon, K., and Bollag, G. (2007). Hyperactive Ras in developmental disorders and cancer. Nat. Rev. Cancer *7*, 295–308.

Sheffels, E., Sealover, N.E., Theard, P.L., and Kortum, R.L. (2019). Anchorage-independent growth conditions reveal a differential SOS2 dependence for transformation and survival in RAS-mutant cancer cells. Small GTPases, 1–12.

Simanshu, D.K., Nissley, D.V., and McCormick, F. (2017). RAS Proteins and Their Regulators in Human Disease. Cell *170*, 17–33.

Su, F., Viros, A., Milagre, C., Trunzer, K., Bollag, G., Spleiss, O., Reis-Filho, J.S., Kong, X., Koya, R.C., Flaherty, K.T., et al. (2012). RAS mutations in cutaneous squamous-cell carcinomas in patients treated with BRAF inhibitors. N. Engl. J. Med. *366*, 207–215.

Waters, A.M., Ozkan-Dagliyan, I., Vaseva, A.V., Fer, N., Strathern, L.A., Hobbs, G.A., Tessier-Cloutier, B., Gillette, W.K., Bagni, R., Whiteley, G.R., et al. (2017). Evaluation of the selectivity and sensitivity of isoform- and mutation-specific RAS antibodies. Sci. Signal. *10*, eaao3332.

Williams, J.G., Drugan, J.K., Yi, G.S., Clark, G.J., Der, C.J., and Campbell, S.L. (2000). Elucidation of binding determinants and functional consequences of Ras/Raf-cysteine-rich domain interactions. J. Biol. Chem. *275*, 22172–22179.

Yao, Z., Yaeger, R., Rodrik-Outmezguine, V.S., Tao, A., Torres, N.M., Chang, M.T., Drosten, M., Zhao, H., Cecchi, F., Hembrough, T., et al. (2017). Tumours with class 3 BRAF mutants are sensitive to the inhibition of activated RAS. Nature *548*, 234–238.

Zhang, C., Spevak, W., Zhang, Y., Burton, E.A., Ma, Y., Habets, G., Zhang, J., Lin, J., Ewing, T., Matusow, B., et al. (2015). RAF inhibitors that evade paradoxical MAPK pathway activation. Nature *526*, 583–586.

Zhou, Y., Prakash, P., Liang, H., Cho, K.J., Gorfe, A.A., and Hancock, J.F. (2017). Lipid-Sorting Specificity Encoded in K-Ras Membrane Anchor Regulates Signal Output. Cell *168*, 239–251.e16.

STAR★METHODS

KEY RESOURCES TABLE

REAGENT or RESOURCE	SOURCE	IDENTIFIER
Antibodies		
B-Raf (H-145) rabbit polyclonal	Santa Cruz Biotechnology	cat# sc-9002; RRID:AB_2067494
B-Raf (F-7) mouse monoclonal	Santa Cruz Biotechnology	cat# sc-5284; RRID:AB_2721130
C-Raf (C-12) rabbit polyclonal	Santa Cruz Biotechnology	cat# sc-133; RRID:AB_632305
C-Raf mouse monoclonal	BD Pharmagen	cat# 610152; RRID:AB_397553
A-Raf (C-20) rabbit polyclonal	Santa Cruz Biotechnology	cat# sc-408; RRID:AB_630882
H-Ras (C-20) rabbit polyclonal	Santa Cruz Biotechnology	cat# sc-520; RRID:AB_631670
N-Ras (F155) mouse monoclonal	Santa Cruz Biotechnology	cat# sc-31; RRID:AB_628041
K-Ras mouse monoclonal	Sigma	cat# WH0003845M1; RRID:AB_1842235
pS217/221-MEK rabbit polyclonal	Cell Signaling Technology	cat# 9121; RRID:AB_331648
Rluc rabbit polyclonal	MBL International	cat# PM047; RRID:AB_1520866
GFP mouse monoclonal	Roche	cat# 11814460001; RRID:AB_390913
GFP rat monoclonal	MBL International	cat# D153-3; RRID:AB_591817
Pan-Ras [EPR3255] rabbit monoclonal	Abcam	cat# 108602; RRID:AB_10891004
Pan-Ras [Ras10] mouse monoclonal	EMD Millipore	cat# 05-516; RRID:AB_11211664
Actin (I-19) goat polyclonal	Santa Cruz Biotechnology	cat# sc-1616; RRID:AB_630836
Donkey anti-goat IgG-HRP	Santa Cruz Biotechnology	cat# sc-2020; RRID:AB_631728
Donkey anti-rabbit IgG-HRP	GE Healthcare	cat# NA934; RRID:AB_772206
Sheep anti-mouse IgG-HRP	GE Healthcare	cat# NA931; RRID:AB_772210
Goat anti-rat IgG-HRP	Cell Signaling Technology	cat# 7077; RRID:AB_10694715
Chemicals, Peptides, and Recombinant Proteins		
Vemurafenib (PLX4032)	SelleckChem	Cat# S1267
Dabrafenib (GSK2118436)	SelleckChem	Cat# S2807
LY3009120	SelleckChem	Cat# S7842
PLX7904	SelleckChem	Cat# S7964
SB-590885	SelleckChem	Cat# S2220
Coelenterazine-h	Promega	Cat# S2011
Halo Oregon Green ligand	Promega	Cat# G2802
Epidermal Growth Factor (EGF)	ThermoFisher	cat# PHG0311
GST-RBD	Millipore	cat# 14-863
X-tremeGENE 9	Roche/Sigma	cat# 06365809001
Collagen, Human Placenta Type IV	Millipore/Sigma	cat# C7521
Critical Commercial Assays		
CellTiter-Glo 2.0	Promega	cat# G9241
TransIT®-Lenti Transfection Reagent	Mirus	cat# MIR 6603
Mission Lentiviral Packaging Mix	Sigma	cat# SHP001
GeneArt Seamless Cloning and Assembly Kit	Life Technologies	cat# A13288
QuickChange II Kit	Agilent	cat# 200523
Deposited Data		
Raw data of immunoblots and live cell imaging	Mendeley Data	https://doi.org/10.17632/r6vvxjpskf.1
Experimental Models: Cell Lines		
293FT (human)	Invitrogen	cat# R70007
Phoenix-Eco (human)	ATCC	cat# CRL-3214; RRID:CVCL_H717

(*Continued on next page*)

Continued

REAGENT or RESOURCE	SOURCE	IDENTIFIER
NIH 3T3 (mouse)	ATCC	cat# CRL-1658; RRID:CVCL_0594
HeLa (human, female)	ATCC	cat# CCL-2; RRID:CVCL_0030
SW480 (human, male)	ATCC	cat# CCL-228; RRID:CVCL_0546
RL95-2 (human, female)	ATCC	cat# CRL-1671; RRID:CVCL_0505
H358 (human, male)	ATCC	cat# CRL-5807; RRID:CVCL_1559
T24 (human, female)	ATCC	cat# HTB-4; RRID:CVCL_0554
MCF10A (human, female)	ATCC	cat# CRL-10317; RRID:CVCL_0598
Ras−/− MEF + KRas Q61L (mouse)	NCI-Ras Initiative	N/A
Ras−/− MEF + HRas Q61L (mouse)	NCI-Ras Initiative	N/A
Oligonucleotides		
CRISPR A-Raf sgRNA (TGGTCTACCGACTCATCAAG)	This paper	N/A
CRISPR B-Raf sgRNA (GGGCCAGGCTCTGTTCAACG)	This paper	N/A
CRISPR C-Raf sgRNA (GCCGAACAAGCAAAGAACAG)	This paper	N/A
CRISPR H-Ras sgRNA (ACGGAATATAAGCTGGTGG)	Sheffels et al., 2019	N/A
CRISPR K-Ras sgRNA (TCATTGCACTGTACTCCTCT)	Sheffels et al., 2019	N/A
CRISPR NT sgRNA (CCATATCGGGGCGAGACATG)	Sheffels et al., 2019	N/A
shCRaf (CGGAGATGTTGCAGTAAAGAT)	Open Biosystems	TRCN0000001066
Recombinant DNA		
pLHCX-WT-Raf^{Reg}-Rluc8 (A-, B-, C-Raf)	This paper	N/A
pLHCX-R > L-Raf^{Reg}-Rluc8 (A-, B-, C-Raf)	This paper	N/A
pLHCX-Raf^{FL}-Rluc8 (A-, B-, C-Raf)	This paper	N/A
pLHCX-C-Raf^{Reg}/B-Raf N'-segment-Rluc8	This paper	N/A
pLHCX-C-Raf^{Reg}/B-Raf RBD/CRD-Rluc8	This paper	N/A
pLHCX-B-Raf^{Reg}/C-Raf N'-segment-Rluc8	This paper	N/A
pLHCX-B-Raf^{Reg}/C-Raf RBD/CRD-Rluc8	This paper	N/A
pLHCX-B-Raf^{Reg} N'segment mutants-Rluc8	This paper	N/A
pLHCX-B-Raf^{FL} kinase domain mutants-Rluc8	This paper	N/A
pLHCX-R188L-B-Raf^{FL}-Rluc8	This paper	N/A
pUBC-Raf-mCherry (B-, C-Raf)	NCI-Ras Initiative	N/A
pCMV5-Venus-Ras^{Q61R} (H-, N-, K-Ras4A, 4B)	NCI-Ras Initiative	N/A
pCMV5-Venus-Ras^{G12V} (H-, N-, K-Ras4B)	NCI-Ras Initiative	N/A
pCMV5-Venus-Ras^{G12D} (H-, N-, K-Ras4B)	NCI-Ras Initiative	N/A
pCMV5-Venus-Ras^{G13D} (H-, N-, K-Ras4B)	NCI-Ras Initiative	N/A
pCMV5-Venus-Ras^{Q61L} (H-, N-, K-Ras4B)	NCI-Ras Initiative	N/A
pCMV5-Venus-WT Ras (H-, N-, K-Ras4B)	NCI-Ras Initiative	N/A
pCMV5-Halo-Ras^{G12V} (H-, K-Ras4B)	NCI-Ras Initiative	N/A
EGFP-K-Ras4B^{G12V} PBR mutants	Zhou et al., 2017	N/A
pCMV-Venus-H-Ras^{Q61R}/K-Ras4B HVR	NCI-Ras Initiative	N/A
pCMV-Venus-K-Ras^{Q61R}/H-Ras HVR	NCI-Ras Initiative	N/A
pLKO.1 lentiviral vector	Open Biosystems/Dharmacon	cat# RHS4080
pLKO.1 shCRaf lentiviral construct	Open Biosystems/Dharmacon	cat# RHS3979-201733340; TRCN0000001066
pLentiCRISPRv2	Addgene	cat# 52961
Software and Algorithms		
GraphPad Prism	GraphPad	https://www.graphpad.com
ImageJ	ImageJ	https://imagej.nih.gov/ij/

LEAD CONTACT AND MATERIALS AVAILABILITY

Further information and requests for resources and reagents should be directed to and will be fulfilled by the Lead Contact, Deborah Morrison (morrisod@mail.nih.gov). Plasmids and cell lines are available for use upon request to the Lead Contact.

EXPERIMENTAL MODEL AND SUBJECT DETAILS

Cell Lines and Culture Conditions

293FT, NIH 3T3, Phoenix-Eco, RL95-2, and RAS-deficient MEFs were cultured in DMEM. H358 cells were cultured in RPMI, T24 cells in McCoy's 5a, and SW480 in L-15. All media was supplemented with 10% fetal bovine serum (FBS), 2 mM L-glutamine, and 1% penicillin/streptomycin. MCF10A cells were cultured in DMEM/F12 supplemented with 5% horse serum, 0.5 μg/mL hydrocortisone, 20 ng/mL EGF, 100 ng/mL cholera toxin, 10 μg/mL insulin, and 1% penicillin/streptomycin. All cell lines were cultured at 37°C under 5% CO_2 except for SW480 cells, which were cultured at 37°C under atmospheric conditions. Ras-deficient MEFs were sequenced by the provider (NCI-Ras Initiative) to confirm loss of endogenous Ras and integration of the transgene.

METHOD DETAILS

DNA Constructs

The full-length Raf kinases and the Raf regulatory domain proteins were tagged at the C terminus with the Rluc8 enzyme and cloned into the pLHCX-CMV vector. The Raf regulatory domain constructs encode amino acids 1-288 of A-Raf, amino acids 1-435 of B-Raf, and amino acids 1-327 of C-Raf. Chimeric Raf proteins with various regions in the Raf regulatory domain exchanged were constructed using the GeneArt Seamless Cloning and Assembly Kit from Life Technologies. The Raf regions exchanged are based on the following amino acid designations: B-Raf N'-segment: amino acids 1-154, B-Raf RBD/CRD: amino acids 155-280, C-Raf N'-segment: amino acids 1-55, C-Raf RBD/CRD: amino acids 56-184. The Ras family members were tagged at the N terminus with the Venus fluorophore and cloned into the pCMV5 vector. For Ras HVR-exchanged constructs, the HVR of K-Ras4B was defined as amino acids 165-188, and the HVR of H-Ras as amino acids 165-189. Point mutations were generated by site-directed mutagenesis using the QuickChange II Kit from Agilent.

BRET Assay

293FT cells were seeded into 12-well dishes at a concentration of $1x10^5$ cells/well. 16 h after plating, Venus-tagged and Rluc8-tagged constructs were transfected into cells using a calcium phosphate protocol. A 12-point saturation curve was generated in which the concentration of the energy donor construct (Rluc8) was held constant (62.5 ng) as the concentration of the energy acceptor plasmid (Venus) increased (0-1.0 μg). Live cells were collected 48 h after transfection, washed, and plated in PBS. The Rluc8 cofactor coelenterazine-h was added to a final concentration of 3.375 μM, and the BRET signal read 2 min after addition. The BRET signal was measured at 535 nm (bandwidth 30 nm) on the PHERAstar *Plus* plate reader (BMG Labtech) and the Rluc8 signal was simultaneously measured at 475 nm (bandwidth 30 nm). Venus fluorescence was measured independently using an excitation wavelength of 485 nm (5 nm bandwidth), and the emission spectra measured at 530 nm (5 nm bandwidth) on the Tecan Infinite M1000 plate reader. The BRET value for each data point was calculated by dividing the BRET ratio (BRET/Rluc8) by the background signal. The acceptor/donor ratio was equalized against a control where equal quantities of Venus and Rluc8 constructs were transfected. Data was analyzed using GraphPad Prism. Non-linear regression was used to plot the best fit hyperbolic curve and values for $BRET_{max}$ and $BRET_{50}$ were obtained from the calculated best fit curves.

Transfection, Lysis, and Co-immunoprecipitation

The indicated cell lines were plated at ~70% confluency 18-24 h prior to transfection. Cells were then transfected using the XtremeGENE9 transfection reagent per the manufacturer's instructions, using a 2:1 ratio of XtremeGENE9 to DNA. For cell lysis, cells were washed twice with ice cold PBS and lysed for 15 min at 4°C in1% NP-40 buffer (20mM Tris [pH 8.0], 137 mM NaCl, 10% glycerol, 1% NP-40 alternative, 0.15 U/mL aprotinin, 1 mM phenylmethylsulfonyl fluoride, 0.5 mM sodium vanadate, 20 μM leupeptin). Lysates were clarified by centrifugation at 14,000 rpm for 10 min at 4°C, following which the protein content was determined by Bradford assays. Lysates containing equivalent amounts of protein were incubated with the appropriate antibody and protein G Sepharose beads for 2 h at 4°C on a rocking platform. Complexes were washed extensively with 1% NP-40 buffer and then examined by immunoblot analysis along with aliquots of equalized lysate.

Live-cell Imaging

293FT or MCF10A cells expressing the indicated Halo- and mCherry-tagged proteins were plated onto collagen-coated glass surfaces (10 μg/mL human placenta type IV collagen). On the day of live cell imaging experiments, cells were washed with media lacking phenol red and incubated with the Halo Oregon green ligand for 15-30 min at 37°C. Cells were then washed in phenol red-free media and maintained in growth media lacking phenol red for the duration of image acquisition using either Zeiss Axiovert Z1 and LSM710.

Raf-RBD Pull-down Assays

To monitor the GTP-bound state of Ras, equalized cell lysates containing 5 μM $MgCl_2$ were incubated with GST-tagged Raf-RBD bound to glutathione-Sepharose beads (Millipore) for 1 h at 4°C on a rocking platform. Complexes were washed extensively with 1% NP-40 buffer and then examined by immunoblot analysis.

shRNA and CRISPR/Cas9 Vectors

For depletion of C-Raf protein levels in NIH 3T3 cells, pLKO.1 lentiviral vectors expressing shC-Raf (TRCN0000001066) sequences were obtained from Open Biosystems. For CRISPR/Cas9 studies, a non-targeting (NT), single guide RNA (sgRNA) or sgRNAs targeting the *A-Raf, B-Raf*, *C-Raf*, *H-Ras*, or *K-Ras* gene were each cloned into pLentiCRISPRv2 (Sanjana et al., 2014).

Recombinant Lentiviruses and Cell Infection

For protein depletion experiments, lentiviral particles expressing the desired targeting constructs were generated by co-transfecting the pLKO.1 or pLentiCRISPRv2 constructs with the MISSION lentiviral packaging mix (Sigma) into 293T cells using the Mirus Trans-IT lenti transfection kit. 48 h post-transfection, viral supernatants were collected, centrifuged twice at 1500 rpm for 7 min, and either stored at −80°C or used directly. Cells were infected with viral supernatants containing 8 μg/mL polybrene. 48 h post-infection, cells were placed into selection media containing 6 μg/mL puromycin for 4 days and then shifted into media containing 3 μg/mL puromycin for an additional 6 days, prior to analysis. For protein expression studies, lentiviral particles were generated by co-transfecting the pUBC-Raf-mCherry or pCMV-Halo-Ras^{G12V} constructs with packaging plasmids pMD2.G and psPAX2 (3:1:2 ratio) into 293T cells using XtremeGENE9. 48 h post-transfection, viral supernatants were collected, centrifuged twice at 1500 rpm for 7 min, and either stored at −80°C or used directly. MCF10A cells were infected with lentivirus supernatants containing 8 μg/mL polybrene for 24 h, following which growth media supplemented with the appropriate antibiotic selection was added (Puromycin: 1 μg/mL, Hygromycin: 40 μg/mL).

NIH 3T3 Focus Formation Assay

Recombinant retroviruses expressing Halo-H-Ras^{G12V} or Halo-K-Ras^{G12V} constructs were generated by transfecting the pBabe-Halo-Ras constructs into Phoenix-Eco cells using the X-tremeGENE9 protocol described above. Viral supernatants were collected 3 days post-transfection, centrifuged twice at 1500 rpm for 7 min, and either stored at −80°C or used directly. Control (shNeg) or C-Raf-depleted (shC-Raf) NIH 3T3 cells were plated into 60 mm dishes at a concentration of 2×10^5/dish. After 18 h, cells were infected with the indicated recombinant retrovirus in media containing 4% FBS and 8 μg/mL polybrene for 24 h. Cells were trypsinized and plated into two 100 mm dishes, one of which contained 5 μg/mL puromycin. After two weeks of culture, cells were fixed with 3.7% formaldehyde and stained with 1% methylene blue.

Cell Proliferation Assay

Cell proliferation was assessed using the CellTiter-Glo 2.0 Reagent (Promega) with luminescence determined using a GloMax Discover Plate Reader (Promega). 1×10^3 cells were seeded into white-walled cell culture-coated 96-well plates (Promega). Cell number was assessed 24 h after plating (day 1) and then every 48 h for 7 days. Data were analyzed as an increase in luminescence over day 1.

Transformation and Spheroid Growth Assays

Transformation of T24 cells was assessed by CSC/spheroid frequency as previously described (Inouye et al., 2000). Briefly, serially diluted T24 cells were seeded into ultra-low attachment 96-well, flat-bottomed plates (1 cell /well – 1000 cells/well, Corning Corstar #3474), with 24 wells per condition. Cells were cultured for 7-10 days, and wells with spheroids > 100 μm were scored as spheroid positive. CSC/CIC frequency was calculated by ELDA website (http://bioinf.wehi.edu.au/software/elda/) (Hu and Smyth, 2009). Spheroid growth of R95-2, H358 and SW480 cells were conducted as described in (Sheffels et al., 2019). RL95-2, H358 or SW480 cells were seeded at 500-1000 cells/well in ultra-low attachment 96-well round bottomed plates (Corning Costar #7007). Cell number was assessed 18 h after plating to allow spheroids to form (day 0), and then at day 7 using CellTiter-Glo 2.0 reagent (Promega), which measures ATP content as a surrogate of overall cell number. Spheroid growth for each cell line was normalized to the CellTiter Glo signal at day 0, and the results are expressed as a fold-increase over day 0.

QUANTIFICATION AND STATISTICAL ANALYSIS

BRET data were transferred to GraphPad Prism for statistical analysis and curve fitting. Data was plotted as the acceptor to donor ratios versus mBRET values. Non-linear regression was used to fit a hyperbolic curve to the dataset and determine R-squared values. The $BRET_{max}$ and $BRET_{50}$ values as well as the corresponding 95% confidence intervals were calculated using GraphPad Prism8 software. For cell proliferation and spheroid growth assays, replicate wells (n = 6 per experiment) were seeded into 96-well plates and cell number was quantified at the indicated times. Data represent 3 independent experiments and are presented as mean ±

SD. Significance was determined by ANOVA using the Tukey's multiple comparisons test and calculatedusing GraphPad Prism8 software. The co-immunoprecipitation, live cell imaging, and BRET experiments shown are representative and reflect at least 3 independent experiments.

DATA CODE AND AVAILABILITY

The datasets analyzed during this study are available at cBioPortal [http://www.cbioportal.org] and COSMIC [https://cancer.sanger.ac.uk/cosmic]. Raw data of immunoblots and live cell imaging are available through Mendeley Data (https://doi.org/10.17632/r6vvxjpskf.1). This study did not generate any code.

NIH NATIONAL CANCER INSTITUTE

SOS signaling in RAS-mutated cancers

Subscribe

June 29, 2020, by Erin Sheffels and Rob Kortum

Rob Kortum earned his Ph.D. with Rob Lewis at the University of Nebraska Medical Center, and trained with both Larry Samelson and Deborah Morrison at NCI. He is an assistant professor of Pharmacology at Uniformed Services University in Bethesda, MD.

Erin Sheffels trained with Dr. Kortum and earned her Ph.D. in May 2020. She plans to do her postdoctoral work with Gina Razidlo at Mayo Clinic.

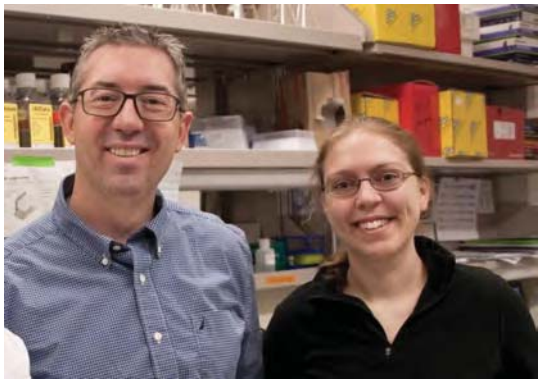

Rob Kortum, MD, PhD, and Erin Sheffels, PhD

RAS-mutated tumors were originally thought to proliferate independently of upstream signaling inputs, but we now know that receptor tyrosine kinase-dependent activation of both mutant RAS and non-mutated wild-type (WT) RAS plays an important role in modulating downstream effector signaling and driving therapeutic resistance in RAS-mutated cancers. The contributions of wild-type RAS to proliferation and transformation in RAS-mutated cancer cells places renewed interest in upstream signaling molecules, including the RasGEFs SOS1 and 2, as potential therapeutic targets in RAS-mutated cancers.

RAS isoforms have a hierarchy of abilities to activate RAS effectors

Mutant RAS-dependent transformation requires both Raf/MEK/ERK and PI3K/AKT effector pathway activation. However, while HRAS, NRAS, and KRAS can all interact with PI3K and RAF, a series of seminal papers showed that they activate these effectors to different extents, such that there is an inverse relationship in their ability to activate Raf and PI3K: mutant HRAS is a potent activator of PI3K but a poor activator of RAF, and conversely KRAS is a potent activator of Raf but a poor activator of PI3K (1-3). We are beginning to understand the mechanism for the differential activation of RAF proteins. The Morrison laboratory recently showed that BRAF preferentially interacts with KRAS via an interaction between the KRAS(4B) polybasic region and an acidic N-terminal region in BRAF (4). The ability to directly associate with both BRAF and CRAF makes KRAS a more potent activator of the RAF/MEK/ERK cascade. While the precise mechanism for differential PI3K activation between HRAS and KRAS remains unclear, a major contributor seems to be the polybasic stretch in the hypervariable region of KRAS; mutating basic residues in the KRAS(4B) HVR inhibits Raf/MEK/ERK

signaling but enhances PI3K/AKT phosphorylation (5). These differences in activation abilities impact the dependence of *RAS*-mutated cancers on upstream signals. For example, PI3K/AKT pathway activation is dependent on RTK signaling in *KRAS*-mutated colorectal (6) and lung (7) adenocarcinoma cells. A potential role for the WT RAS isoforms is to activate the effector pathways that mutant RAS does not strongly activate, making the cellular outcome a product of signaling by both WT and mutant RAS.

Mutant RAS can activate WT RAS via SOS

Mutant RAS can activate WT RAS independently of RTK input by at least two interdependent mechanisms. First, SOS1 can be allosterically activated by RAS, allowing increased activation of WT RAS. When assessing the crystal structure of SOS1, the Kuryian and Bar-Sagi labs found an allosteric RAS^{GTP} binding pocket distinct from the SOS1 catalytic domain that, when occupied, relieves SOS1 autoinhibition (8). This RAS^{GTP} binding increases SOS1 catalytic activity by up to 500-fold, setting up a RAS^{GTP}–SOS1–WT RAS positive feedback loop that allows for processive localized WT RAS activation at the plasma membrane. Further downstream, PI3K/AKT signaling can phosphorylate eNOS, which can nitrosylate and activate WT HRAS (9). RTK signaling can also activate WT RAS independently from mutant RAS. The McCormick laboratory built on previous work to show that canonical RTK-dependent WT RAS activation supplements basal signaling from mutated RAS to promote proliferation in *RAS*-mutated tumor cell lines, and combined inhibition of WT and mutated RAS is required to induce cell killing (3, 10). These mechanisms are not mutually exclusive and may cooperate in some contexts (11-13).

These models all indicate that SOS plays a role in activating WT RAS in mutant *RAS* cancers. Data from our lab and others suggests that SOS1 and SOS2 may play non-overlapping roles to promote WT RAS activation in *RAS* mutated tumor cells. For SOS1, allosteric signaling and RTK-dependent activation are both important for *KRAS*-mutated cancer cells depending on the cellular context: SOS1 is required for WT HRAS and NRAS activation in an animal model of KRAS-induced leukemia (14), mutant KRAS–SOS1–WT RAS allosteric signaling promotes growth of *KRAS* mutant pancreatic cancer cell xenografts (15), and both allosteric signaling and EGFR-SOS1 signaling contribute to growth of KRAS-mutated colorectal cancer cells (16). In contrast, we found that RTK–SOS2–WT RAS signaling, but not allosteric SOS2 activation, is a critical mediator of PI3K signaling in the context of mutant RAS (17) and protects *KRAS*-mutated cancer cells from anoikis (18).

SOS proteins as therapeutic targets in RAS-mutant cancers

In *KRAS*-mutated cancer cells, single agent MEK inhibitor treatment is ineffective because it relieves ERK-dependent negative feedback signaling, enhancing RTK-SOS-WT RAS signaling to the Raf/MEK/ERK and PI3K/AKT pathways and leading to therapeutic resistance (19-22). Similar relief of negative feedback signaling drives rapid resistance to $KRAS^{G12C}$ inhibitors (23, 24). In both cases, this resistance is driven by multiple RTKs. CRISPR screens revealed that both $KRAS^{G12C}$ inhibitors (25) and MEK inhibitors (26) require either broad inhibition of proximal RTK signaling or targeting of PI3K/mTOR survival signaling to enhance their efficacy and delay therapeutic resistance. Recent pre-clinical studies showed that co-treatment with allosteric SHP2 inhibitors can overcome both $KRAS^{G12C}$ (23, 24) and MEK (27, 28) inhibitor resistance, leading to more durable responses. Furthermore, we

found that *SOS2* deletion inhibited RTK-WT RAS-PI3K signaling and synergized with MEK inhibitors in *KRAS* mutated cell lines (17).

While there are currently no SOS2-specific inhibitors, Bayer Pharmaceuticals published a SOS1 inhibitor suitable for *in vitro* studies (29). Furthermore, Boehringer Ingelheim has developed orally available SOS1 inhibitors (30) and started recruiting patients with advanced *KRAS*-mutated solid tumors in 2019 for a Phase 1 clinical trial (NCT04111458). SOS1 inhibition is mechanistically most similar to SHP2 inhibition (31), suggesting that SOS1 inhibition could similarly enhance the efficacy of $KRAS^{G12C}$- and MEK-inhibitors. Indeed this appears to be true for combined SOS1/MEK inhibition, as preliminary data from Boehringer Ingelheim showed marked cooperativity between SOS1- and MEK-inhibition in multiple G12 and G13 *KRAS*-mutated PDX models (30). Furthermore, since $KRAS^{G12C}$ allosteric inhibitors can only bind $KRAS^{GDP}$, inhibiting SOS1 has the potential advantage of directly enhancing the efficacy of $KRAS^{G12C}$ inhibitors by increasing the amount of mutant $KRAS^{G12C}$ accessible to drug (29), in addition to inhibiting feedback activation of WT RAS. While further studies are required, the possibility of inhibiting SOS1 has enormous clinical potential as a combination therapy.

WT RAS signaling is an important modifier of *KRAS*-mutated oncogenesis, and inhibition of WT RAS signaling may be required for effective treatment of *KRAS*-mutated cancers. Understanding the mechanisms by which the ubiquitously expressed RasGEFs SOS1 and SOS2 promote WT RAS activation is an important step in determining the best ways to limit WT RAS signaling. The ability to pharmacologically manipulate SOS1/2 signaling may lead to optimized therapeutic combinations that can be used to treat *KRAS*-mutated cancers.

Selected References

1. Voice JK, Klemke RL, Le A, Jackson JH, 1999. **Four human ras homologs differ in their abilities to activate Raf-1, induce transformation, and stimulate cell motility.** J Biol Chem [PubMed Abstract]
2. Yan J, Roy S, Apolloni A, Lane A, Hancock JF, 1998. **Ras isoforms vary in their ability to activate Raf-1 and phosphoinositide 3-kinase.** J Biol Chem [PubMed Abstract]
3. Hamilton M, Wolfman A, 1998. **Oncogenic Ha-Ras-dependent mitogen-activated protein kinase activity requires signaling through the epidermal growth factor receptor**. J Biol Chem [PubMed Abstract]
4. Terrell EM, Durrant DE, Ritt DA, Sealover NE, Sheffels E, Spencer-Smith R, Esposito D, Zhou Y, Hancock JF, Kortum RL, Morrison DK, 2019. **Distinct Binding Preferences between Ras and Raf Family Members and the Impact on Oncogenic Ras Signaling**. Mol Cell [PubMed Abstract]
5. Zhou Y, Prakash P, Liang H, Cho KJ, Gorfe AA, Hancock JF, 2017. **Lipid-Sorting Specificity Encoded in K-Ras Membrane Anchor Regulates Signal Output**. Cell [PubMed Abstract]
6. Ebi H, Corcoran RB, Singh A, Chen Z, Song Y, Lifshits E, Ryan DP, Meyerhardt JA, Benes C, Settleman J, Wong KK, Cantley LC, Engelman JA, 2011. **Receptor tyrosine kinases exert dominant control over PI3K signaling in human KRAS mutant colorectal cancers**. J Clin

Invest [PubMed Abstract]

7. Molina-Arcas M, Hancock DC, Sheridan C, Kumar MS, Downward J, 2013. **Coordinate direct input of both KRAS and IGF1 receptor to activation of PI3 kinase in KRAS-mutant lung cancer**. Cancer Discov [PubMed Abstract]
8. Margarit SM, Sondermann H, Hall BE, Nagar B, Hoelz A, Pirruccello M, Bar-Sagi D, Kuriyan J, 2003. **Structural evidence for feedback activation by Ras.GTP of the Ras-specific nucleotide exchange factor SOS**. Cell [PubMed Abstract]
9. Lim KH, Ancrile BB, Kashatus DF, Counter CM, 2008. **Tumour maintenance is mediated by eNOS**. Nature [PubMed Abstract]
10. Young A, Lou D, McCormick F, 2013. **Oncogenic and wild-type Ras play divergent roles in the regulation of mitogen-activated protein kinase signaling**. Cancer Discov [PubMed Abstract]
11. Boykevisch S, Zhao C, Sondermann H, Philippidou P, Halegoua S, Kuriyan J, Bar-Sagi D, 2006. **Regulation of ras signaling dynamics by Sos-mediated positive feedback**. Curr Biol [PubMed Abstract]
12. Roose JP, Mollenauer M, Ho M, Kurosaki T, Weiss A, 2007. **Unusual interplay of two types of Ras activators, RasGRP and SOS, establishes sensitive and robust Ras activation in lymphocytes**. Mol Cell [PubMed Abstract]
13. Das J, Ho M, Zikherman J, Govern C, Yang M, Weiss A, Chakraborty AK, Roose JP, 2009. **Digital signaling and hysteresis characterize ras activation in lymphoid cells**. Cell [PubMed Abstract]
14. You X, Kong G, Ranheim EA, Yang D, Zhou Y, Zhang J, 2018. **Unique dependence on Sos1 in KrasG12D -induced leukemogenesis**. Blood [PubMed Abstract]
15. Jeng HH, Taylor LJ, Bar-Sagi D, 2012. **Sos-mediated cross-activation of wild-type Ras by oncogenic Ras is essential for tumorigenesis**. Nat Commun [PubMed Abstract]
16. Depeille P, Henricks LM, van de Ven RA, Lemmens E, Wang CY, Matli M, Werb Z, Haigis KM, Donner D, Warren R, Roose JP, 2015. **RasGRP1 opposes proliferative EGFR-SOS1-Ras signals and restricts intestinal epithelial cell growth**. Nat Cell Biol [PubMed Abstract]
17. Sheffels E, Sealover NE, Wang C, Kim DH, Vazirani IA, Lee E, M Terrell E, Morrison DK, Luo J, Kortum RL, 2018. **Oncogenic RAS isoforms show a hierarchical requirement for the guanine nucleotide exchange factor SOS2 to mediate cell transformation**. Sci Signal [PubMed Abstract]
18. Sheffels E, Sealover NE, Theard PL, Kortum RL, 2019. **Anchorage-independent growth conditions reveal a differential SOS2 dependence for transformation and survival in RAS-mutant cancer cells**. Small GTPases [PubMed Abstract]
19. Turke AB, Song Y, Costa C, Cook R, Arteaga CL, Asara JM, Engelman JA, 2012. **MEK inhibition leads to PI3K/AKT activation by relieving a negative feedback on ERBB receptors**. Cancer Res [PubMed Abstract]
20. Pettazzoni P, Viale A, Shah P, Carugo A, Ying H, Wang H, Genovese G, Seth S, Minelli R, Green T, Huang-Hobbs E, Corti D, Sanchez N, Nezi L, Marchesini M, Kapoor A, Yao W, Francesco ME,

Petrocchi A, Deem AK, Scott K, Colla S, Mills GB, Fleming JB, Heffernan TP, Jones P, Toniatti C, DePinho RA, Draetta GF, 2015. **Genetic events that limit the efficacy of MEK and RTK inhibitor therapies in a mouse model of KRAS-driven pancreatic cancer**. Cancer Res [PubMed Abstract]

21. Sos ML, Fischer S, Ullrich R, Peifer M, Heuckmann JM, Koker M, Heynck S, Stückrath I, Weiss J, Fischer F, Michel K, Goel A, Regales L, Politi KA, Perera S, Getlik M, Heukamp LC, Ansén S, Zander T, Beroukhim R, Kashkar H, Shokat KM, Sellers WR, Rauh D, Orr C, Hoeflich KP, Friedman L, Wong KK, Pao W, Thomas RK, 2009. **Identifying genotype-dependent efficacy of single and combined PI3K- and MAPK-pathway inhibition in cancer**. [PubMed Abstract]
22. Manchado E, Weissmueller S, Morris JP 4th, Chen CC, Wullenkord R, Lujambio A, de Stanchina E, Poirier JT, Gainor JF, Corcoran RB, Engelman JA, Rudin CM, Rosen N, Lowe SW, 2016. **A combinatorial strategy for treating KRAS-mutant lung cancer**. Nature [PubMed Abstract]
23. Xue JY, Zhao Y, Aronowitz J, Mai TT, Vides A, Qeriqi B, Kim D, Li C, de Stanchina E, Mazutis L, Risso D, Lito P, 2020. **Rapid non-uniform adaptation to conformation-specific KRAS(G12C) inhibition**. Nature [PubMed Abstract]
24. Ryan MB, Fece de la Cruz F, Phat S, Myers DT, Wong E, Shahzade HA, Hong CB, Corcoran RB, 2020. **Vertical Pathway Inhibition Overcomes Adaptive Feedback Resistance to KRASG12C Inhibition**. Clin Cancer Res [PubMed Abstract]
25. Lou K, Steri V, Ge AY, Hwang YC, Yogodzinski CH, Shkedi AR, Choi ALM, Mitchell DC, Swaney DL, Hann B, Gordan JD, Shokat KM, Gilbert LA, 2019. **KRASG12C inhibition produces a driver-limited state revealing collateral dependencies**. Sci Signal [PubMed Abstract]
26. Anderson GR, Winter PS, Lin KH, Nussbaum DP, Cakir M, Stein EM, Soderquist RS, Crawford L, Leeds JC, Newcomb R, Stepp P, Yip C, Wardell SE, Tingley JP, Ali M, Xu M, Ryan M, McCall SJ, McRee AJ, Counter CM, Der CJ, Wood KC, 2017. **A Landscape of Therapeutic Cooperativity in KRAS Mutant Cancers Reveals Principles for Controlling Tumor Evolution**. Cell Rep [PubMed Abstract]
27. Fedele C, Ran H, Diskin B, Wei W, Jen J, Geer MJ, Araki K, Ozerdem U, Simeone DM, Miller G, Neel BG, Tang KH, 2018. **SHP2 Inhibition Prevents Adaptive Resistance to MEK Inhibitors in Multiple Cancer Models**. Cancer Discov [PubMed Abstract]
28. Ruess DA, Heynen GJ, Ciecielski KJ, Ai J, Berninger A, Kabacaoglu D, Görgülü K, Dantes Z, Wörmann SM, Diakopoulos KN, Karpathaki AF, Kowalska M, Kaya-Aksoy E, Song L, van der Laan EAZ, López-Alberca MP, Nazaré M, Reichert M, Saur D, Erkan MM, Hopt UT, Sainz B Jr, Birchmeier W, Schmid RM, Lesina M, Algül H, 2018. **Mutant KRAS-driven cancers depend on PTPN11/SHP2 phosphatase**. Nat Med [PubMed Abstract]
29. Hillig RC, Sautier B, Schroeder J, Moosmayer D, Hilpmann A, Stegmann CM, Werbeck ND, Briem H, Boemer U, Weiske J, Badock V, Mastouri J, Petersen K, Siemeister G, Kahmann JD, Wegener D, Böhnke N, Eis K, Graham K, Wortmann L, von Nussbaum F, Bader B, 2019. **Discovery of potent SOS1 inhibitors that block RAS activation via disruption of the RAS-SOS1 interaction**. Proc Natl Acad Sci U S A [PubMed Abstract]
30. Gerlach D, Gmachl M, Ramharter J, The J, Fu S-C, Trapani F, Kessler D, Rumpel K, Botesteanu

D-A, Ettmayer P, Arnhof H, Gerstberger T, Kofink C, Wunberg T, Vellano CP, Heffernan TP, Marszalek JR, Pearson M, McConnell DB, Kraut N, Hofmann MH, 2020. **BI-3406 and BI 1701963: Potent and selective SOS1::KRAS inhibitors induce regressions in combination with MEK inhibitors or irinotecan**. AACR Virtual Meeting 1, abstract currently unavailable.

31. Nichols RJ, Haderk F, Stahlhut C, Schulze CJ, Hemmati G, Wildes D, Tzitzilonis C, Mordec K, Marquez A, Romero J, Hsieh T, Zaman A, Olivas V, McCoach C, Blakely CM, Wang Z, Kiss G, Koltun ES, Gill AL, Singh M, Goldsmith MA, Smith JAM, Bivona TG, 2018. **RAS nucleotide cycling underlies the SHP2 phosphatase dependence of mutant BRAF-, NF1- and RAS-driven cancers**. Nat Cell Biol [PubMed Abstract]

< Older Post
RAS Mutation Tropism

Newer Post >
Deploying a RAS pipeline against the SARS-CoV-2 pandemic

We welcome your comments on this post. All comments must follow our comment policy.

Archive

2018 (7)

2017 (9)

2016 (11)

2015 (15)

2014 (5)